Guidance Notes on

Nonlinear Finite Element Analysis of Marine and Offshore Structures

January 2021

GUIDANCE NOTES ON

NONLINEAR FINITE ELEMENT ANALYSIS OF MARINE AND OFFSHORE STRUCTURES
JANUARY 2021

American Bureau of Shipping
Incorporated by Act of Legislature of
the State of New York 1862

© 2021 American Bureau of Shipping. All rights reserved.
ABS Plaza
1701 City Plaza Drive
Spring, TX 77389 USA

Foreword *(2021)*

With the continuous increase in the size and complexity of marine and offshore structures, new and innovative design concepts are constantly being envisaged by engineers. With the development of powerful computers, more and more engineers turn to advance nonlinear numerical simulation tools in order to better understand complex engineering processes of new structural concepts that may not be adequately covered by the current Rules and standards. Also, advanced nonlinear numerical tools are widely used in situations where a structural engineer wants to apply more advanced analysis methods that go beyond the standard Rule requirements in order to investigate the behavior of the structure in the inelastic regime, to assess the actual safety margin of the structure, or to gain a better understanding of alternative load paths, failure mode interactions, and collapse sequences.

Nonlinear finite element analysis (NLFEA) is currently one of the most advanced structural analysis approaches. It takes into account various sources of nonlinearity such as material, geometry, and boundary condition nonlinearities such as contact. NLFEA has been developed over the last 60 years and is considered mature enough to be applied in daily structural design and analysis. However, the application of NLFEA is still challenging because many technical aspects need to be carefully considered. Nonlinear analysis solutions can be non-unique, convergence is not always obtained, and there is often no mathematical error estimation available. While NLFEA is a powerful numerical analysis tool, improper application can yield unreliable and inconsistent results.

These Guidance Notes address the main technical aspects of using NLFEA and provide the best practices and general recommendations for achieving more reliable results when analyzing yielding and plastic deformations, buckling, ductile static fracture, and dynamic low-cycle fatigue fracture of marine and offshore structures made of steel. Application examples included in these Guidance Notes are structural collapse analysis of a stiffened panel, hull-girder ultimate strength calculations in intact and damaged conditions, dynamic analysis of a container stacks, and impact analysis of a stiffened panel.

The objective of this document is to provide guidance for using NLFEA for cases that are not covered by the ABS Rules and Guides, or for those involving novel structural designs and loading situations where NLFEA may provide a better insight into the adequacy of a proposed design.

Additional considerations may be needed for some specific cases, especially when a novel design or application is being evaluated. In case of any doubt about the application of these Guidance Notes, ABS should be consulted.

The January 2021 edition updates the examples in Appendix 1.

These Guidance Notes become effective on the first day of the month of publication.

Users are advised to check periodically on the ABS website www.eagle.org to verify that this version of these Guidance Notes is the most current.

We welcome your feedback. Comments or suggestions can be sent electronically by email to rsd@eagle.org.

Terms of Use

The information presented herein is intended solely to assist the reader in the methodologies and/or techniques discussed. These Guidance Notes do not and cannot replace the analysis and/or advice of a qualified professional. It is the responsibility of the reader to perform their own assessment and obtain professional advice. Information contained herein is considered to be pertinent at the time of publication but may be invalidated as a result of subsequent legislations, regulations, standards, methods, and/or more updated information and the reader assumes full responsibility for compliance. Where there is a conflict between this document and the applicable ABS Rules and Guides, the latter will govern. This publication may not be copied or redistributed in part or in whole without prior written consent from ABS.

GUIDANCE NOTES ON

NONLINEAR FINITE ELEMENT ANALYSIS OF MARINE AND OFFSHORE STRUCTURES

CONTENTS

SECTION 1
Introduction

1 General

The stiffness of a discretized structure in a numerical analysis is characterized by its stiffness matrix $\boldsymbol{K}$. When the structure is in static equilibrium, $\boldsymbol{K}$ relates the vector of external nodal loads, $\boldsymbol{f}$, to the vector of nodal displacements, $\boldsymbol{u}$, as follows:

$$\boldsymbol{f} = \boldsymbol{K}\boldsymbol{u} \tag{1.1}$$

A structure is said to be nonlinear whenever its stiffness changes with changing loads. The stiffness matrix $\boldsymbol{K}$ can be a function of the structure's geometric and material properties and change continuously as the applied load $\boldsymbol{f}$ changes. This requires an incremental and iterative solution of the governing equations of the nonlinear system.

Most marine and offshore structures exhibit nonlinear behavior prior to reaching their maximum load bearing capacity (*ultimate strength*) after which a progressive collapse and total failure occur. When analyzing various structures, including marine and offshore structures, it is common to plot the relationship between a dominant load acting on the structure and the appropriately chosen measure of the structure's deflection (e.g., a hull girder vertical bending moment plotted against a hull girder curvature or a compressive force on the stiffened panel plotted against an average axial displacement of the loaded edge of the panel in the direction of the applied load). These curves are usually called the *load-displacement* (*P*-Δ) or *load-shortening curves*.

An example of a *P*-Δ curve is shown in Section 1, Figure 1 for a typical structure exhibiting nonlinear behavior. Initial response of the structure to the applied load is usually linear up to the proportionality limit with a constant stiffness matrix $\boldsymbol{K}$. If the load is increased even further, the structure begins to behave in a nonlinear manner due to changes in $\boldsymbol{K}$. At the point of ultimate strength (largest maxima in the load-displacement curve), the structure reaches its maximum load bearing capacity. At this point, any increase in the applied load will lead to an accelerated response of the structure, as the static equilibrium can no longer be established.

Nonlinear finite element analysis (NLFEA) is an advanced, robust, and widely used numerical procedure for analyzing structural problems involving nonlinearities and will be discussed in detail in Section 3.

1.1 Principles of Structural Design Evaluation

A marine or offshore structure needs to withstand various static and dynamic loads throughout its entire design life. Rules and standards for marine and offshore structures usually rely on the following three structural design evaluation principles [1]:

1) *Working Stress Design* (WSD) where the calculated working stress in a structural component does not exceed a fraction of the yield stress of the material.

2) *Critical Buckling Strength Design* (CBSD) where the calculated stress in components susceptible to buckling does not exceed the critical buckling stress which is usually equal to the elastic buckling stress corrected by a factor that considers plasticity.

3) *Limit State Design* (LSD) where a reliability theory is used to calculate the actual safety margin of the structure subjected to extreme loads. The limit state is defined as the state of the structure beyond which it is no longer fit for its intended use. Limit states are further categorized as follows [1]:

a) *Ultimate Limit State* (ULS) represents the state of a structure at which the maximum load carrying capacity is reached when the structure is subjected to extreme loads.

b) *Accidental Limit State* (ALS) represents a state of the structure at which the maximum load-carrying capacity of the structure is reached when the structure is subjected to accidental loads such as loads due to explosion, collision, and grounding.

c) *Fatigue Limit State* (FLS) represents the state of a structure at which the maximum capacity of the structure to withstand cyclic loads is reached.

d) *Serviceability Limit State* (SLS) represents the state of a structure at which the normal functional or operational parameter limits are reached (e.g., local deformation limit).

FIGURE 1
Load-Displacement Curve of a Typical Structure

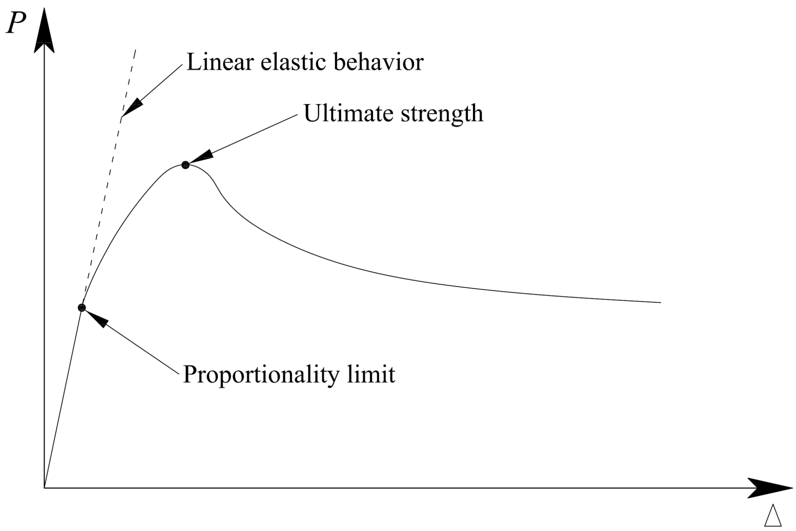

Although WSD and CBSD are generally sufficient for many types of vessels, the use of the more sophisticated LSD approach may be justified in certain cases. The LSD approach requires very precise calculations of both the ultimate capacity of the structure and the extreme loads. An accurate and general way to assess the reliability of the structure for all relevant failure modes is to characterize all the random variables affecting the loads and the structural capacity using their full probability distributions. Reliability theory is then used to calculate the probability of failure of the structure (reliability = 1 – probability of failure).

Frequently, for marine and offshore structures, the full probabilistic limit state approach is not used due to the lack of statistical data and complexity of the approach. Approximate probabilistic methods are often used such as the *Safety Index* (SI) method and the *Partial Safety Factors* (PSF) method (see [2] and [1] for more details). The latter is widely adopted in the marine and offshore industries. It uses the established set of deterministic factors (PSFs) which factor up the characteristic load and factor down the characteristic load limit (capacity or resistance) such that the required level of structural safety can be obtained considering the consequence of each failure mode (see Section 1, Figure 2). For loads, the characteristic value implies that there is a small probability of exceeding this value. For load limit, the characteristic value implies that there is a small probability of being below this value. The following condition is to be satisfied:

$$\gamma_P P_C \leq P_{L,C}/\gamma_L \qquad (1.2)$$

where

γ_P = PSF accounting for the uncertainty in the calculated load

γ_L = PSF accounting for the uncertainty in the calculated load limit (capacity or resistance)

P_C = characteristic load

$P_{L,C}$ = characteristic load limit

FIGURE 2
Partial Safety Factors for LSD Approach

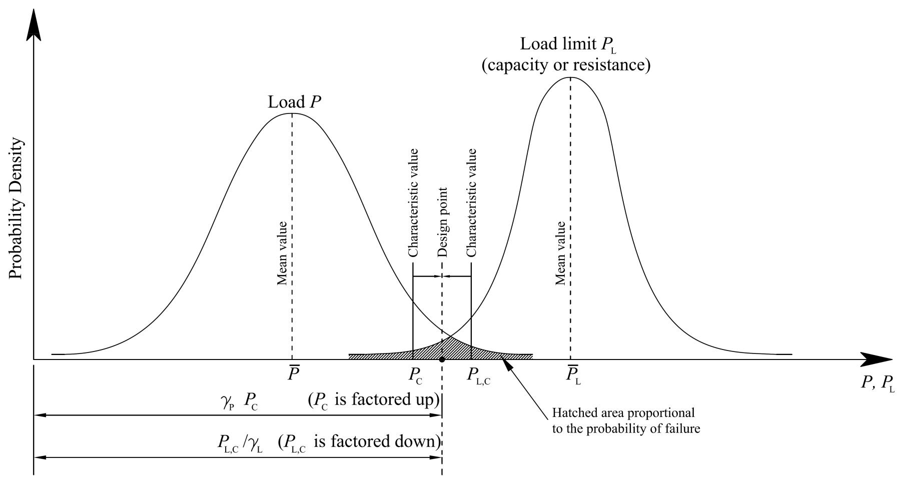

The calculation of load characteristic values is outside of the scope of these Guidance Notes. However, when the NLFEA is used to determine the characteristic load limit using the recommendations contained in these Guidance Notes regarding finite element (FE) model, material model, and analysis parameters, the calculated load limit may be considered as a characteristic value with a 5% probability that the actual load limit is lower than the calculated load limit. The statistical variability of other parameters affecting the load limit that are not specified in these Guidance Notes, such as plate thickness, should be considered when calculating the statistical properties of the characteristic load limit.

1.2 Application of NLFEA

With the increase in computing capacity, and with the NLFEA achieving maturity, its usage by engineers in the marine and offshore industries has grown rapidly. The cases where the NLFEA is most applied are:

i) When the Rules or standards call for the application of LSD approach. In contrast to WSD and CBSD approaches, LSD approach requires the use of a nonlinear analysis to calculate the limit state of the structure and to assess the actual safety margin against a certain type of failure. The examples may include the calculation of hull girder ultimate strength (reference should be made to Parts 5A, 5B, 5C, and 5D of the ABS *Marine Vessel Rules*, as applicable for specific vessel type) in the intact and damaged conditions (residual strength) and the investigation of the collapse sequence of a stiffened panel.

ii) When current Rules or standards do not cover a certain aspect of a structural design or for novel designs and loading situations where the NLFEA may be used to provide a better insight into the adequacy of a proposed design

iii) When it is necessary to assess the adequacy of the structure following an accident such as collision, impact with ice, grounding, or explosion

iv) When it is necessary to assess the *crashworthiness* of a vessel (i.e., the ability of a vessel to absorb the energy of the collision while protecting its occupants and cargo)

v) For static and dynamic analysis of structures containing members for which the assumption of linearity does not hold. An example of such a structure is a container stack with twistlocks and lashing rods, which both exhibit nonlinear structural behavior

vi) Whenever a contact between two surfaces or objects needs to be analyzed and whenever friction needs to be simulated

vii) When it is necessary to analyze repeated yielding of the structure and the associated low-cycle fatigue

viii) To assess the redundancy of complex structures (i.e., the ability of a structure to shed loads from a failed member to surrounding intact members and to establish alternative load paths)

ix) To assess the interaction of various failure modes and complete collapse sequence of complex structures

x) To analyze manufacturing or repair processes involving plastic deformations and residual stresses

xi) Multi-physics analysis (fluid-structure interaction – FSI, thermal-structural coupling, etc.)

xii) To gain insights into complex engineering processes otherwise only accessible by experiments

The recommendations and best practices contained within these Guidance Notes may be applied in the NLFEA of all types of limit states (ULS, ALS, FLS, SLS).

1.3 Types of Structural Failures

The objective of the LSD approach is to find the loads that cause structural failure at the local member level, or at the global level involving the overall collapse of the entire structure. Since most marine and offshore structures behave nonlinearly before reaching the ultimate state, LSD may require the use of NLFEA. Nonlinearities may come from the geometry of the structure, its material, boundary conditions, or from the combination of these factors. For structures made of steel, such as marine and offshore structures, the most common and basic types of failure are [2]:

i) Large local plasticity

ii) Buckling (bifurcation or nonbifurcation)

iii) Fracture

- Static (ductile and brittle)
- Dynamic (high-cycle and low-cycle fatigue)

Usually, the failure of a structural component, or the entire structure, involves a combination of the above basic failure types. The typical load-displacement curves for members failing due to large local plasticity and buckling are shown in Section 1, Figure 3.

1.3.1 Large Local Plasticity

Large local plasticity is the dominant failure mode in sturdy members which are not susceptible to buckling. After the proportionality limit has been reached, the growth of the local plastic regions gradually decreases the stiffness of the structure represented by the slope of the load-displacement curve. As the stiffness becomes very small, the deflection starts to rapidly increase (see Section 1,

Figure 3a). There may not be a well-defined failure point, and the failure load is usually defined as the load at which the deflection of the structure starts to increase rapidly.

1.3.2 Bifurcation Buckling

Buckling, or instability, occurs in slender members under axial or in-plane compressive loads. *Bifurcation* (branching) *buckling* is an idealized model assuming a perfect structure without any geometric or load eccentricities and without any local imperfections or residual stresses. Under these assumptions, there will be no deflection of the member in any direction other than the direction of the applied load until a load reaches a certain critical value. After this point, called the *bifurcation point*, multiple solutions may exist as the load-displacement path branches. The member's lateral deflection may stay at zero (unstable solution) or may start to rapidly increase in different directions without any increase in the axial load (stable solutions) as seen in Section 1, Figure 3b for an idealized beam.

The bifurcation buckling model is appropriate for many actual slender members, such as beams and pillars with initial eccentricities and imperfections, where the lateral deflection is very small prior to the onset of buckling (see Section 1, Figure 3b). The initial load and geometric eccentricities and imperfections determine to which side the member will buckle. Slender stiffened panels and plates may have some reserve strength (positive stiffness) after the initial bifurcation buckling, as illustrated in Section 1, Figure 3c.

1.3.3 Nonbifurcation Buckling

Nonbifurcation buckling occurs when the initial deflection of the member increases with the applied axial or in-plane compressive loads and progressively weakens the structure from the beginning of load application. Nonbifurcation buckling usually occurs in beams, pillars, plates, and stiffened panels with significant lateral load in combination with in-plane and axial compressive loads. Due to the coupling between the in-plane or axial loads and the lateral deflection of the member, the structural response is nonlinear from the beginning of load application. Similarly to large local plasticity, there is no clear onset of buckling or maxima in the load-displacement curve (see Section 1, Figure 3d). Instead, the member is considered to have failed when a limit value of the deflection has been reached.

FIGURE 3
Load-Displacement Curves for Large Plasticity and Buckling

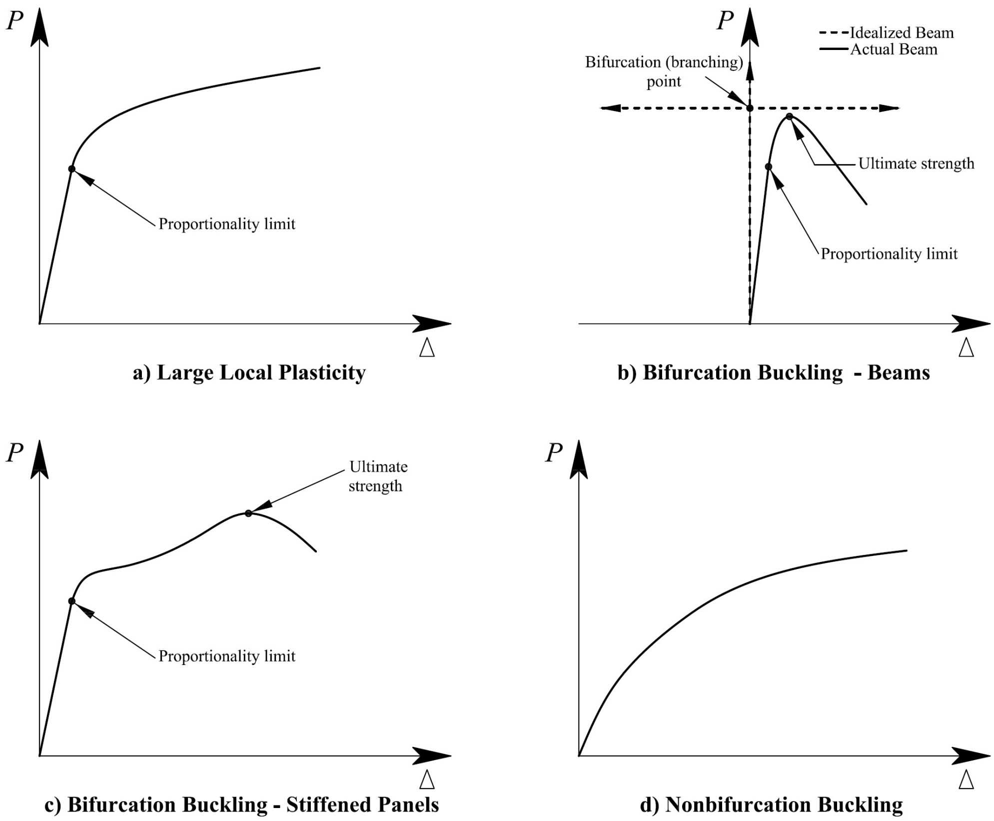

1.3.4 Static Fracture

A *static fracture* is the rupture of a structural component under the action of static loads. For ductile materials, such as typical steel grades used for marine and offshore structures, significant plastic deformation will occur before static fracture, giving sufficient warning of the imminent failure. On the other hand, brittle materials do not exhibit large plastic deformations before static fracture. Steels may become brittle at very low temperatures, depending mainly on their chemical composition. However, steel grades used for marine and offshore structures are engineered to have sufficient ductility, even at low temperatures.

1.3.5 High-cycle and Low-cycle Fatigue

High-cycle fatigue failure occurs when many cycles of moderate dynamic loads are applied to the structure causing crack initiation and growth to the point where fracture occurs. High-cycle fatigue is governed by the elastic stress range and is analyzed using a linear damage accumulation law called Miner's Rule. On the other hand, *low-cycle fatigue* occurs when the structure is subjected to a relatively low number of large dynamic load cycles causing plastic deformations. Low-cycle fatigue is governed by the strain range [3] (strain-based approach to fatigue).

2 Scope and Overview of these Guidance Notes

The objective of these Guidance Notes is to provide the best practices and general recommendations for analyzing marine and offshore structures using NLFEA. The main technical aspects of NLFEA are addressed in these Guidance Notes to help the reader to better understand and evaluate the analysis results and to aid in troubleshooting possible issues with solution convergence.

These Guidance Notes cover:

- Different sources of structural nonlinearities (see Section 2)

- Main technical aspects of NLFEA, such as analysis type, iterative algorithm, time-domain integration, model extent, mesh size, element type, boundary conditions, load application, geometric imperfections, contact, numerical solution stabilization, etc. (see Section 3)
- Quality control (see Section 4)
- Application examples (see Appendix 1)

The recommendations of these Guidance Notes for using NLFEA are applicable to marine and offshore structures made of steel. All types of structural failures listed in 1/1.3 are covered except for brittle failure and high-cycle fatigue. Brittle failure rarely occurs in marine and offshore structures due to high quality control of the steel manufacturing and construction processes. Linear high-cycle fatigue analysis procedure and the associated acceptance criteria may be found in ABS *Guide for Spectral-Based Fatigue Analysis for Vessels* and ABS *Guide for Spectral-Based Fatigue Analysis for Floating Production, Storage and Offloading (FPSO) Installations*.

Design loads and acceptance criteria for NLFEA results regarding various failure modes may be found in ABS Rules or other applicable Standards.

3 Associated ABS Documents

- ABS *Rules for Building and Classing Marine Vessels (Marine Vessel Rules)*
- ABS *Guide for Certification of Container Securing Systems*
- ABS *Guide for Spectral-Based Fatigue Analysis for Vessels*
- ABS *Guide for Spectral-Based Fatigue Analysis for Floating Production, Storage and Offloading (FPSO) Installations*
- ABS *Guidance Notes on Accidental Load Analysis and Design for Offshore Structures*
- ABS *Guidance Notes on Ice Class*

4 Abbreviations

ABS : American Bureau of Shipping

ALS : Accidental Limit State

CAD : Computer Aided Design

CBSD : Critical Buckling Strength Design

COR : Center of Roll

CPC : Corner Post Compression

DOF : Degree of Freedom

FAT : Fully Automatic Twistlock

FE : Finite Element

FEA : Finite Element Analysis

FLS : Fatigue Limit State

FPSO : Floating Production, Storage and Offloading

FSI : Fluid-Structure Interaction

HHT : Hilber-Hughes-Taylor

HS : Higher-Strength Steel

ISO : International Organization for Standardization

ISSC : International Ship and Offshore Structures Congress

LRT : Lashing Rod Tension

LSD : Limit State Design

MPC : Multi Point Constraint

MS : Mild Steel (Ordinary-Strength Steel)

NLFEA : Nonlinear Finite Element Analysis

N-R : Newton-Raphson

PSF : Partial Safety Factors

SAT : Semi-Automatic Twistlock

SI : Safety Index

SLS : Serviceability Limit State

TT : Twistlock Tension

ULS : Ultimate Limit State

WSD : Working Stress Design

5 Definitions

Accidental Limit State. State of a structure at which the maximum load-carrying capacity of the structure is reached when the structure is subjected to accidental loads.

Backstress. Stress tensor by which the yield surface shifts according to the kinematic hardening model.

Bauschinger Effect. Asymmetry of yield stress in tension and subsequent compression of the material caused by the shifting of the yield surface in one direction.

Bifurcation Buckling. Idealized model assuming no eccentricities in structure or loads where there is no response in the buckling mode until a critical buckling load is reached. At that point, the solution bifurcates (branches) into multiple load-displacement paths.

Characteristic Value of Load or Load Limit. Load design value with a certain small probability of being exceeded or a load limit design value with a certain small probability of not being exceeded.

Combined Kinematic and Isotropic Hardening. Hardening model which assumes simultaneous isotropic expansion and kinematic shift of the yield surface.

Contact Pair. A pair of geometric entities or element sets on the same or on different bodies which may potentially come into contact during the analysis.

Corner Angle. Angle between element edges at a corner.

Coulomb Friction Model. Model where friction is proportional to the force acting normal to the contact surfaces.

Crashworthiness. The ability of a vessel to absorb the energy of the collision while protecting its occupants and cargo.

Critical Buckling Strength Design . Design principle in which the calculated stress in components susceptible to buckling does not exceed the critical buckling stress.

Critical Time Increment (for Explicit Analysis). The maximum size of a time increment allowing for a stable and accurate solution. It is approximately equal to the time it takes a stress wave to propagate across the smallest finite element dimension.

Cycle-Dependent Creep. The increase of the mean strain when the material is subjected to biased stress cycles.

Cycle-Dependent Relaxation. The shifting of the mean stress towards zero when the material is subjected to biased strain cycles.

Cyclic Hardening. Phenomenon where the maximum stress reached in each of the hysteresis loops of a symmetric strain-controlled loading cycle gradually increases.

Displacement Control. Analysis approach in which the displacement application is controlled.

Drilling Stiffness. Rotational stiffness of a shell element about the direction normal to plane of the element.

Element Aspect Ratio. Ratio of maximum to minimum element edge length.

Engineering Stress and Strain. Stress and strain calculated based on the initial cross section and length of a test specimen, respectively.

Explicit Time Integration. Time integration in which the displacements and velocities at the next time increment are nonlinear functions of the displacements and velocities at the previous time increments only and can be calculated explicitly without the iterative solution process.

Fatigue Limit State. State of a structure at which the maximum capacity of the structure to withstand cyclic loads is reached.

Flow Curve. Uniaxial stress-plastic strain curve that defines the flow rule.

Flow Rule. Relationship between the plastic strain increment and the stress increment once the stress state is on the yield surface.

Follower Loads. Loads that follow the nodal translation and rotation of the structure.

Geometric Nonlinearity. Type of nonlinearity that occurs in structures that exhibit large displacements and rotations such that the applied loads and/or the stiffness of the structure become dependent on the structure's geometry.

Hard Contact. Type of pressure-overclosure relationship where the contact pressure is zero when the surfaces are not in contact and where there is no penetration of one surface into another.

Hardening Rule. Rule that describes how the yield surface evolves when plastic straining occurs.

High-Cycle Fatigue. Many cycles of moderate dynamic loads are applied to the structure causing crack initiation and growth to the point where fracture occurs.

Hourglassing. Numerical issue that is characterized by the occurrence of spurious, zero strain energy bending modes of first-order elements with reduced integration.

Implicit Time Integration. Time integration in which the displacements and velocities at the next time increment are nonlinear functions of the displacements and velocities at the next and previous time increments. It requires an iterative solution process.

Isotropic Hardening. Hardening model which assumes that the yield surface expands equally in all directions when plastic straining occurs.

Jacobian. Measure of the element's deviation from an ideal shape.

Kinematic Hardening. Hardening model which assumes that the yield surface does not change in size or shape, but simply shifts in the stress space.

Large Local Plasticity. Growth of the local plastic regions that gradually decreases the stiffness of the structure.

Limit State Design. Design principle in which the reliability theory is used to calculate the true safety margin of the structure subjected to extreme loads.

Load Control. Analysis approach in which the load application is controlled.

Load-Displacement Curve. Relationship between a dominant load acting on the structure and the appropriately chosen measure of the structure's deflection.

Load-Shortening Curve. See "Load-Displacement Curve".

Low-Cycle Fatigue. Relatively low number of large dynamic load cycles causing plastic deformations and fracture.

Mass Scaling. Artificial increasing of material density in order to increase the critical time increment during explicit analysis.

Material Nonlinearity. Nonlinearity stemming from the nonlinear material behavior as characterized by a nonlinear uniaxial stress-strain function.

Necking. Localization of strains in a ductile material. In a tensile test of a cylindrical specimen, necking is manifested as a local reduction of cylinder radius.

Nonbifurcation Buckling. Type of buckling that occurs when the initial deflection of the member increases with the applied axial or in-plane compressive loads and progressively weakens the structure from the beginning of load application.

Numerical Stabilization. Introduction of artificial damping elements at the nodes where the ratio of displacement increments to load increments is very high.

Partial Safety Factors. Deterministic factors which factor up the characteristic load and factor down the characteristic load limit of a structure such that the required level of structural safety can be obtained considering the consequence of each failure mode.

Penalty Method. Numerical method used to enforce the contact pressure-overclosure relationship.

Plastic Shakedown. Stabilization of the cyclic hardening over a certain number of cycles.

Ratchetting. See "Cycle-Dependent Creep".

Reversed Mass Scaling. Technique which consists of reducing the material density in order to minimize the inertial effects during the quasi-static analysis.

Safety Index. Inverse of the coefficient of variation of the margin between the actual load and the load limit value (capacity). It determines the degree of safety of the structure.

Selective Subcycling. Technique used during the explicit analysis to reduce the total computation time. It is used when a small number of elements with a very small critical time increment govern the total computation time. Instead of integrating all the elements with this very small time increment, the remaining elements are integrated with their significantly larger critical time increment.

Serviceability Limit State. State of a structure at which the normal functional or operational parameter limits are reached.

Shear Locking. Excessive stiffness in bending of first-order fully integrated finite elements caused by spurious shear strains.

Skewness Angle. Difference between the right angle and the smallest angle between intersecting element mid-lines.

Smooth Step. Mathematical function that gradually increases the load application rate from zero to a maximum value and then gradually decreases the load application rate to zero towards the end of the analysis.

Snap-Back. Unstable structural response that occurs when the displacement is gradually incremented.

Snap-Through. Unstable structural response that occurs when a structure suddenly assumes another configuration under the action of an external load.

Static Fracture. Rupture of a structural component under the action of static loads.

True Stress and Strain. Stress and strain calculated based on a specimen's instantaneous cross-section and instantaneous strain increment, respectively.

Ultimate Limit State. State of a structure at which the maximum load carrying capacity is reached when the structure is subjected to extreme loads.

Ultimate Strength. Maximum load-bearing capacity of the structure.

Volumetric Locking. Excessive stiffness of fully integrated elements to deformations that cause no change in the volume of the element. Volumetric locking is caused by spurious pressure stresses.

Warping Angle. Out-of-plane element warping.

Working Stress Design. Design principle in which the calculated working stress in a structural component does not exceed a fraction of the yield stress of the material.

Yield Condition. Combination of stresses in a certain structural component when the material starts to yield.

Yield Surface. Mathematical function describing the yield condition.

6 Symbols

a	Distance between the strong stiffened panel supports in the x direction
A	Overall stiffened panel length

b	Spacing of stiffened panel stiffeners; plate breadth; grounding damage breadth
b_f	Breadth of flange
B	Total breadth of the stiffened panel in the *y* direction
c	Dilatational wave speed
$\boldsymbol{C}$	Damping matrix
C	Parameter of the Cowper-Symonds model
d	Collision damage breadth
d_1, d_2, d_3, d_4, d_5	Parameters of the Johnson-Cook ductile fracture criteria
E	Modulus of elasticity
f	Function
$\boldsymbol{f}$	Vector of external nodal loads
F	Force
Fx	Compressive load in *x* direction
Fy	Compressive load in *y* direction
h	Collision or grounding damage height
h_w	Height of the stiffener web
H	Half-length of one structural fold of a thin plate
$\boldsymbol{K}$	Stiffness matrix
K	Constant of the power-hardening true stress-strain relationship
K_t	Tangent stiffness
L	Finite element length
m	Number of half-waves between the stiffened panel strong supports in the x direction
$\boldsymbol{M}$	Mass matrix
n	Strain-hardening exponent of the power-hardening true stress-strain relationship
n_s	Number of stiffeners between strong longitudinal supports
P	Load
P_C	Characteristic load
$P_{L.C}$	Characteristic load limit
q	Parameter of the Cowper-Symonds model
r	Radius of the indenter
R	Residual load
Rx_{i-j}	Rotation around the *x* axis of edge connecting corners *i* and *j*
Ry_i	Rotation around the *y* axis of corner *i*
Ry_{i-j}	Rotation around the *y* axis of edge connecting corners *i* and *j*
Rz_i	Rotation around the *z* axis of corner *i*
Rz_{i-j}	Rotation around the *z* axis of edge connecting corners *i* and *j*

S	Current cross-sectional area of the test specimen
S_0	Initial cross-sectional area of the test specimen
$S(t)$	Smooth step function
t	Time or plate thickness
t_f	Thickness of flange
t_p	Thickness of plate
t_w	Thickness of web
T	Time period over which the full load is applied such that S(T) =1
$\boldsymbol{u}$	Vector of nodal displacements
$\bar{u}_p$	Equivalent plastic displacement
$\bar{u}_{pf}$	Equivalent plastic displacement at fracture
Ux_i	Translation in the *x* direction of corner *i*
Ux_{i-j}	Translation in the *x* direction of edge connecting corners *i* and *j*
Uy_i	Translation in the *y* direction of corner *i*
Uz_i	Translation in the *z* direction of corner *i*
V_0	Initial speed of the dynamic load
w	Vertical displacement
$\boldsymbol{\alpha}$	Backstress tensor
α	Parameter of Hilber-Hughes-Taylor implicit time integration scheme
β	Parameter of Hilber-Hughes-Taylor implicit time integration scheme
γ	Parameter of Hilber-Hughes-Taylor implicit time integration scheme
γ_L	PSF accounting for the uncertainty in the calculated load limit
γ_P	PSF accounting for the uncertainty in the calculated load
δ	Average displacement of the structural element
$\delta_{y,flange}$	Transverse displacements of the stiffener flange nodes
$\delta_{y,web}$	Transverse displacements of the stiffener web nodes
$\delta_{z,flange}$	Vertical displacements of the stiffener flange nodes
$\delta_{z,panel}$	Vertical displacement of the stiffened panel nodes
$\delta_{z,plate}$	Vertical displacement of the stiffened panel plate nodes
$\delta_{z,web}$	Vertical displacements of the stiffener web nodes
Δ	Displacement
ΔP	Load increment
ε	True strain
$\dot{\varepsilon}$	Strain rate
ε_{cf}	Critical fracture strain

ε_{el}	Elastic portion of the true strain
ε_{eng}	Engineering strain
ε_{ij}^{p}	Components of the plastic strain rate tensor
ε_{p}	True plastic strain
$\bar{\varepsilon}_{p}$	Equivalent plastic strain
$\varepsilon_{sh,\,eng}$	Engineering strain at the start of the strain hardening region
$\varepsilon_{u,\,eng}$	Engineering strain at the point where ultimate engineering stress is reached
$\varepsilon_{y,\,eng}$	Engineering strain at the onset of yielding
v	Poisson ratio
ρ	Density
σ	True stress
$\sigma_1, \sigma_2, \sigma_3$	Principal stresses in the three orthogonal directions
σ_Y	Yield stress
$\sigma_{Y,\,eng}$	Engineering yield stress
$\sigma_{U,\,eng}$	Engineering ultimate stress
$\sigma(\varepsilon)$	Static true flow curve
$\sigma(\varepsilon)_{dyn}$	Dynamic true flow curve
φ	Rotation angle

SECTION 2
Sources of Structural Nonlinearity

1 General

There are three main sources of nonlinearity in solid mechanics:

1) Geometric nonlinearity

2) Material nonlinearity

3) Boundary condition nonlinearity

Since the solution methods of the NLFEA should be adjusted according to the type of nonlinearity, all three sources of nonlinearity are described separately in the next Subsections.

2 Geometric Nonlinearity

Geometric nonlinearity occurs in structures such as beams and shells that exhibit large displacements and rotations such that the applied loads and/or the stiffness of the structure become dependent on the structure's instantaneous geometry. A few classical examples of geometric nonlinearity are given in the following Paragraphs, and more details can be found in [4].

2.1 Bifurcation Buckling (Instability)

A simple example features an idealized rigid beam supported by an elastic rotational spring and loaded with an axial compression force, F, without any eccentricities, as shown in Section 2, Figure 1. After the force reaches a critical value that depends on the length of the beam and the stiffness of the rotational spring, the solution of the nonlinear problem starts to bifurcate (branch). This critical point is called the bifurcation point, after which three different solutions are possible: an unstable trivial solution in which there is no rotation of the beam, and two stable symmetric solutions with either positive or negative rotation of the beam, , as shown in Section 2, Figure 1. Initial eccentricities in the geometry or the load, that are common in structures, will determine which of the two stable solutions is followed as the compressive force is increased.

2.2 Large Displacements

Another example of geometric nonlinearity is shown in Section 2, Figure 2, where a system of two connected elastic rods is subjected to large displacements by a force, F, acting at their connection point. As the rods are stretched, the axial forces in the rods grow and progressively resist the applied vertical force as the angle of the rods with respect to the horizontal increases. Therefore, the force needed for an incremental increase in the vertical displacement, w, grows with the vertical displacement, as shown with the force-displacement curve in Section 2, Figure 2.

2.3 Snap-Through Problem

The *snap-through* problem occurs when a structure suddenly assumes another configuration under the action of an external load. An example of such nonlinear behavior is shown in Section 2, Figure 3. This example is very similar to the example in 2/2.2, but in this case, the elastic rods form an isosceles triangle with the horizontal in their initial unloaded configuration. The force displacement curve for this problem is also shown in Section 2, Figure 3. As the force, F, reaches a critical value at point A, an instability occurs, and the structure instantaneously snaps through from one equilibrium state at point A to another equilibrium state at point B.

FIGURE 1
Load-Displacement Curves for Bifurcation Buckling of a Rigid Beam

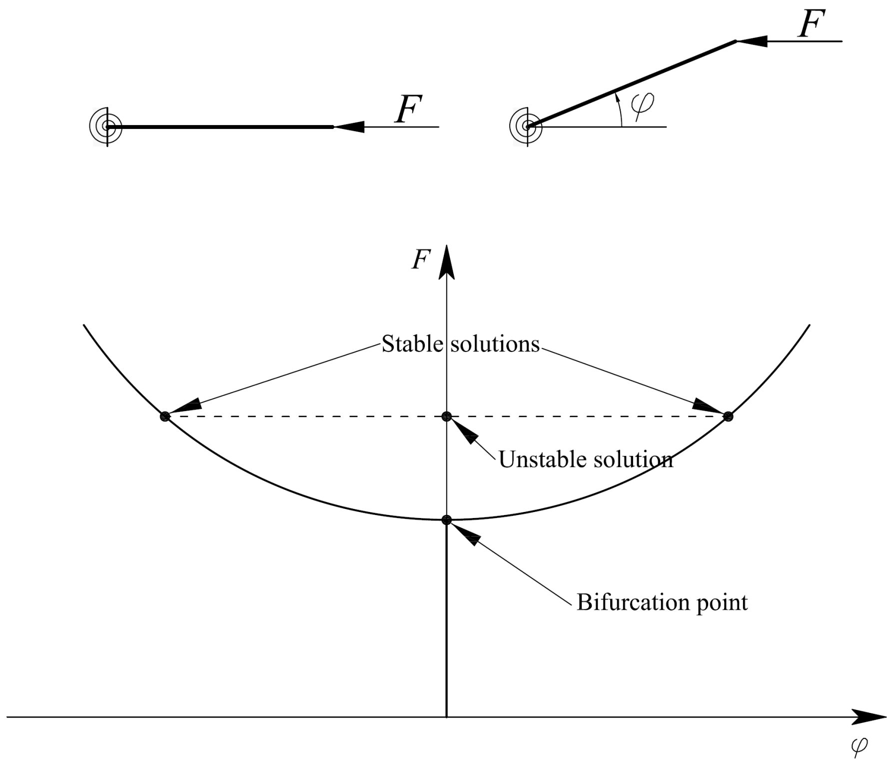

FIGURE 2
Load-Displacement Curves for Large Deflection of an Elastic System

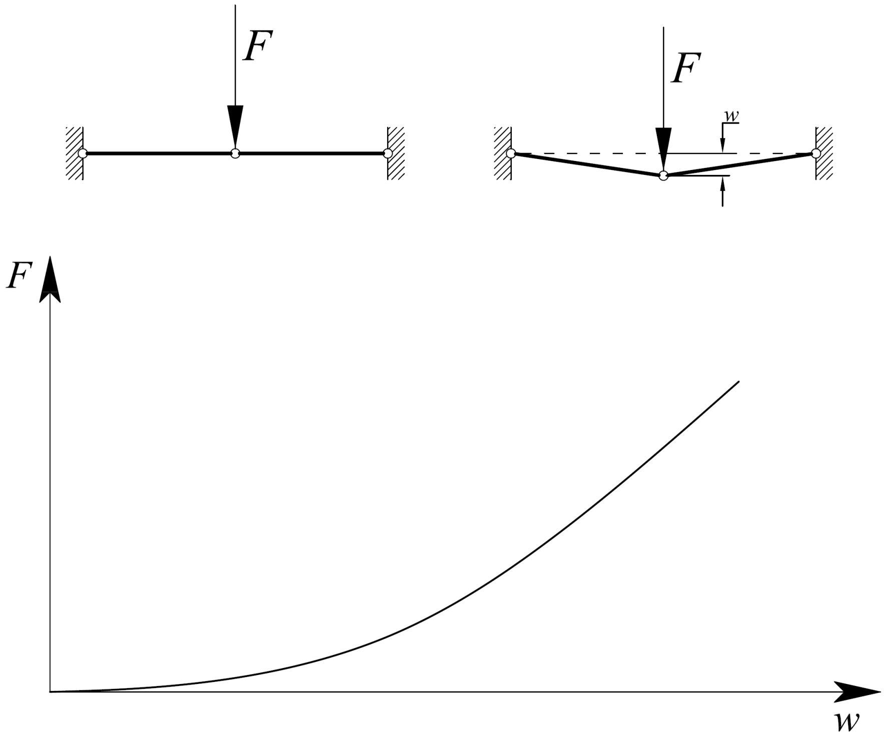

FIGURE 3
Load-Displacement Curves for Snap-Through of an Elastic System

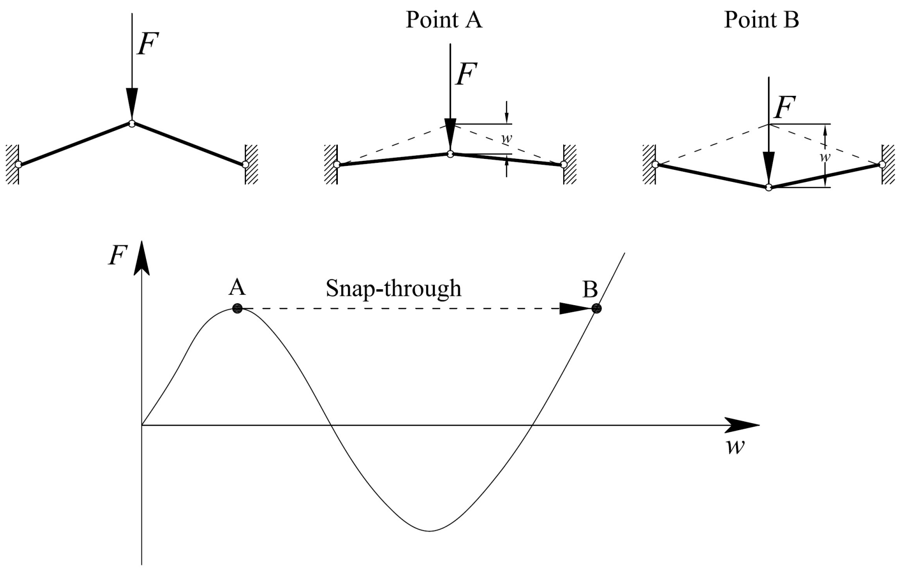

3 Material Nonlinearity

Geometric nonlinearities occur when the structure's displacements are large. If the strains are large as well, then *material nonlinearity* may also affect the structure's behavior. Many materials, including steel, exhibit nonlinear behavior which is characterized by a nonlinear uniaxial stress-strain function. Section 2, Figure 4 shows an idealized elastic-perfectly plastic material behavior where the initial slope of the elastic region sharply decreases to zero allowing the material to strain indefinitely with no further increase in stress. Most real materials exhibit some strain hardening until the ultimate stress of the material is reached.

Similar to geometric nonlinearity, which can be the cause of structures' instability (bifurcation buckling, snap-through, snap-back), material nonlinearity can also cause instability in the form of necking, plastic hinges, or shear bands.

FIGURE 4
Material Nonlinearity – Elastic-Perfectly Plastic Material

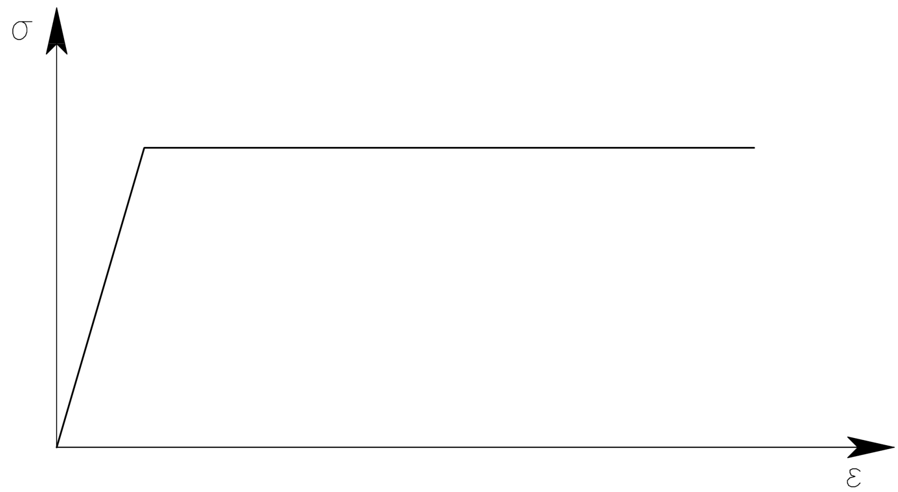

4 Boundary Condition Nonlinearity

Boundary conditions may be the sources of nonlinearity in cases where, for example, two bodies come into contact with one another or in cases where the loads or load paths depend on the deformation of the structure. The *follower loads* that follow the nodal translation and rotation of the structure fall into the latter category. An example of these follower loads is a liquid pressure that always acts normal to the deformed surface.

SECTION 3

Main Aspects of NLFEA

1 General

This Section addresses the following main aspects of the NLFEA:

- Incremental-iterative solution process
- Iteration algorithms
- Numerical stabilization
- Analysis type
- Model extent
- Loading approach
- Boundary conditions
- Material model
- Geometric imperfections
- Ductile fracture modeling
- Contact modeling
- Mesh quality and size
- Element choice

The following Subsections discuss each of these aspects and provide general guidance and recommendations.

2 Incremental-Iterative Solution Process

In a linear analysis, the solution is calculated directly in one step by solving a system of linear equations. However, in order to trace the solution path in a nonlinear analysis, the load (or prescribed displacement) should be divided into a series of smaller *increments*. For each load increment equilibrium, a solution is found by performing several *iterations,* each of which is computationally comparable to a solution of a linear system. Therefore, nonlinear analysis may be computationally much more demanding compared to the linear analysis. Section 3, Figure 1 shows the basic incremental-iterative approach to solving nonlinear problems with two load increments ($\Delta P1$ and $\Delta P2$) and three iterations within each of the two load increments.

In most commercial NLFEA programs, the load is prescribed as a function of time. In a static analysis, the time is usually specified from zero to one, and it does not have a physical meaning. It only tells the program how to increment the load from its initial value at time equal to zero to its final value at time equal to one. In this case, each load increment is specified as a fraction of total time over which the load is prescribed.

Load incrementation in many commercial NLFEA programs is controlled automatically by the software in order to reduce the computation time, although manual control is also available. For most nonlinear problems, automatic increment control is sufficient and recommended. The user should only specify the size of the first load increment. A reasonable value of the initial load increment should be provided. A value that is too large or too small will require significant subsequent reductions or growth of the load increment resulting in wasted computing effort. Prior knowledge or experience related to similar problems can aid in selecting a reasonable initial increment. Otherwise a value of 10% of the maximum load may be used. The manual increment control should only be used in rare circumstances when convergence cannot be achieved by any other means. Also, iteration algorithms have a finite radius of convergence, which means that a load increment that is too large may prevent the nonlinear solver from converging to a solution.

FIGURE 1
Incremental-Iterative Solution Process

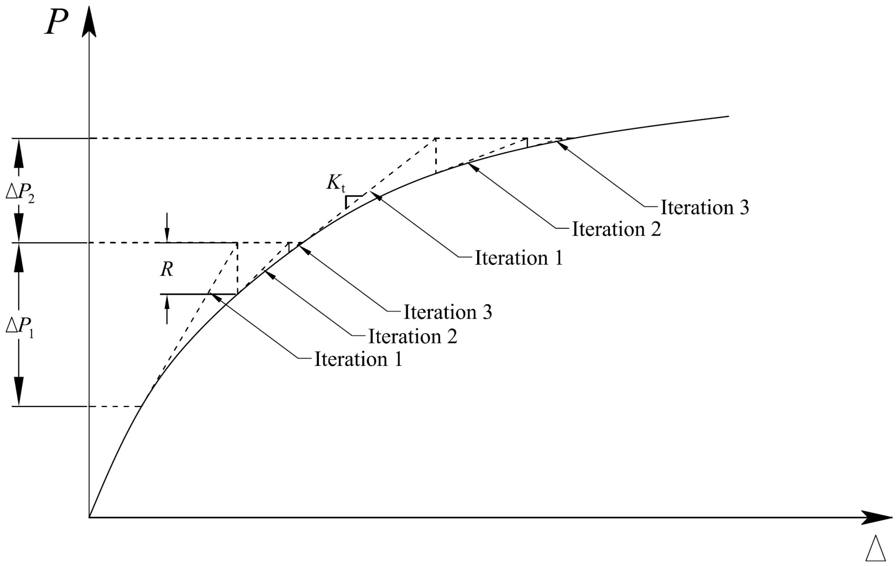

At each load increment, the nonlinear solver begins the iterative process to find the equilibrium solution and stops when convergence is achieved as judged by the tolerances specified in the solver. The solution at each load increment is said to be converged when certain residuals are below the specified tolerances. Usually, the iterative solver monitors the difference between the external and internal loads, called the residual load, *R* (see Section 3, Figure 1), and stops when *R* falls below a small tolerance value that is set as a solver default or edited by the user. There may be other convergence checks specific to each implementation of the iterative solver. It is not recommended to change the default tolerance values for the convergence checks unless the analyst has an in-depth knowledge of the nonlinear solver and how the changes may affect the solution accuracy. Any such changes should be well documented and supported.

3 Iteration Algorithms

When the stiffness matrix is dependent on either the displacement vector or the load vector, or both, the problem is nonlinear and will require an iterative algorithm to solve it. The three main iteration algorithms are:

1) Newton-Raphson (N-R) Algorithm for static or dynamic implicit analysis

2) Modified N-R (Quasi N-R) Algorithm for static or dynamic implicit analysis

3) Arc Length (Riks) for static analysis only

3.1 Newton-Raphson Algorithms

The N-R algorithm [2] updates the tangent stiffness, K_t (see Section 3, Figure 1) at each iteration in order to find progressively better estimates of the equilibrium solution with progressively smaller residual loads R.

The modified N-R algorithm is similar to the N-R algorithm but uses a constant tangent stiffness for all the iterations within a particular load increment. Not having to calculate K_t at each iteration considerably reduces the computational effort. However, the modified N-R method usually requires more iterations to achieve comparable accuracy as the N-R method, thus offsetting the efficiency gain.

3.2 Arc Length (Riks) Algorithm

The Arc Length algorithm [5], also known as the Riks algorithm [6] controls both the load incrementation process and the iteration process used to eliminate the unbalanced loads. This method considers the load increment, ΔP, as an additional unknown and solves simultaneously for loads and displacements. The progress of the solution is measured by the "arc length" along the static load-displacement curve. Since the load is a part of the solution and not prescribed using a certain function, it is possible to analyze global post-ultimate strength or post-buckling behavior. In order to use the Arc Length method, all loads acting on the structure need to be proportional, meaning they can all be scaled with a single parameter.

The Arc-Length algorithm is not well suited for analyzing bifurcation buckling problems. Usually, when using the Arc-Length algorithm, initial imperfections should be applied to the structure (see 3/10). In that case, there will be a continuous response by the structure before the critical buckling load is reached, and bifurcation buckling will be avoided.

3.3 Choice of the Iteration Algorithm

The choice of the iteration algorithm will depend upon the analysis type (see 3/5), load control approach (see 3/7), and the expected load-displacement behavior of the structure. Section 3, Figure 2 shows a very general load-displacement curve of a highly nonlinear structure experiencing snap-through (see 2/2.3) and snap-back behavior. As opposed to snap-through behavior that occurs when the load is gradually incremented (load control approach), snap-back behavior occurs when the displacement is gradually incremented (displacement control approach). At point C, called the turning point, the structure may snap back to point D as illustrated in Section 3, Figure 2.

FIGURE 2
General Load-Displacement Curve

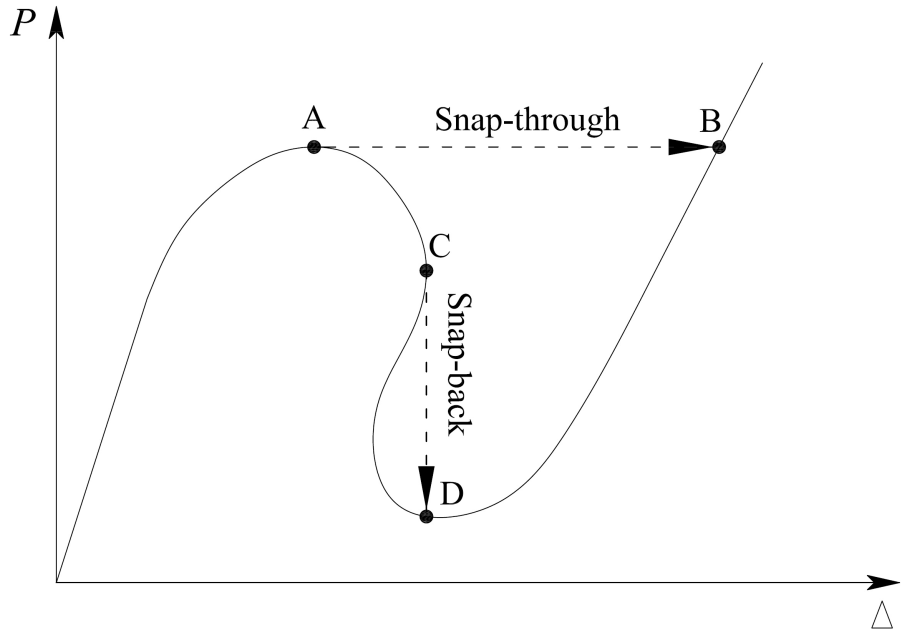

When static analysis with load control is used, N-R algorithms cannot, in general, find the equilibrium solutions past the first maxima (limit point) in the load-displacement curve (point A in Section 3, Figure 2). This is because the algorithm relies on a positive tangent stiffness (or positive definite tangent stiffness matrix in strict mathematical terms). At point A, the tangent stiffness becomes negative, and the structure starts to release the energy to stay in equilibrium. The analysis may pick up at another point with positive tangent stiffness on the load-displacement curve (point B in Section 3, Figure 2), but the section of the load-displacement curve between points A and B cannot be traced, in general.

It is possible to continue tracing the load-displacement curve past the point A if static analysis with displacement control is used in combination with the N-R algorithms. However, such analysis will stop at point C where the snap-back instability occurs. The displacement-controlled analysis may pick up at point D, but the section of the load-displacement curve between points C and D cannot be traced, in general.

Implicit dynamic analysis (see 3/5.2.1) also uses the N-R algorithms. However, it should be realized that an accelerated response of the structure initiates at point A under the load control or point C under the displacement control. Even if the structure is heavily dampened and stabilized, as in the quasi-static analysis (see 3/5.3), the inertial effects may prevent the establishment of a quasi-static equilibrium once the accelerated response has initiated.

The Arc Length method is recommended for static analysis of highly nonlinear unstable problems including the snap-through and snap-back problems. Because the loads and displacements are solved simultaneously, this method enables achieving the equilibrium solutions along the entire load-displacement curve (points A-C-D-B in Section 3, Figure 2) , which makes it the only method that can trace the static equilibrium solutions between points C and D. Since the Arc Length method controls the loads on the entire structure using a single global parameter, it may not be well suited for analyzing cases with local instabilities such as local buckling or necking in a complex structure like a vessel's hull girder. Also, the Arc Length method cannot be used in full dynamic or quasi-static analyses.

4 Numerical Stabilization

NLFEA can become numerically unstable due to sudden local or global geometric instabilities (bifurcation buckling, snap-through, snap-back) and/or material instabilities (necking, shear band). The instability comes from the fact that the displacements or strains at the onset of instability become very large, even though the load increment is kept relatively small. Global instabilities can frequently be assessed using the Arc-Length method (see 3/3.2 and 3/3.3). However, the Arc-Length method may not work if the instabilities are local such that a part of the structure releases the strain energy while the neighboring parts of the structure accumulate it. Such local instabilities often arise in the limit state analysis of complex structures (e.g., ultimate strength analysis of a hull girder) and must be treated either dynamically (see 3/5.2 and 3/5.3) or/and numerically stabilized using artificial damping.

Numerical stabilization is based on the introduction of artificial damping elements at the nodes where the ratio of displacement increments to load increments is very high. Numerical stabilization can be used in both static and dynamic analyses. In a static analysis, damping is proportional to the ratio of the nodal displacement increment and the load increment, where the load increment is expressed as a fraction of total time. In a dynamic analysis, artificial damping has a physical meaning and is proportional to the nodal velocity.

The amount of damping needed to stabilize a certain problem is not known in advance. The proper amount of damping will depend on the type of system being analyzed, the analysis type, the mesh size, and the extent of the model. Experience with a similar type of problem and some trial-and-error simulations can help determine the right amount of damping. Too much damping can lead to unrealistically stiff structures and will affect the final static or dynamic equilibrium. Too little damping will not be able to stabilize the problem.

It is important to verify that, after the problem has been stabilized and the convergence has been achieved, the accumulated stabilization energy is less than 5% of the model's total strain energy (internal energy) at each increment of the analysis. The accumulated stabilization energy is readily available as an output in most commercial NLFEA programs.

Most commercial NLFEA programs offer automatic numerical stabilization of unstable problems. This is the preferred method of stabilization since the program automatically applies artificial damping only to the nodes with high local velocity, while keeping the accumulated stabilization energy below a user-specified small fraction (5% is recommended) of the model's total strain energy at each increment of the analysis.

5 Analysis Type

The following main analysis types of NLFEA are briefly described in this Subsection:

1) Static analysis

2) Dynamic analysis

3) Quasi-static analysis

5.1 Static Analysis

During a static analysis, loads or displacements are applied incrementally. At each load increment, static equilibrium (Eq. 1.1) is found using an iterative numerical algorithm (e.g., N-R or Arc Length), as described in 3/3.1 and 3/3.2. Inertial effects are not accounted for, as well as time-dependent material effects such as creep. However, strain rate effects on material plasticity can be taken into account. When the N-R iteration algorithm is used and local instabilities (local buckling, material necking, etc.) are expected to occur, numerical stabilization techniques should be applied as in 3/4.

5.2 Dynamic Analysis

Nonlinear dynamic analysis uses either implicit (Backward Euler or Hilber-Hughes-Taylor) or explicit (Central Difference) direct time integration schemes to propagate the solution across all time increments. Both integration methods solve the dynamic system of equations:

$$\boldsymbol{f} = \boldsymbol{M}\ddot{\boldsymbol{u}} + \boldsymbol{C}\dot{\boldsymbol{u}} + \boldsymbol{K}\boldsymbol{u} \quad (3.1)$$

where

$\boldsymbol{M}$	=	mass matrix
$\boldsymbol{C}$	=	damping matrix
$\boldsymbol{u}$	=	vector of time dependent nodal displacements
$\boldsymbol{f}$	=	vector of time dependent external nodal loads

5.2.1 Implicit Dynamic Analysis

When *implicit time integration* is used, the displacements and velocities at the current time step are nonlinear functions of the displacements and velocities at the current and previous time steps, thus requiring an iterative solution using the N-R algorithms at each time increment of the analysis.

The most commonly used implicit time integration scheme is the Hilber-Hughes-Taylor (HHT) [7], which is an extension of the Newmark β-method. Another commonly used scheme is the Backward Euler. All numerical integration schemes introduce some level of artificial (non-physical) numerical damping. The Backward Euler scheme introduces more numerical damping compared to the HHT scheme and is usually used when quasi-static analysis (see 3/5.3) is performed.

The HHT time integration scheme is controlled by three parameters: α, β, and γ. Parameter α varies in the range $-\frac{1}{2} \leq \alpha \leq 0$ and controls the amount of numerical damping. It is highly recommended to set the other two parameters as follows:

$$\beta = \frac{1}{4}(1-\alpha)^2 > 0 \text{ and } \gamma = \frac{1}{2} - \alpha \geq \frac{1}{2} \quad \text{(3.2)}$$

This preserves the unconditional stability of the HHT integration scheme for linear problems or linear portions of nonlinear problems, which means that the time increment in a linear implicit dynamic analysis can be arbitrarily large, and that the converged solution at a given time instant can be obtained in only one time increment. The same stability characteristics cannot be guaranteed in a nonlinear analysis, but the unconditionally stable HHT scheme in a linear analysis will also have desirable characteristics in a nonlinear analysis. Section 3, Table 1 shows the recommended time integration schemes and parameter values for various types of implicit dynamic analyses.

HHT with α= 0 is also called the Trapezoidal Rule and has no numerical damping. However, some numerical damping is always desirable to improve the convergence behavior and reduce the high-frequency solution noise.

Automatic time incrementation is recommended, which allows the implicit solver to minimize the computation time while achieving convergence at each time increment.

For transient analyses involving high-frequency vibrations (e.g., whipping of the hull girder caused by slamming), it is recommended to limit the maximum time increment to 1/100 of the total simulated time span or 1/10 of the smallest natural vibration period of interest, whichever is smaller.

TABLE 1
Recommended Unconditionally Stable Time Integration Schemes

Time Integration Scheme	*Parameters*			*Damping*	*Typical Applications*
	α	β	γ		
Backward Euler	NA			Significant	Quasi-static analysis
HHT	0	0.25	0.5	Zero	Transient analysis involving very high-frequency vibrations
	–0.05	0.27563	0.55	Very small	Transient analysis involving high-frequency vibrations
	–0.41421	0.5	0.91421	Medium	Collision analysis
	$-1/3$	$4/9$	$5/6$	Maximum (for HHT)	Quasi-static analysis

For dynamic analyses involving moderate energy dissipation mechanisms where high-frequency vibration modes are not of interest (e.g., collision analysis), the maximum time increment should be limited to $1/10$ of the total simulated time span.

For quasi-static analysis (see 3/5.3), there is no need to use the upper bound for the time increment. The automatic time incrementation will use large time increments when possible to achieve maximum computation efficiency.

5.2.2 Explicit Dynamic Analysis

When *explicit time integration* is used, the displacements and velocities at the current time step are nonlinear functions of the displacements and velocities at the previous time steps only and can be calculated explicitly without the iterative solution process. This means that each time increment of the explicit method is computationally much more efficient compared to the implicit method. However, the Central Difference integration scheme is conditionally stable, unlike the unconditionally stable implicit time integration schemes (see 3/5.2.1). The size of the *critical time increment* (allowable time increment) in the explicit analysis is approximately equal to the time it takes a stress wave (dilatational wave) to propagate across the smallest finite element dimension. Section 3, Table 2 shows the critical time increment for explicit dynamic analysis for rod, shell, and solid finite elements.

TABLE 2
Critical Time Increments in Explicit Analysis

Finite Element	*Critical Time Increment Δt_c*
Rod	$\Delta t_c = \frac{L}{c} = L\sqrt{\frac{\rho}{E}}$
Shell	$\Delta t_c = \frac{L}{c} = L\sqrt{\frac{(1-\nu^2)\rho}{E}}$
Solid	$\Delta t_c = \frac{L}{c} = L\sqrt{\frac{(1+\nu)(1-2\nu)\rho}{E(1-\nu)}}$

where

L = smallest finite element dimension in the mesh

c = dilatational wave speed

v = Poisson ratio

E = modulus of elasticity

ρ = density

The critical time increment for beam elements is computed in a similar way. However, L is equal to the length of the beam only for the axial deformation mode and is computed differently for bending, shear, and torsion deformation modes. In practice, the critical time increment of the beam element can be smaller compared to other element types of similar size present in the mesh. For that reason, attention should be paid when using beam elements in the explicit dynamic analysis of marine and offshore structures.

The critical time increment of the explicit analysis, even without the beam elements, is likely to be much smaller compared to the time increment of the implicit analysis. Therefore, the time saved on avoiding iterations can be offset by the large number of required time increments.

In order to reduce the computation time, it is necessary to increase the critical time increment (see Section 3, Table 2) or to reduce the total simulated time. This can be done using four different techniques:

1) Increasing the size L of the smallest element in the mesh by a factor f increases the time increment and decreases the computation time by the same factor. The effect can be even larger if by increasing L, the number of nodes in the model reduces significantly. Increasing L may decrease the accuracy of the finite element solution.

2) Artificially increasing the material density, ρ, by a factor f^2 will reduce the required number of time increments (and the total simulation time) by a factor f. This is called *mass scaling*. Increasing the mass density will increase the inertial forces and may significantly affect the solution. Therefore, the mass scaling factor f should be chosen carefully. Inertial forces should be monitored during the solution to make sure they do not become dominant. For quasi-static problems, kinetic energy of the system should be monitored to make sure it does not become larger than 5% of the internal strain energy, except at the beginning of the analysis where this ratio may exceed 5% due to very small strain energy. In order to minimize the inertial effects, mass scaling can be applied selectively to only the elements whose critical time increment is below a specified value. This can be accomplished in most commercial NLFEA programs.

3) Artificially speeding up the simulation by increasing the load application rates by a factor f will reduce the computation time by the same factor. This has the same effect on the simulation results as mass scaling and the same precautions should be made in terms of monitoring the inertial forces. In addition to this, speeding up the simulation should not be done if time/rate dependent material behavior is specified in the analysis.

4) In cases where there is a relatively small number of very small elements governing the critical time increment and where all the other elements in the model are significantly larger, the total computation time can be considerably reduced if the two groups of elements are integrated separately using different critical time increments. In that case, the bigger group of larger elements is integrated using a correspondingly larger time increment which can significantly speed-up the simulation. This technique is called *selective subcycling*.

Due to the large number of time increments needed in the explicit dynamic analysis, the small numerical roundoff errors in each time increment can quickly accumulate into a significant error.

Therefore, it is strongly suggested to use double precision float numbers when running an explicit analysis.

5.2.3 Implicit vs. Explicit Dynamic Analysis

Both implicit and explicit time integration schemes can be used for a wide range of dynamic problems. In many cases, the choice will not be obvious and will depend on the specifics of the analyzed system. The following paragraphs present some general guidance.

The computation cost of the explicit analysis depends linearly on the number of elements in the model. The computation cost of the implicit analysis rises more rapidly with the number of elements in the model. Therefore, explicit analysis will be computationally very effective for large problems, (e.g., ultimate strength analysis of a 2-hold hull girder model or collision analysis of two vessels).

The explicit method is usually more efficient than the implicit method for solving highly dynamic and discontinuous events over a short period of time (e.g., impact and explosions).

The explicit method can usually achieve convergence in cases where the implicit method fails, since it does not require iteration.

Although both time integration schemes can be used to solve quasi-static problems (see 3/5.3), a slight preference should be given to the implicit scheme, since it provides more options for damping the solution and minimizing inertial effects. For example, the inertial effects can be minimized by reducing the material density, which is called *reversed mass scaling*. This will not impact the solution time of the implicit scheme, but it will have a detrimental effect on the critical time increment of the explicit scheme (see 3/5.2.2). Likewise, increasing the load application time may not have a big impact on the computational time when implicit analysis is used due to the fact that larger time increments may be used, but it will proportionally increase the computation time of the explicit analysis where the critical time increment remains unchanged.

5.3 Quasi-Static Analysis

Quasi-static analysis is a dynamic analysis whose purpose is to estimate the static response of the structure by minimizing the inertial effects, which are only introduced to mitigate the unstable behavior of the structure. It is mainly used when static analysis fails to converge. Examples may include the ultimate and post-ultimate strength analysis of a hull girder or a collapse analysis of a stiffened panel or a web frame. The maxima (limit point) in the load-displacement curve (point A in Section 3, Figure 2) can be passed using either load control or displacement control approaches. However, when the structure reaches its ultimate capacity at point A, any further incremental increase in the external load, which can no longer be sustained by the structure, will initiate the accelerated response of the structure. At this point, it becomes increasingly more difficult to dampen and stabilize the structure, and its kinetic energy may quickly grow to over 5% of the internal strain energy of the system. At that point, the solution can no longer be considered as quasi-static.

There are three ways to minimize the inertia effects and to achieve a quasi-static equilibrium using dynamic analysis:

1) Loads are applied over a long time period, which increases the number of time increments when explicit analysis is used.

2) Density of the structural material is deliberately lowered by an order of magnitude (reversed mass scaling). This will have a negative effect on the critical time increment for explicit analysis but will not affect the implicit analysis.

3) Numerical and/or structural and material damping is used, which also stabilizes the system and improves convergence.

In addition to the above-mentioned ways of minimizing the inertia effects, another useful approach to minimize the inertia effects (especially at the beginning of the analysis when the internal strains in the structure are small) is to use a *smooth step* function to apply the loads or displacements. The smooth step function gradually increases the load application rate from zero to a maximum value and then gradually decreases the load application rate to zero towards the end of the analysis, as can be seen in Section 3, Figure 3.

The mathematical expression for the smooth step function is as follows:

$$S(t) = \left(\frac{t}{T}\right)^2\left(3 - 2\frac{t}{T}\right)^2 \quad \ldots \quad (3.3)$$

where

t	=	time
T	=	time period over which the full load is applied such that $S(T) = 1$

FIGURE 3
Smooth Step Function

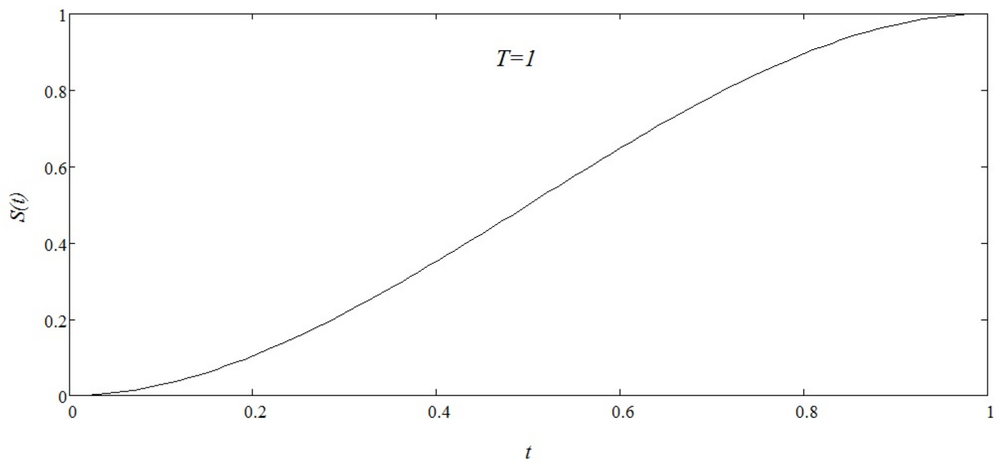

The smooth step function can also be useful in dynamic analysis, where it is necessary to gradually ramp up the dynamic cyclic loads to their full amplitudes in order to avoid excessive noise in the results at the beginning of the simulation.

Both time integration schemes can be used to obtain a stable quasi–static solution in cases where static analysis fails. However, a quasi-static solution should be verified by comparing the kinetic and internal energies of the system throughout the solution sequence. Kinetic energy should always be below 5% of the internal strain energy of the system, except at the beginning of the analysis where this ratio may exceed 5% due to very small strain energy. In addition to checking the ratio of kinetic and internal strain energies of the system, a quasi-static solution should be further verified by checking if the slope of the linear portion of the load-displacement curve is the same as the corresponding slope from a purely linear static analysis.

6 Model Extent

Excessive computation cost may prohibit the consideration of the entire structure when performing NLFEA. When only a part of the structure is modeled, the loads and supports at its boundaries should be carefully considered.

The boundaries of the model should be located sufficiently away from the locations of interest so that the accuracy of the NLFEA results is not adversely affected by the boundary conditions. Sometimes a sensitivity study of the effects of the boundary proximity will be necessary in order to reliably define the model extent.

Symmetry of the structure and/or loads may be considered in order to reduce the model extent.

Section 3, Table 3 contains general recommendations for the model extent in some typical marine and offshore structure analysis situations.

7 Loading Approach

As mentioned in 3/2, the loading on the FE model should be applied incrementally during the NLFEA. While in the linear structural analysis the load application sequence is irrelevant, this is not the case with NLFEA. In NLFEA, different load components cannot be analyzed separately and then scaled and superimposed to get the final response of the structure. The response of the structure, its ultimate strength, and collapse sequence will depend on the load path/sequence of application chosen for the analysis.

It is recommended to apply the loads on the structure following a sequence in which they appear on the actual structure. For marine and offshore structures, this means incrementally applying the hydrostatic and gravity loads first. After that, the dynamic loads coming from waves, currents, and wind should be incrementally applied. In the case of stiffened panel loads, the hydrostatic pressure should be applied first followed by biaxial and shear stresses arising from the static hull girder sectional forces. The biaxial and shear stresses arising from the dynamic hull girder sectional forces should be applied last until their target is reached, or the structure collapses, whichever comes first.

The pressure causes tensile stresses in the panel plate and may significantly change its initial deflection. In some cases, the pressure generated panel deflection may be in the opposite direction to the deflections of the fundamental buckling mode of the panel, thereby increasing the panel ultimate strength under in-plane compression. For stiffened panels with variable amount of pressure (e.g., due to changing draft of the vessel), the ultimate strength of the panel should be checked for all possible combinations of pressure and in-plane loads, and the most conservative result should be taken as the final ultimate strength of the panel.

TABLE 3
Model Extent Recommendations

Type of Analysis	*Load Type*	*Longitudinal Extent*	*Transverse Extent*	*Vertical Extent*
Buckling of stiffener with attached plating[(1)]	Uniaxial compression and pressure	½ + 1 + ½ bays[(2)]	½ of stiffener spacing on either side of the stiffener	Stiffener and the attached plate
Stiffened panel structural collapse[(1)]	Uniaxial compression	½ + 1 + ½ bays[(2)]	Between strong longitudinal supports	Stiffeners and the attached plate
	Biaxial compression, shear, and pressure	½ + 2 + ½ bays[(2)]	Between strong longitudinal supports	Stiffeners and the attached plate
Hull girder ultimate strength analysis (intact hull)	Vertical bending moment	1 bay[(2)]	Breadth of the vessel	Depth of the vessel
	Vertical and horizontal bending and pressure	½ + 1 + ½ holds	Breadth of the vessel	Depth of the vessel

Type of Analysis	*Load Type*	*Longitudinal Extent*	*Transverse Extent*	*Vertical Extent*
Hull girder residual strength analysis (damaged hull)	Vertical bending moment	The extent of damage, but no less than ½ + 1 + ½ holds	Breadth of the vessel	Depth of the vessel
	Vertical and horizontal bending and pressure	The extent of damage, but no less than ½ + 1 + ½ holds	Breadth of the vessel	Depth of the vessel
Impact with ice	Line loads and patch load (ABS *Guidance Notes on Ice Class*)	Sufficiently beyond the length of the applied ice patch load(3)	From side shell to centerline	Between deck above structural region of interest and turn of bilge
Ship-to-ship collision	Impact with bulbous bow of striking ship	1 hold	From side shell to centerline	Depth of the vessel

Notes:

1 For stiffeners and stiffened panels, the longitudinal direction coincides with the direction of the stiffeners, and the vertical direction is perpendicular to the plating.

2 Bay is the area between adjacent transverse frames.

3 For ice class vessels, the model longitudinal extent needs to be sufficient such that the boundary conditions do not significantly influence the results of the NLFEA.

Some structures may undergo large deflections. As a result, the load direction and/or magnitude may change. This should be carefully considered during the analysis.

When performing NLFEA, there are two main types of incremental loading approach:

- Displacement control
- Load control

7.1 Displacement Control

This loading approach consists of incrementing the displacements of the structure's boundary. In case of the hull girder under bending moments, rigid body rotation of the model end cross sections (curvature) is incremented.

Displacement control is primarily used because it is easy to trace the behavior of the structure in the post-collapse region beyond the limit point (point A in Section 3, Figure 2). However, it requires special post processing of the stress results in order to find the forces and moments at various cross sections of interest inside the structure. Another issue of pre-imposing a curvature on the FE model is that the real-world behavior of marine and offshore structures is not controlled by displacements, but by loads (forces and moments), and the input of the displacement may not accurately represent the failure process as described in [8].

Care should be taken when displacement control is applied to asymmetric structures (e.g., asymmetrically damaged hull girder). In this case, incrementing the rotation of the end cross sections around the horizontal axis will result in the development of the horizontal bending moment in addition to the intended vertical bending moment, if the neutral axis of the model is not allowed to rotate. However, if boundary conditions applied at the ends of a sufficiently long FE model of the hull (e.g., ½ + 1 + ½ holds – see Section 3, Table 3) prevent the development of internal axial forces, then the neutral axis of the hull away from the ends will be allowed to shift and rotate.

7.2 Load Control

This loading approach consists of incrementing the loads (force, moment, pressure). The major drawback of this approach is that it is not possible, in general, to obtain the negative slope portion of the load-displacement curve when using the N-R iteration algorithm in a static analysis. This creates uncertainty on the calculated ultimate strength value (i.e., the confidence that the ultimate capacity of a structure has been reached without being able to identify the highest peak in the load-displacement curve). This is especially important if the load-displacement curve of the structure has more than one peak. The loss of convergence during static analysis will, of course, occur just as the first peak is being reached. Therefore, unless the first peak is also the highest, it will usually be impossible to find the ultimate strength of the structure using load control during a static analysis with N-R algorithms.

The Arc-Length algorithm (see 3/3.2) can trace the static solution into the post ultimate strength region. In practice, however, for complex marine and offshore structures, the Arc-Length algorithm may fail to converge as soon as local instabilities start to occur. If the static analysis using Arc-Length algorithm fails to converge beyond the first peak of the load-displacement curve, then the quasi-static analysis (see 3/5.3) may offer a solution. However, it may be quite difficult to control the kinetic energy of the system beyond the first peak of the load-displacement curve, as mentioned in 3/5.3.

8 Boundary Conditions

Every NLFEA will require some level of assumptions regarding the boundary conditions. The importance of realistically representing the boundary conditions in the finite element model is even more important for nonlinear analyses than for linear analyses. When assumptions regarding the boundary conditions need to be made, they should be made in such a way as to lead to a conservative response of the structure.

Using assumptions that are valid for small displacement linear analysis for NLFEA should be done cautiously. For example, the assumption that the hull girder cross sections remain plane is valid inside the simple beam theory but ceases to hold when shear and torsion effects are included as part of the Timoshenko beam theory. However, this assumption is considered adequate in many linear analyses, especially for vessels with closed cross-sections. In a nonlinear analysis, it becomes less accurate, especially as certain parts of the structure begin to yield or buckle. The assumption can still be made in NLFEA, but only when the locations of interest are sufficiently away from the end cross sections.

The examples of typical boundary conditions for the analysis of stiffened panels, hull girders, and container stacks are given in Appendix 1. Boundary conditions for the analysis of side structure of a vessel subject to ice loads are given in the ABS *Guidance Notes on Ice Class*.

9 Material Model

Mild and high tensile strength steels used for building marine and offshore structures are elasto-plastic materials. They are characterized by an elastic region up to the yield point and an elasto-plastic region consisting of a yield plateau and a strain hardening region where the material yield point increases when the structure is unloaded and subsequently reloaded, as shown in Section 3, Figure 4. When the initial yield stress, σ_Y, is exceeded, plastic strains (deformations) start to develop in the structure. In the case of unloading at point A, the stress response follows a straight line to point B with the same elastic modulus, E. The elastic strain, ε_{el}, is recovered at point B, but the plastic strain, ε_p, remains. When the structure is loaded again (point B to point A), the stress response follows the same path as on unloading. However, this time the material will start to yield at $\sigma_{Y1} \geq \sigma_Y$. Therefore, the material hardens due to the plastic strains.

The material model used in the NLFEA should be able to adequately describe the material behavior during monotonic loading, unloading, reversed loading, and repeated cyclic loading if needed as in the low-cycle fatigue analyses.

The commonly used J2 metal plasticity theory [9] provides high-fidelity models for elasto-plastic materials such as mild and high tensile steels used in the marine and offshore industries and consists of the following three main elements:

1) Yield condition

2) Flow rule

3) Hardening rule

FIGURE 4
Typical Stress-Strain Curve of Steel

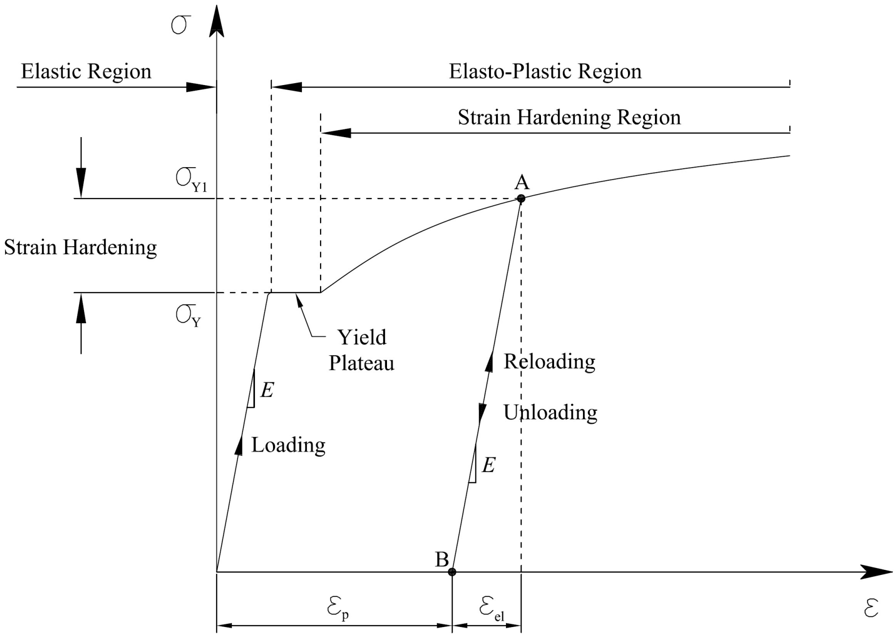

9.1 Yield Condition

The yield condition defines the combination of stresses in a certain structural component wherein the material starts to yield. It is recommended that the von Mises yield criterion (also called the octahedral shear stress yield criterion) is used in the NLFEA. The criterion states that the material starts to yield when the value of the equivalent von Mises stress reaches the yield stress of the material:

$$\frac{1}{\sqrt{2}}\sqrt{(\sigma_1-\sigma_2)^2+(\sigma_2-\sigma_3)^2+(\sigma_3-\sigma_1)^2}=\sigma_Y \quad \text{(3.4)}$$

where

$\sigma_1, \sigma_2, \sigma_3$	=	principal stresses in the three orthogonal directions
σ_Y	=	yield stress

The *yield surface* is a cylinder of radius σ_Y with an axis along the line $\sigma_1 = \sigma_2 = \sigma_3$. In the case of plane stress where $\sigma_3 = 0$, the yield surface is an ellipse with its major axis along the line $\sigma_1 = \sigma_2$, as shown in Section 3, Figure 5.

All stress states inside the yield surface are in the elastic domain and all stress states on the yield surface are in the elasto-plastic domain. It should also be noted that the yield surface shifts and/or changes size as the plastic strains develop in the material, but the stress states always stay on the yield surface. It is not possible for the stress state to be outside the yield surface. The von Mises yield criterion is built into most of the commercial NLFEA programs and does not require any special input from the user.

FIGURE 5
Von Mises Yield Surface for Plain Stress

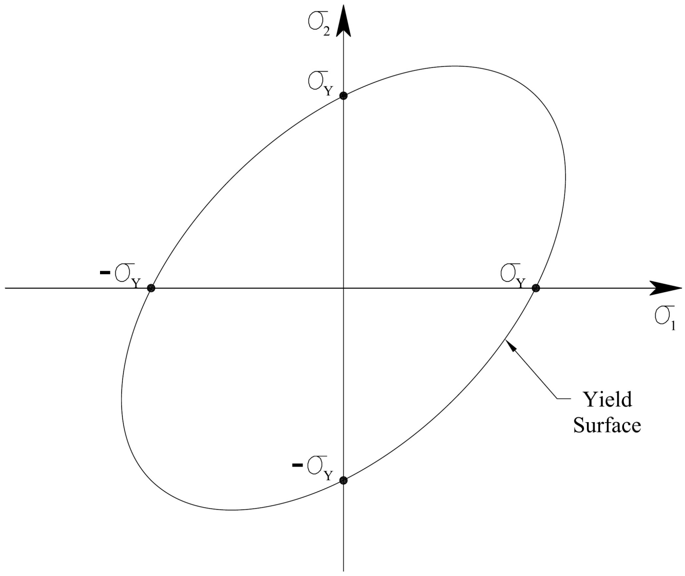

9.2 Flow Rule

The flow rule describes the relationship between the plastic strain increment and the stress increment once the stress state is on the yield surface. In other words, it describes how the plastic straining develops (flows). The plastic strain increment direction is usually assumed to be normal to the yield surface (see 3/9.1). Due to this association between the plastic strain increment direction and the yield surface normal, the rule is called the associated flow rule and is used in most commercial NLFEA programs by default.

According to the plasticity theory, the relationship between the plastic strain increments and stress increments (the flow rule) can be described by a single uniaxial stress-plastic strain curve for all possible stress states. This stress-strain curve is called the *flow curve* and is usually the only input required from the user to define the flow rule. The uniaxial tension test data, if available, should be used. If this is not the case, the design stress-strain curves for mild and high tensile steels from 3/9.4 may be used instead.

9.3 Hardening Rule

The hardening rule describes how the yield surface evolves when plastic straining occurs. Three basic hardening models are usually used and are available in most commercial NLFEA programs:

1) Kinematic hardening

2) Isotropic hardening

3) Combined kinematic and isotropic hardening

9.3.1 Kinematic Hardening

The kinematic hardening model assumes that the yield surface does not change in size or shape, but simply shifts in the stress space by a tensor, $\boldsymbol{\alpha}$, called *backstress*. The shifting of the yield surface in one direction causes the asymmetry of yield stress in tension and subsequent compression of the material. For example, the material subjected to tension will yield at σ_Y. If the loading is then reversed and compression force is applied, the material will yield at a value that is smaller, in absolute terms, compared to σ_Y (see Section 3, Figure 6 for a case of uniaxial stress). This earlier yielding on load reversal is called the *Bauschinger effect* and is observed in most engineering metals. Therefore, the chosen hardening model for marine and offshore steels should contain the kinematic hardening component if reversed loading is applied during the analysis.

A simplified version of the general (nonlinear) kinematic hardening model is the linear kinematic hardening model where stresses after yielding depend linearly on plastic strains. Therefore, the linear kinematic hardening model should only be used if the bilinear stress-strain curve is an adequate representation of the material, which is seldom the case.

9.3.2 Isotropic Hardening

The isotropic hardening model assumes that the yield surface expands equally in all directions when plastic straining occurs. In this case, the material in subsequent compression starts to yield at the new yield stress, σ_{Y_1}, which is greater in absolute terms than the initial yield stress of the material, σ_Y (see Section 3, Figure 7). Therefore, the isotropic hardening model predicts the opposite of the Bauschinger effect. The isotropic hardening model should only be used on its own if reversed loading is not applied during the analysis (e.g., ultimate strength analysis of a hull-girder or a local structure).

FIGURE 6
Kinematic Hardening Model

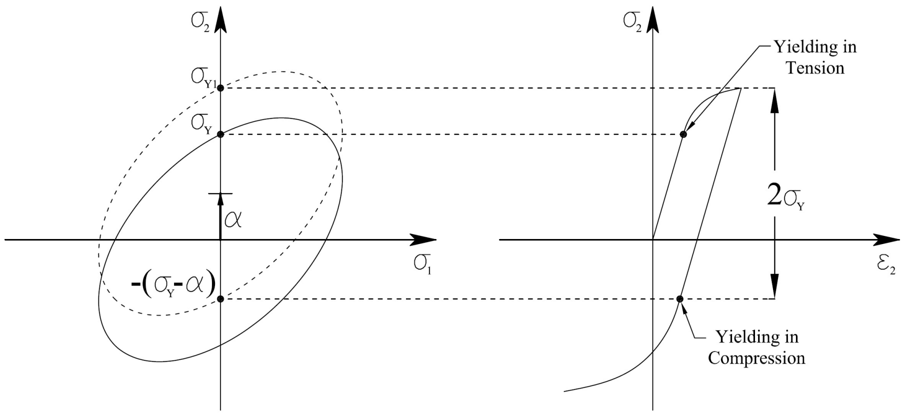

FIGURE 7
Isotropic Hardening Model

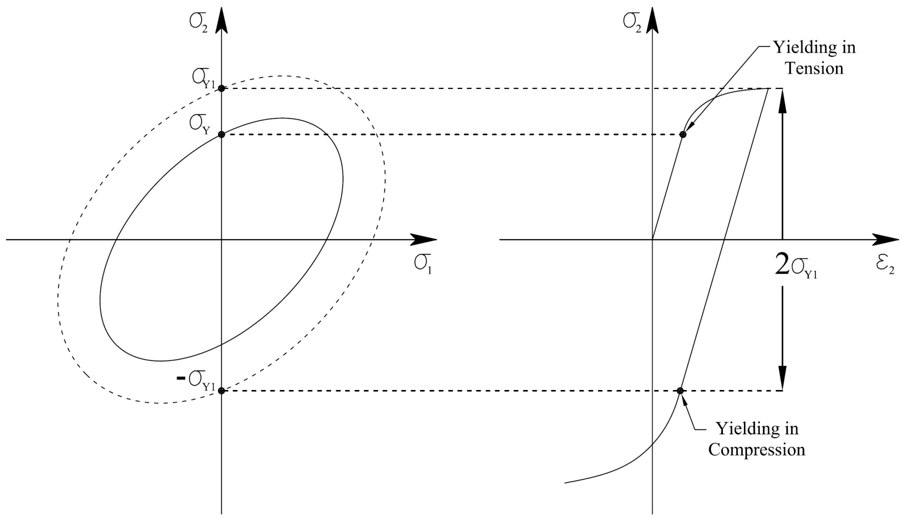

9.3.3 Combined Kinematic-Isotropic Hardening

The combined model assumes a simultaneous isotropic expansion and kinematic shift of the yield surface. This is the preferred hardening model in situations where reversed loading is applied during the analysis. This model is also very suitable for cases where repeated cyclic loading is applied, as in the case of the low-cycle fatigue analysis. The combined hardening model enables modeling of the following cyclic behavior of the material:

i) *Bauschinger Effect (see 3/9.3.1)*. This effect is taken into account by the kinematic hardening component of the combined model. The linear kinematic hardening component on its own can model the Bauschinger effect, but the nonlinear kinematic hardening component will better capture the actual plastic stress-strain portions of the cyclic hysteresis loops. It is recommended to superimpose multiple nonlinear kinematic hardening components by using a certain number of backstresses. In general, the number of superimposed nonlinear kinematic hardening components, defined by the number of specified backstresses, should be equal to the number of specified stress-plastic strain points of the flow curve.

ii) *Cyclic Hardening* with *Plastic Shakedown*. Cyclic hardening is characteristic of mild and high tensile steels used in the marine and offshore industries and refers to the phenomenon wherein the maximum stress reached in each of the hysteresis loops of a symmetric strain-controlled loading cycle gradually increases (see Section 3, Figure 8). If the increase of the stress stabilizes over a certain number of cycles, the structures has reached the stabilized plastic shakedown. Only the combined hardening model with nonlinear kinematic component(s) can predict these two phenomena.

iii) *Cycle-dependent Creep or Ratchetting*. This phenomenon occurs when the material is subjected to biased stress cycles (having non-zero mean stress). In that case, the mean strain of each hysteresis loop may start to shift towards larger strains (see Section 3, Figure 9a). The ratchetting may stabilize and stop after a certain number of cycles, it may establish a constant rate, or it may accelerate leading to a failure. If a nonlinear kinematic hardening model is used without the isotropic model, the predicted ratchetting rate will be constant (constant strain shift). If the isotropic hardening model is added, the ratchetting rate may decrease. More improvements in modeling the ratchetting behavior are achieved by using the isotropic hardening model in combination with a superposition of the linear kinematic hardening model and several nonlinear kinematic hardening models.

iv) *Cycle-dependent Relaxation*. This phenomenon occurs when the material is subjected to biased strain cycles, as in an asymmetric strain experiment having non-zero mean strain. In that case, the mean stress of each of the hysteresis loops tends to zero (see Section 3, Figure 9b). The nonlinear kinematic hardening component of the combined model can predict this behavior.

FIGURE 8
Cyclic Hardening and Plastic Shakedown

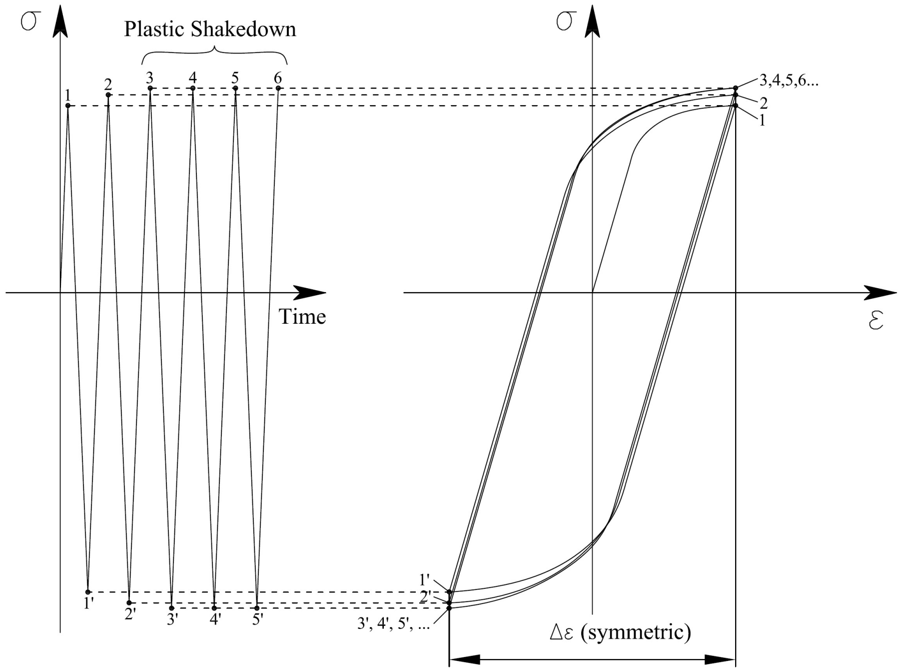

FIGURE 9
Cycle-Dependent Creep and Relaxation

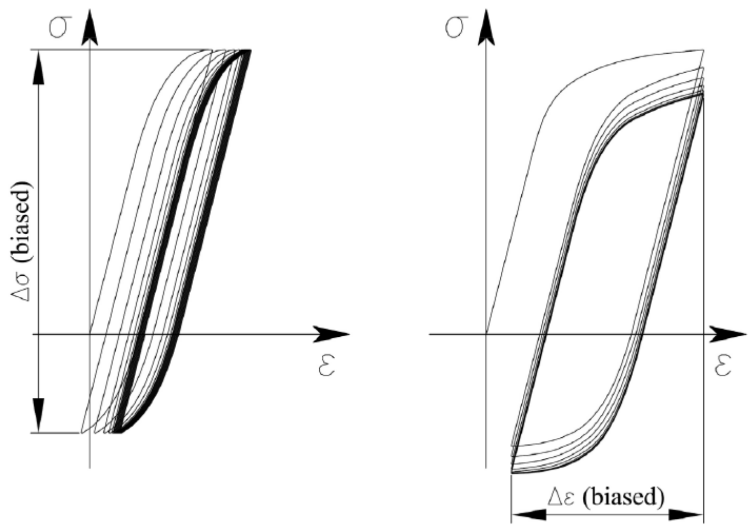

(a) Cycle-Dependent Creep (Ratchetting) **(b) Cycle-Dependent Relaxation**

During cyclic loading of the material, some or all the above-mentioned phenomena may occur. Therefore, for such applications, the use of the combined isotropic and kinematic hardening model is recommended. The kinematic hardening model should be a superposition of a linear and multiple nonlinear components.

Different commercial NLFEA packages may have different implementations of various hardening models. The determination of parameters of such models is outside the scope of these Guidance Notes. Some general guidelines are provided below. Usually, the NLFEA program documentation will contain details on how to calibrate the parameters of hardening models based on test data.

The parameters of the isotropic hardening model may be calibrated directly from the strain-controlled cyclic test data for the material in question. Because the isotropic hardening model does not predict different hardening behavior at different strain ranges, attention should be given to performing the calibration test at a constant strain range corresponding to the strain range expected during the analysis.

The parameters of the kinematic hardening model may be calibrated based on the stress-plastic strain data from a monotonic uniaxial tension test. In this way, the kinematic hardening parameters are essentially calibrated based on the first half-cycle and will only be relevant if the analysis consists of only a few cycles.

For analyses consisting of many cycles, especially where a stabilized response is of interest, the parameters of the kinematic hardening model should be calibrated based on the stabilized stress-plastic strain hysteresis loop curve from a symmetric strain-controlled cyclic test. Some commercial NLFEA programs will perform the calibration automatically based on the supplied test data.

Cyclic stress-plastic strain curves for a particular material may be used as an approximation of the stabilized stress-plastic strain hysteresis loop curve, but it needs to be expanded by a scale factor of two [3]. Care should also be taken to supply the test data in the format that is required by the NLFEA program.

9.4 Stress-Strain Curves (Flow Curves)

When reversed loading or cyclic loading does not have to be modeled, usually the only material parameters that need to be supplied are the elastic parameters (Poisson ratio, v, elastic modulus, E, and yield stress, σ_Y), mass density, ρ, and the uniaxial stress-strain curve describing the nonlinear plastic flow (flow curve). Ideally, the material parameters should be obtained from tests of the selected material. In the case when the uniaxial test data sets are not available for the materials used in the NLFEA, the data presented in this Subsection may be used as characteristic design material properties.

The stress-strain pairs from the uniaxial tension tests are usually given in terms of *engineering stresses* and *strains*, where both physical quantities are calculated based on the initial cross section and length of a test specimen, respectively. On the other hand, most commercial NLFEA require the definition of the flow curve in terms of the *true stresses* and *strains*, which are calculated based on the specimen's instantaneous cross-section and instantaneous strain increments, respectively. The relationships between true and engineering stresses and strains are given as:

$$\sigma = \sigma_{eng}\left(\varepsilon_{eng} + 1\right) \quad (3.5)$$

$$\varepsilon = \ln\left(\varepsilon_{eng} + 1\right) \quad (3.6)$$

where

σ = true stress

ε = true strain

σ_{eng} = engineering stress

ε_{eng} = engineering strain

Eq. 3.5 and 3.6 are only valid up to the onset of necking, when the ultimate tensile stress is reached. After necking, the true stresses and strains may be obtained using precise measurements of the instantaneous cross-sectional area of the specimen:

$$\sigma = \frac{F}{S} \quad (3.7)$$

$$\varepsilon = \ln\left(\frac{S_0}{S}\right) \quad (3.8)$$

where

F = instantaneous axial tension

S = current cross-sectional area of the test specimen

S_0 = initial cross-sectional area of the test specimen

In addition to the true flow curves, commercial NLFEA programs usually require that the true stresses be defined versus the plastic portion, ε_p, of the total true strain ε. True plastic strains can be calculated by subtracting the elastic strains from the total true strains as follows:

$$\varepsilon_P = \varepsilon - \varepsilon_{el} = \varepsilon - \frac{\sigma}{E} \quad (3.9)$$

where

$\varepsilon_{el} = \frac{\sigma}{E}$ = elastic portion of the true strain (see also Section 3, Figure 4).

The engineering stress-strain curves for most steels used in marine and offshore structures exhibit a softening region after the ultimate stress point is reached. This region is characterized by the negative slope of the flow curve and occurs due to necking (localized deformation of the specimen's cross section during uniaxial tests). The true stress-strain curves for most steels used in marine and offshore structures will usually not have the softening region as shown in Section 3, Figure 10.

FIGURE 10
True vs. Engineering Flow Curves

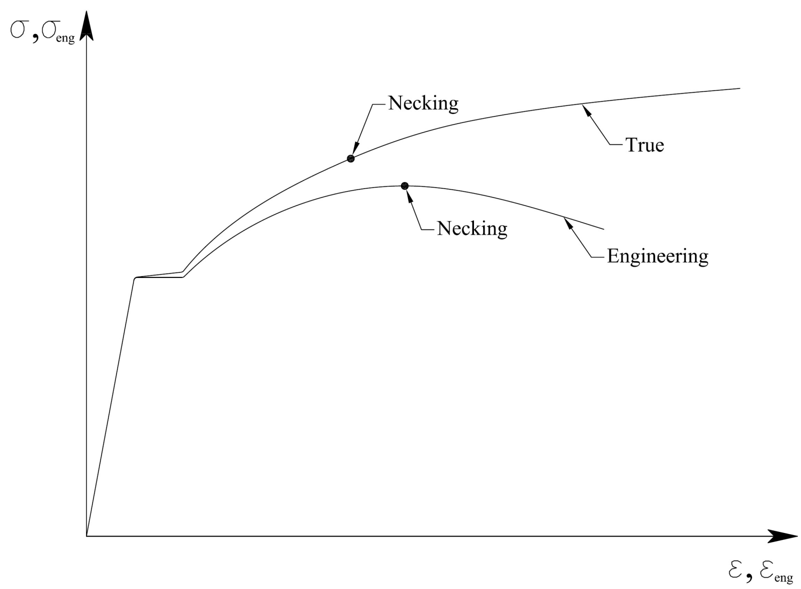

The proposed model for the true flow curves is based on calibration analysis on over 500 engineering stress-strain data sets for structural carbon steels with the yield stress ranging from 235 N/mm^2 (23.96 kgf/mm^2, 34084 psi) to 960 N/mm^2 (97.89 kgf/mm^2, 139236 psi), as specified in [10]. The model is a combination of a bi-linear and a nonlinear strain hardening model. The model only requires the knowledge of the elastic modulus, E, the engineering yield stress, $\sigma_{Y,eng}$, and the engineering ultimate stress, $\sigma_{U,eng}$. All three parameters are usually readily available to the engineer for any steel grade.

The true flow curve is given as follows:

$$\sigma(\varepsilon) = \begin{cases} E(e^{\varepsilon}-1)e^{\varepsilon} & \text{if } \varepsilon \le \ln(\varepsilon_{y,eng}+1) \\ \sigma_{Y,eng}e^{\varepsilon} & \text{if } \ln(\varepsilon_{y,eng}+1) < \varepsilon \le \ln(\varepsilon_{sh,eng}+1) \\ \left\{ \sigma_{Y,eng} + (\sigma_{U,eng}-\sigma_{Y,eng})\left\{\left(1-\frac{2}{\sqrt[5]{401}}\right)\left[\frac{(e^{\varepsilon}-1)-\varepsilon_{sh,eng}}{\varepsilon_{u,eng}-\varepsilon_{sh,eng}}\right]\right\} \right. & \text{if } \ln(\varepsilon_{sh,eng}+1) < \varepsilon \le \ln(\varepsilon_{u,eng}+1) \\ \left. + \frac{2\left[\frac{(e^{\varepsilon}-1)-\varepsilon_{sh,eng}}{\varepsilon_{u,eng}-\varepsilon_{sh,eng}}\right]}{\left\{1+400\left[\frac{(e^{\varepsilon}-1)-\varepsilon_{sh,eng}}{\varepsilon_{u,eng}-\varepsilon_{sh,eng}}\right]^5\right\}^{1/5}} \right\} e^{\varepsilon} & \\ K\varepsilon^n & \text{if } \varepsilon > \ln(\varepsilon_{u,eng}+1) \end{cases} \quad (3.10)$$

where

$$\varepsilon_{y,eng} = \frac{\sigma_{Y,eng}}{E} \quad \ldots \quad (3.11)$$

$$\varepsilon_{sh,eng} = 0.1\frac{\sigma_{Y,eng}}{\sigma_{U,eng}} - 0.055 \quad , \quad \text{but} \quad 0.015 \le \varepsilon_{sh,eng} \le 0.03 \quad \ldots \quad (3.12)$$

$$\varepsilon_{u,eng} = 0.6\left(1-\frac{\sigma_{Y,eng}}{\sigma_{U,eng}}\right) \quad , \quad \text{but} \quad \varepsilon_{u,eng} \ge 0.06 \quad \ldots \quad (3.13)$$

$$K = \sigma_{U,eng}\left(\frac{e}{n}\right)^n \quad \ldots \quad (3.14)$$

$$n = \ln(\varepsilon_{u,eng}+1) \quad \ldots \quad (3.15)$$

The material model is schematically explained in Section 3, Figure 11, where the axes are the true stress and true strain. It should be noted that:

$\varepsilon_{y,eng}$ = engineering strain at the onset of yielding

$\varepsilon_{sh,eng}$ = engineering strain at the start of the strain hardening region

$\varepsilon_{u,eng}$ = engineering strain at the point where ultimate engineering stress $\sigma_{u,eng}$, is reached (the onset of necking)

The material model parameters for common steel grades used in the marine and offshore industries are shown in Section 3, Table 4.

The recommended design true flow curve plots for common marine and offshore steels are shown in Section 3, Figure 12.

Appendix 2 contains design true flow curves for common steel grades used in the marine and offshore industries. Both total true strains and plastic true strains are given in the tables.

9.5 Strain-Rate Effects

The effect of strain rate on the mechanical properties of the material are often neglected during the NLFEA of marine and offshore structures. However, in cases of high-speed collision or impact analyses, these effects may become important.

In general, material flow curves harden, and the fracture strain decreases as the strain rate increases. Strain-rate hardening should be modeled using the Cowper-Symonds equation to stretch the true flow curve along the y-axis by a constant factor that depends on the strain rate, $\dot{\varepsilon}$:

$$\sigma(\varepsilon)_{dyn} = \sigma(\varepsilon)\left[1 + \left(\frac{\dot{\varepsilon}}{C}\right)^{1/q}\right] \quad \text{.......................................} (3.16)$$

where

$\sigma(\varepsilon)_{dyn}$ = dynamic true flow curve

$\sigma(\varepsilon)$ = static true flow curve

C, q = parameters of the Cowper-Symonds model

C and q should be calibrated based on the experimental data. In the absence of more relevant experimental data, the parameter values from Section 3, Table 5 may be used when the plastic strains during the analysis are small.

FIGURE 11
Schematic Description of the Recommended Material Model

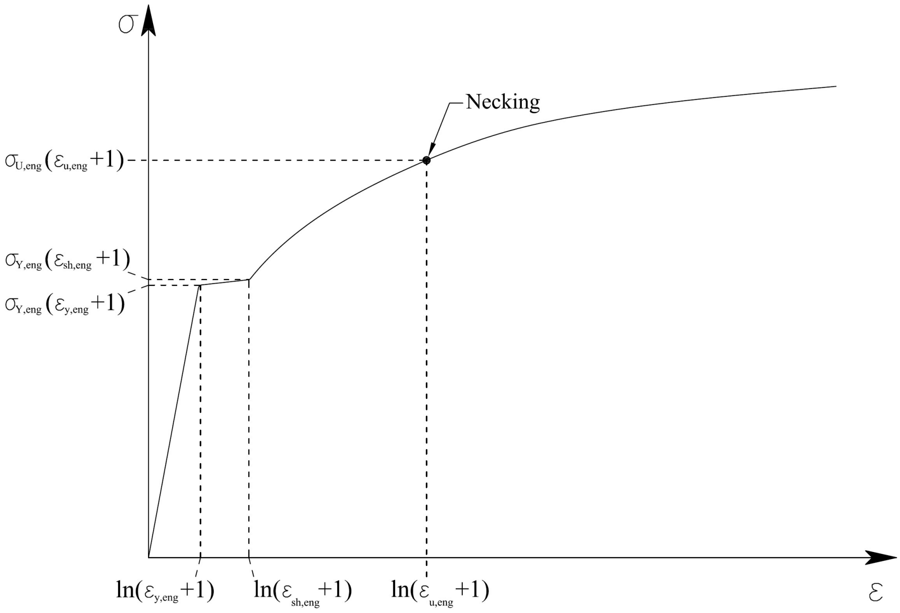

FIGURE 12
Design True Flow Curves for Common Marine and Offshore Steels

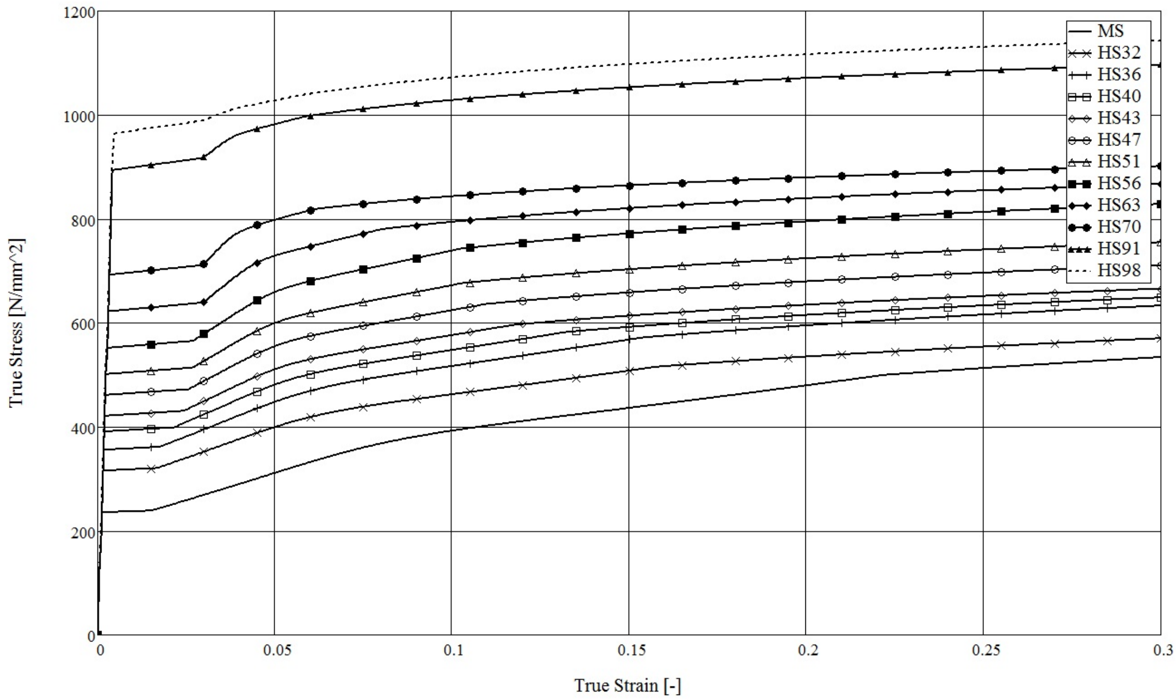

TABLE 4
Material Model Parameters for Common Steel Grades

Steel Grade	*E* *N/mm²* *(kgf/mm², psi)*	*v*	*ρ* *kg/m³* *(lb/ft³)*	σ_Y *N/mm²* *(kgf/mm², psi)*	σ_U *N/mm²* *(kgf/mm², psi)*	ε_y *%*	ε_{sh} *%*	ε_u *%*	*n*	*K* *N/mm²* *(kgf/mm², psi)*
MS	210,000 (21414, $30.46 \cdot 10^6$)	0.3	7850 (490)	235 (23.96, 34084)	400 (40.79, 58015)	0.11	1.50	24.75	0.221	697 (71.07, 101091)
HS32	210,000 (21414, $30.46 \cdot 10^6$)	0.3	7850 (490)	315 (32.12, 45687)	440 (44.87, 63817)	0.15	1.66	17.05	0.157	689 (70.26, 99931)
HS36	210,000 (21414, $30.46 \cdot 10^6$)	0.3	7850 (490)	355 (36.20, 51488)	490 (49.97, 71069)	0.17	1.74	16.53	0.153	761 (77.60, 110374)
HS40	210,000 (21414, $30.46 \cdot 10^6$)	0.3	7850 (490)	390 (39.77, 56565)	510 (52.01, 73969)	0.19	2.15	14.12	0.132	760 (77.50, 110229)
HS43	210,000 (21414, $30.46 \cdot 10^6$)	0.3	7850 (490)	420 (42.83, 60916)	530 (54.05, 76870)	0.20	2.42	12.45	0.117	766 (78.11, 111099)
HS47	210,000 (21414, $30.46 \cdot 10^6$)	0.3	7850 (490)	460 (46.91, 66717)	570 (58.12, 82672)	0.22	2.57	11.58	0.110	810 (82.60, 117481)

Steel Grade	E N/mm² (kgf/mm², psi)	v	ρ kg/m³ (lb/ft³)	σ_Y N/mm² (kgf/mm², psi)	σ_U N/mm² (kgf/mm², psi)	ε_y %	ε_{sh} %	ε_u %	n	K N/mm² (kgf/mm², psi)
HS51	210,000 (21414, $30.46 \cdot 10^6$)	0.3	7850 (490)	500 (50.99, 72519)	610 (62.20, 88473)	0.24	2.70	10.82	0.103	854 (87.08, 123862)
HS56	210,000 (21414, $30.46 \cdot 10^6$)	0.3	7850 (490)	550 (56.08, 79771)	670 (68.32, 97175)	0.26	2.71	10.75	0.102	937 (95.55, 135900)
HS63	210,000 (21414, $30.46 \cdot 10^6$)	0.3	7850 (490)	620 (63.22, 89923)	720 (73.42, 104427)	0.30	3.00	8.33	0.080	955 (97.38, 138511)
HS70	210,000 (21414, $30.46 \cdot 10^6$)	0.3	7850 (490)	690 (70.36, 100076)	770 (78.52, 111679)	0.33	3.00	6.23	0.061	969 (98.81, 140542)
HS91	210,000 (21414, $30.46 \cdot 10^6$)	0.3	7850 (490)	890 (90.75, 129084)	940 (95.85, 136335)	0.42	3.00	6.00	0.058	1176 (119.92, 170564)
HS98	210,000 (21414, $30.46 \cdot 10^6$)	0.3	7850 (490)	960 (97.89, 139236)	980 (99.93, 142137)	0.46	3.00	6.00	0.058	1226 (125.02, 177816)

TABLE 5
Cowper-Symonds Parameters for Small Plastic Strains

	Cowper-Symonds Parameters	
	C [s⁻¹]	*q [-]*
Mild Steels	40.4	5
High Tensile Steels	3200	5

Since parameters C and q may depend on the plastic strains and the plate thickness as shown in [11], especially for mild steels, it is necessary to use the parameters that are calibrated at the plastic strain level and the plate thickness relevant for the problem to be analyzed by the NLFEA. If the expected strains during the NLFEA are very large, the parameter values from Section 3, Table 5 for mild steel may lead to overestimation of the hardening effect for larger plastic strains. In the absence of more accurate values, the strain rate may be estimated using the following expression:

$$\dot{\varepsilon} = \frac{V_0}{2\delta} \qquad (3.17)$$

where

V_0 = initial speed of the dynamic load

δ = average displacement of the structural element

For ship collisions, the estimated strain rate is in the range of 0.5 s^{-1} to 5 s^{-1}, as stated in [12].

10 Geometric Imperfections

During the fabrication of thin-walled marine and offshore structures (metal cutting, rolling, forming, welding, and heat treatment), some geometric imperfections (nonuniformities in shape, eccentricities, and local imperfections) and residual stresses are inevitably introduced and can affect their structural behavior, especially the ultimate strength. Accidental limit states due to collision, grounding, impact with ice, or explosion are not likely to be affected by the initial imperfections and residual stresses in the structure. However, the initial imperfections may help avoid the numerical instabilities during the solution process, regardless of the type of limit state that is being analyzed.

The shape and size of initial geometric imperfections may have a significant impact on the ultimate limit state of the structure and its collapse mechanism, especially for structures that are sensitive to the initial imperfections. Therefore, a sound understanding of the effect of imperfection patterns and magnitudes on the analyzed or similar structures may be necessary. The geometric imperfections can be treated using the following four different approaches:

1) Impose the measured initial imperfection pattern onto the FE model

2) Linear superposition of buckling eigenmodes from the eigenvalue buckling analysis

3) Direct shape definition through the specification of nodal coordinates

4) Using the deformation shape from a linear static analysis

The following Paragraphs contain recommended practices related to each of the above-mentioned treatments of the geometric imperfections. The imperfection magnitudes given in 3/10.3 can be used in approaches 2, 3, and 4 from the above list and are applicable to the basic building blocks of marine and offshore structures – stiffened panels. Imperfections obtained in this way can be considered as equivalent imperfections that represent the combined effects of the initial imperfections and the residual stresses. Other equivalent imperfection magnitudes may be considered, depending on fabrication tolerances and post weld heat treatment. The choice of equivalent imperfection magnitudes should be documented.

10.1 Imposing Measured Imperfections

This is the most accurate approach to treating the geometric imperfections. However, measurement of random imperfection patterns on real marine and offshore structures is complex and time consuming, and the measured imperfections are usually not available. The measured imperfections, as opposed to the equivalent imperfections, do not account for the effects of residual stresses.

10.2 Linear Superposition of Eigenmodes

This is usually the most convenient method and is recommended for large and complex structures such as a section or the entire hull girder of a vessel. A linear eigenvalue buckling analysis should be performed first. Then, only four eigenmodes should be linearly combined and scaled to obtain the imperfection pattern with the desired amplitudes. The following four buckling modes should be selected:

1) Global buckling mode that best describes the overall buckling of the stiffened panel (plate and stiffeners) between the strong supporting members

2) Local buckling mode that best describes the local buckling of the plate between the stiffeners

3) Local buckling mode that best describes the local buckling of the stiffener web plates

4) Local buckling mode that best describes the local sideways tripping of the stiffeners

More information regarding the recommended geometry of the global and local imperfection patterns as well as their recommended equivalent magnitudes is given in 3/10.3.

Attention should be paid to imposing the relevant boundary conditions during the eigenvalue buckling analysis so that realistic buckling modes can be obtained.

Initial imperfections are usually imposed over the parts of the structure that are susceptible to buckling under compressive loads. In case of the hull girder, imperfections should be applied across the top hull girder flange (deck) when the hull is in sagging, or across the bottom flange (double bottom) when the hull is in hogging. In the longitudinal direction, the imperfections should be specified across three adjacent web frame spacings at the weakest sections of the hull where failure is expected.

This method usually produces the most conservative imperfection pattern because the main plate and stiffener buckling modes will be triggered during the analysis.

10.3 Direct Shape Definition

Direct shape definition uses regular imperfection patterns based on trigonometric functions to describe the initial imperfections by manually offsetting all the nodes in the structure. Attention should be paid to achieving consistency between nodal offsets of separately treated regions of the marine or the offshore structure.

Imperfection patterns based on regular trigonometric functions, and similar to the global and local buckling modes listed in 3/10.2, should be selected for stiffened panels (see Section 3, Figure 13).

10.3.1 Global Imperfections of the Stiffened Panel

The global imperfections of the panel are given as vertical displacements in the z-axis direction of all the panel nodes depending only on the original in-plane (x and y) coordinates of the stiffened panel nodes (see Section 3, Figure 13). The vertical displacements may be calculated as:

$$\sigma_{z,panel} = \frac{a}{750}\cos\frac{\pi x}{a}\sin\frac{\pi y}{B} \quad \text{(3.18)}$$

where

a	=	distance between the strong stiffened panel supports in the x direction (e.g., between web frames)
B	=	total breadth of the stiffened panel in the y direction (see Section 3, Figure 13)

Eq. 3.18 creates one half-wave between the strong supports in the x direction and one half-wave between the strong supports in the y direction, as shown in Section 3, Figure 14. The recommended maximum out-of-plane global deformation of the stiffeners with the attached plating is $a/750$.

If the origin of the coordinate system is shifted in the x direction to the strong transverse support instead of in between the strong transverse supports, then the cosine function in Eq. 3.18 should be replaced with the sine function.

FIGURE 13
Typical Stiffened Panel

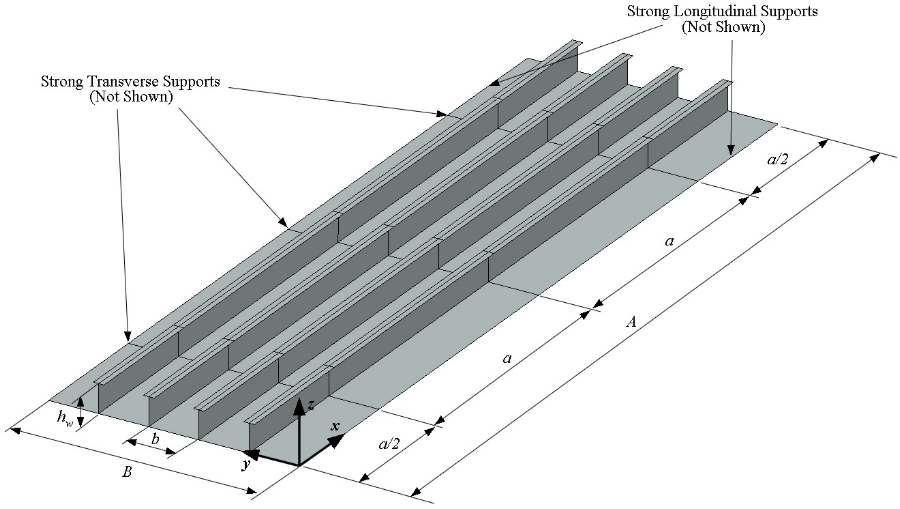

FIGURE 14
Global Stiffened Panel Imperfections (scale = 50x)

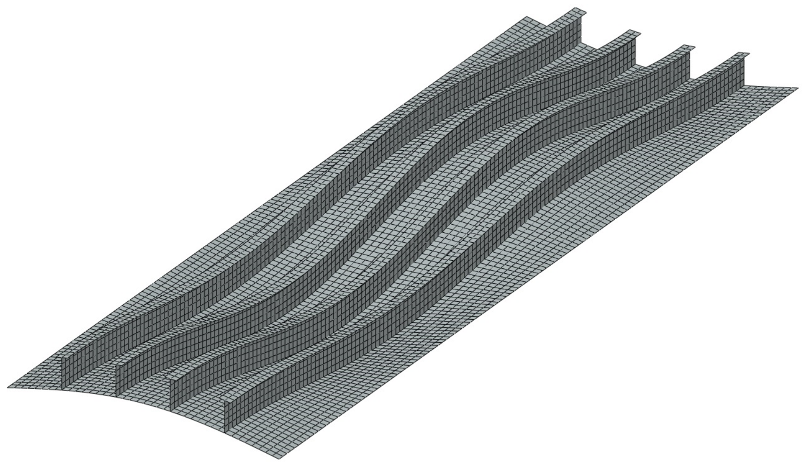

10.3.2 Local Imperfections of the Plate

The local imperfections of the plate are given as vertical displacements in the z-axis direction of all the plate nodes depending only on the original in-plane (x and y) coordinates of the plate nodes. The vertical displacements may be calculated as:

$$\delta_{z,plate} = \frac{b}{200}\cos\frac{m\pi x}{a}\sin\frac{m\pi y}{b} \quad (3.19)$$

where

a = see 3/10.3.1

b = spacing of stiffened panel stiffeners

m = number of half-waves between the strong stiffened panel supports in the x direction

Eq. 3.19 creates m half-waves between the stiffeners in the y direction as shown in Section 3, Figure 15 for m = 5. The recommended maximum out-of-plane local deformation of the plate between the stiffeners is $b/200$.

The number of half-waves, m, may be estimated from the buckling theory of a simply supported plate as the minimum integer satisfying the following inequality from [2]:

$$\sqrt{m(m+1)} \geq \frac{a}{b} \quad (3.20)$$

If the origin of the coordinate system is shifted in the x direction to the strong transverse support instead of in between the strong transverse supports, then the cosine function in Eq. 3.19 should be replaced with the sine function.

FIGURE 15
Local Imperfections of Plate Between the Stiffeners (*m* = 5, scale = 50x)

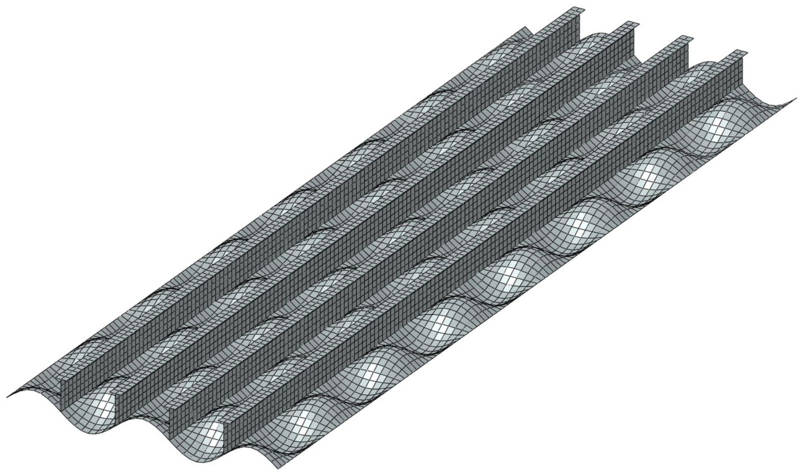

10.3.3 Local Imperfections of the Stiffener Web Plate

The local imperfections of the stiffener web plate are given as transverse displacements in the y-axis direction of all the stiffener web nodes depending only on the original in-plane (x and z) coordinates of the stiffener web nodes (see Section 3, Figure 13). The transverse displacements may be calculated as:

$$\delta_{y,web} = \frac{h_w}{200}\cos\frac{m\pi x}{a}\sin\frac{\pi z}{h_w} \quad (3.21)$$

where

a = see 3/10.3.1

m = see 3/10.3.2

h_w = height of the stiffener web

Eq. 3.21 creates m half-waves between the strong supports in the x direction and one half-wave across the stiffener web height in the z direction as shown in Section 3, Figure 16 for m = 5. The recommended maximum out-of-plane local deformation of the stiffener web plate is $h_w/200$.

If the origin of the coordinate system is shifted in the x direction to the strong transverse support instead of in between the strong transverse supports, then the cosine function in Eq. 3.21 should be replaced with the sine function.

FIGURE 16
Local Imperfections of Stiffener Webs (*m* = 5, scale = 50x)

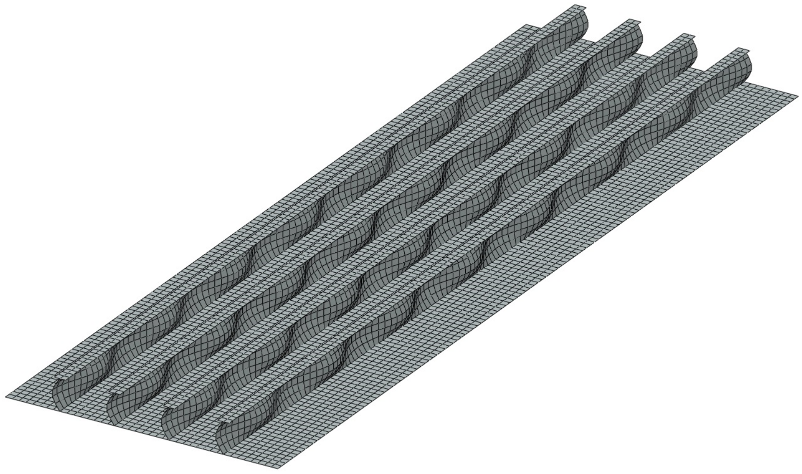

10.3.4 Local Tripping Imperfections of the Stiffener

The local tripping imperfections of the stiffener are given as rotations of the stiffener about the point where it is attached to the plate. The transverse and vertical displacements of the stiffener web nodes may be calculated as:

$$\delta_{y,web} = z\sin\varphi \qquad (3.22)$$

$$\delta_{z,web} = z(\cos\varphi - 1) \qquad (3.23)$$

$$\varphi = \frac{a}{750h_w}\cos\frac{\pi x}{a}\sin\frac{\pi\left(y_{web} - \frac{n_s+1}{2}b\right)}{(n_s-1)b} \qquad (3.24)$$

where

a	=	see 3/10.3.1
b	=	see 3/10.3.2
h_w	=	see 3/10.3.3
n_s	=	number of stiffeners between strong longitudinal supports
φ	=	rotation angle of the stiffener
x, y_{web}, z	=	original coordinates of the stiffener web nodes with y_{web} being constant for each of the stiffeners

The recommended maximum rotation angle of the stiffener is $a/(750h_w)$ radians.

Similarly, for the stiffener flange nodes:

$$\delta_{y,flange} = \sqrt{z^2 + (y - y_{web})^2}\,(\sin(\alpha+\varphi) - \sin(\alpha)) \qquad (3.25)$$

$$\delta_{z,flange} = \sqrt{z^2 + (y - y_{web})^2}\,(\cos(\alpha+\varphi) - \cos(\alpha)) \qquad (3.26)$$

$$\alpha = \tan^{-1}\frac{y - y_{web}}{z} \quad (3.27)$$

$y - y_{web}$ is the difference between the original y coordinate of the flange node and the y coordinate of the corresponding web. Eq. 3.25, 3.26, and 3.27 couple the stiffener flange rotation with the stiffener web rotation, as shown in Section 3, Figure 17.

FIGURE 17
Local Tripping Imperfections of Stiffeners (scale = 50x)

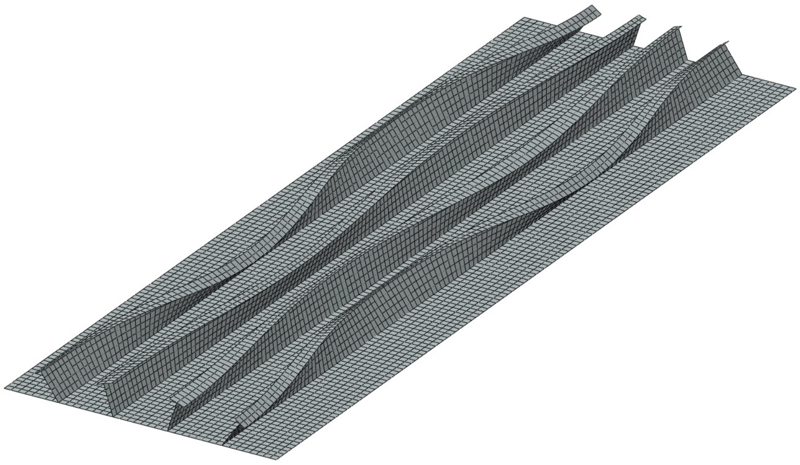

If the origin of the coordinate system is shifted in the x direction to the strong transverse support instead of in between the strong transverse supports, then the cosine function in Eq. 3.24 should be replaced with the sine function.

10.3.5 Combined Imperfections of the Stiffened Panel

The combined global and local imperfections are obtained by linear superposition of all the imperfections calculated in 3/10.3.1 to 3/10.3.4. Section 3, Figure 18 shows the combined initial geometric imperfections of the stiffened panel. Attention should be paid to confirm that the maximum global and local deflections in a certain direction coincide and have the same sign.

FIGURE 18
Combined Imperfections of Stiffened Panel (scale = 25x)

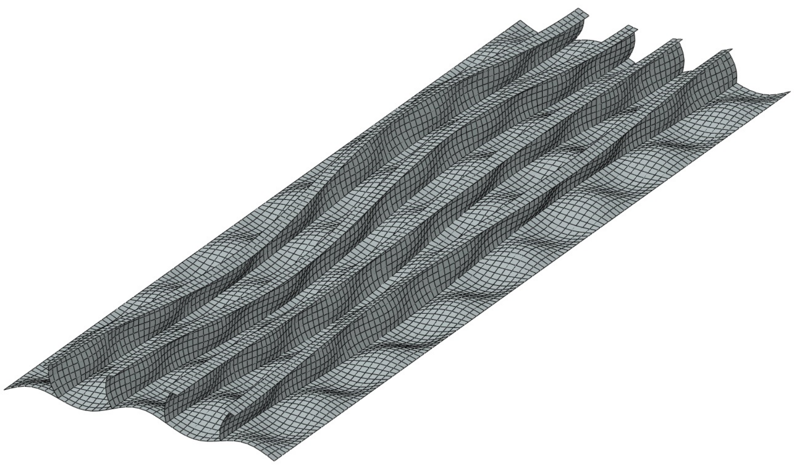

10.4 Deformed Shape from Linear Static Analysis

The deformed structure configuration after the linear static analysis step can be scaled and used as the initial, unstressed configuration for the NLFEA. The scaling should be performed such that the largest out-of-plane deformation of the plate is equal to the sum of global and local amplitudes (i.e., $a/750 + b/200$)

Using the deformed shape from the linear static analysis to prescribe initial geometric imperfections is only applicable to simple structures that are not sensitive to the imperfection shapes.

11 Ductile Fracture Modeling

When simulating ship-to-ship collision, grounding, explosions, and other accidental limit states, it may be important to consider ductile fracture of the material. Fracture of the material will have an impact on the global collapse mechanism of the structure, it will control possible flooding of the compartments, and most importantly, it will affect the total energy absorbed by the structure, which determines its crashworthiness.

Predicting fracture in a material is very complex and requires careful calibration and validation against experimental data. Many ductile fracture criteria have been developed, some of them specifically for use in marine and offshore structures [13]. Many of the ductile fracture criteria predict rupture when the equivalent plastic strain in the material, $\bar{\varepsilon}_p$, becomes equal to or larger than the critical fracture strain, ε_{cf}:

$$\bar{\varepsilon}_p \geq \varepsilon_{cf} \quad (3.28)$$

$\bar{\varepsilon}_p$ is a scalar quantity representing material's accumulated inelastic deformation. It can be expressed using the repeated index notation as follows:

$$\bar{\varepsilon}_p = \int_0^t \sqrt{\frac{2}{3}\dot{\varepsilon}_{ij}^p \dot{\varepsilon}_{ij}^p} dt \quad (3.29)$$

where

$\dot{\varepsilon}_{ij}^p$ = components of the plastic strain rate tensor

t = time over which the straining has occurred

$\dot{\varepsilon}_{ij}^p \dot{\varepsilon}_{ij}^p$ = $(\dot{\varepsilon}_{11}^p)^2 + (\dot{\varepsilon}_{12}^p)^2 + (\dot{\varepsilon}_{13}^p)^2 + (\dot{\varepsilon}_{21}^p)^2 + (\dot{\varepsilon}_{22}^p)^2 + (\dot{\varepsilon}_{23}^p)^2 + (\dot{\varepsilon}_{31}^p)^2 + (\dot{\varepsilon}_{32}^p)^2 + (\dot{\varepsilon}_{33}^p)^2$

Equivalent plastic strain is readily post-processed in most commercial NLFEA programs. According to the plasticity theory, the uniaxial flow curve (σ-ε) can be taken as the equivalent stress-strain ($\bar{\sigma} - \bar{\varepsilon}$) curve, as shown in Section 3, Figure 19. When $\bar{\varepsilon}_p = \varepsilon_{cf}$, ductile fracture is said to have occurred. Some NLFEA define the point where $\bar{\varepsilon}_p = \varepsilon_{cf}$, as the initiation of ductile fracture (point A in Section 3, Figure 19), whereas the actual fracture occurs at a larger critical failure strain ε'_{cf} (point B in Section 3, Figure 19). Between the initiation of fracture and the actual fracture, there is progressive ductile fracture evolution with degradation of both the yield stress (softening) and the material stiffness. At the actual point of fracture, the stiffness of the structure reduces to zero.

The ductile fracture evolution is heavily dependent on the mesh size. NLFEA programs try to minimize this mesh dependency by defining the ductile fracture evolution in terms of the equivalent plastic displacement, $\bar{u}_p$, instead of equivalent plastic strain. $\bar{u}_p$ is zero at ductile fracture initiation and increases to a value $\bar{u}_{pf}$ at fracture. However, it is recommended to, conservatively, neglect the ductile fracture evolution region of the equivalent stress-strain curve by setting:

$$\bar{u}_{pf} = 0 \quad (3.30)$$

where $\bar{u}_{pf}$ is the equivalent plastic displacement at fracture. This is equivalent to assuming that the fracture has occurred at initiation when $\bar{\varepsilon}_p = \varepsilon_{cf}$, as many ductile fracture criteria do.

Critical failure strain, ε_{cf}, depends on stress state in the material, strain rate, and mesh size. However, it has been shown in [14] that ε_{cf} in most reliable ductile fracture criteria for collision simulations of marine structures can be assumed independent of the stress state and the strain rate. A number of commonly used fracture criteria assume that ε_{cf} is a function of the mesh size and plate thickness only:

$$\varepsilon_{cf} = f(L, t) \qquad (3.31)$$

where

L	=	length of the finite element
t	=	plate thickness

Ductile fracture criteria with the form as described with Eq. 3.31, where the critical fracture strain is constant for a certain mesh size and plate thickness, are not usually implemented in commercial NLFEA programs. However, such criteria can be implemented using commonly available and well-known criteria, where ε_{cf} has a constant term, among other terms, and where the ductile damage accumulates linearly. One such criteria is the Johnson-Cook criteria described in [15] that has five parameters d_1, d_2, d_3, d_4, and d_5, of which only d_1 is the constant term. The criteria given by Eq. 3.31 can be implemented using the Johnson-Cook ductile fracture criteria by setting:

$$d_1 = f(L, t)$$
$$d_2 = d_3 = d_4 = d_5 = 0 \qquad (3.32)$$

The criteria described by Eq. 3.31 also assume there is no ductile fracture evolution and, therefore, require $\bar{u}_{pf} = 0$.

FIGURE 19
Ductile Fracture Initiation and Evolution

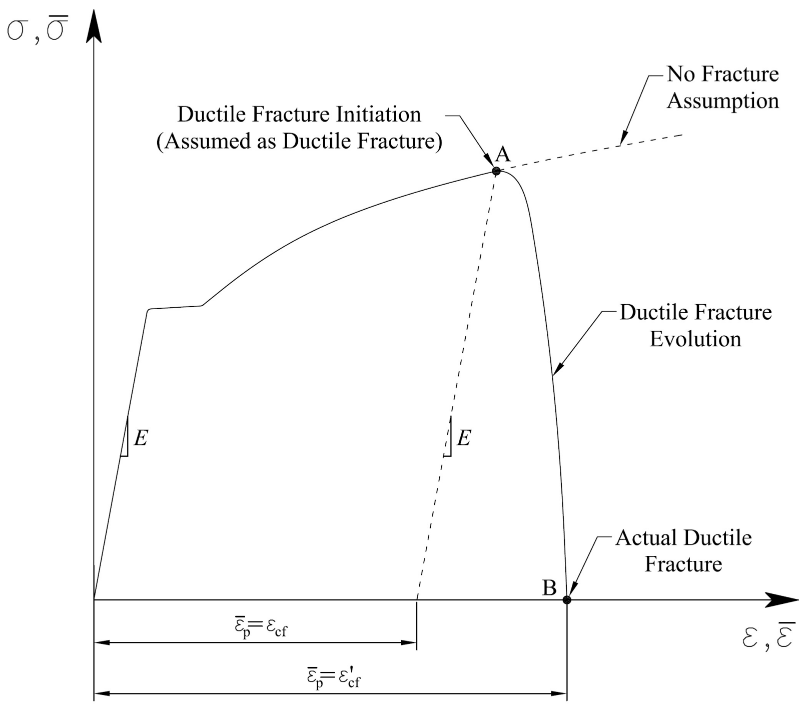

References [13] and [12] describe a number of available fracture criteria that can also be considered. However, care should be taken to use properly calibrated parameters for the material and mesh size used in the NLFEA.

Usually, the NLFEA program will delete an element that has exceeded the ductile fracture criterion in at least one integration point, by default.

It is generally recommended to conduct the analyses involving fracture using explicit dynamic or explicit quasi-static analyses. Implicit dynamic or implicit quasi static analyses as well as the static analysis require iteration algorithms that may fail to converge due to the progressive degradation of yield stress and stiffness, especially in cases where ductile fracture evolution is neglected.

12 Contact Modeling

Modeling contact between two different bodies is necessary in some scenarios, such as ship collisions, grounding, various structural indentations, and multiple container stacks.

When two different bodies come into contact, a contact pressure will develop in the direction perpendicular to the contacting surfaces. The NLFEA solver will determine the amount of contact pressure acting on both contact surfaces based on the user-defined pressure-overclosure relationship. Also, if the contacting surfaces slip relative to each other, frictional forces will develop in the tangential direction. Therefore, contact interface constitutive properties in the normal and tangential direction need to be defined.

12.1 Definition of Contact Interface Constitutive Properties

For the analysis of typical marine and offshore structures where contact modeling is needed, it is recommended to use the *hard contact* pressure-overclosure relationship where the contact pressure is zero when the surfaces are not in contact. When the surfaces are in contact, the pressure is determined based on the constraint of no penetration of one surface into another. It is recommended to use the *penalty method* in order to enforce the hard contact. The penalty method may allow small penetrations. However, this numerical softening may help with the convergence issues. Surfaces that come into contact should be allowed to separate once the contact pressure becomes zero.

If modeling friction is needed, isotropic *Coulomb friction model* is recommended where the friction is proportional to the force acting normal to the contact surfaces. The proportionality factor is the coefficient of friction. For perpendicular ship-to-ship collisions, the friction force will have a very small impact on the analysis. However, for ship-to-ship collisions at an oblique angle (raking collisions) or for ship grounding simulations, friction may become an important factor that should be included in the analysis. The coefficient of friction should be carefully calibrated and validated against the available experimental data. For ship-to-ship collisions, values between 0.23 and 0.3 are typically used.

12.2 Definition of Contact Pairs

Apart from defining the contact interface constitutive properties in the normal and tangential directions, the user may also need to define the surfaces, edges, and vertices on one body that may potentially come into contact with other surfaces, edges, or vertices on the same body or on another body or bodies. This is called *contact pair* definition. Usually surface-to-surface, edge-to-surface, edge-to-edge, and vertex-to-surface types of contact are allowed.

Some commercial NLFEA programs can assign contact pairs automatically, including self-contact. This procedure is recommended as it simplifies the contact modeling considerably, albeit at potentially higher computational cost.

If the contact pairs are defined manually, then all potential contact pairs should be identified first. One entity in the contact pair is defined as "master" and the other one is defined as "slave". When contact pairs are defined automatically by the NLFEA program, each entity in the contact pair is defined as both master and slave. When defining master and slave surfaces for surface-to-surface contact, the following general recommendations should be followed:

i) The larger surface should be selected as the master surface.

ii) If the surfaces are of similar size, the surface of the stiffer body should be selected as the master surface.

iii) If the surfaces are of similar size and stiffness, the surface with a coarser mesh should be selected as the master surface.

12.3 Initial Overclosures and Rough Surface Geometry

Initial overclosures (penetrations) may cause convergence issues and should be resolved. Sometimes the two or more structural components are in contact at the beginning of the analysis. Even though the surfaces of the bodies that are in contact may be smooth, they will be faceted during meshing and the nodes of one surface may penetrate the other surface. Small overclosures at the beginning of the analysis can often be resolved automatically by the NLFEA program without causing any initial strain in the structures. Care should be taken to minimize such initial overclosures as the NLFEA program will exclude the surfaces with significant initial overclosures from contact pairs.

Rough surface geometry caused by coarse mesh will decrease the accuracy of contact pressure and friction force results. It may also cause two surfaces to stick to each other, preventing sliding of the surfaces. Rough surface geometry may be smoothed by refining the mesh in the areas that are expected to come into contact or by using automated surface smoothing contact algorithms if they are available in the NLFEA program.

It should also be recognized that the NLFEA program will take the thickness of the shell elements into account when determining the existence of the contact between two surfaces. Therefore, putting two shell element reference surfaces into initial contact will result in an overclosure equal to $t_1/2 + t_2/2$, where t_1 and t_2 are the thicknesses of the two shell elements.

12.4 Contact Stabilization

Convergence issues related to unwanted rigid body motions can sometimes occur when modeling contact. Some NLFEA programs offer highly automated contact stabilization based on the introduction of artificial viscous damping without significantly affecting the accuracy of the solution. This is similar to the numerical stabilization technique used for improving the convergence of the N-R iterations as explained in 3/4. Contact stabilization should only be used when necessary to stabilize the convergence issues related to contact, and its energy should stay below 5% of the total internal energy of the system throughout the analysis.

13 Mesh Quality and Size

Mesh size and quality parameters are even more important for NLFEA compared to linear finite element analysis (FEA). If the elements undergo significant distortions during the large-displacement nonlinear analysis, the accuracy and reliability of the solution may be reduced. Therefore, special attention should be given to element quality, which can often be defined using the following measures:

i) *Element Aspect Ratio.* Ratio of maximum to minimum element edge length

ii) *Skewness Angle.* Difference between the right angle and the smallest angle between intersecting element mid-lines

iii) *Warping Angle.* Out-of-plane element warping

iv) *Corner Angle.* Angle between element edges at a corner

v) *Jacobian.* Measure of the element's deviation from an ideal shape

In order to increase the accuracy and reliability of the NLFEA, the recommended element quality measure limits for quadrilateral shell and solid brick elements are given in Section 3, Table 6.

Triangle shell or tetrahedral solid elements should not be used in areas of interest. They can be used in areas where finer mesh is transitioned into a coarse mesh, but their usage should be minimized.

Areas of interest will usually have a finer mesh. Due to the high computational cost of the NLFEA, the finer mesh may be transitioned into a coarser mesh away from the areas of interest. Mesh transitions should be done gradually.

TABLE 6
Recommended Quality Measure Limits for Quadrilateral Shell and Solid Brick Elements

Aspect Ratio	*Close to 1 as possible, but not > 3*
Skewness	< 60°
Warping	< 5°
Corner angle	> 45° and < 135°
Jacobian	> 0.6

The size of the mesh will have a very large impact on the computation time of NLFEA. The number of degrees of freedom (DOF) in the system depends on the type of structure, type of loading, expected failure modes, and the type of analysis. It should enable the representation of all relevant failure modes that are to be investigated. For example, the regions of the structure that are expected to have high compressive loads should have a mesh that is fine enough to be able to capture the main buckling failure modes of all structural members in that region. However, at a certain mesh size, further refinements will have a very small impact on the accuracy of the results. Therefore, a mesh sensitivity study should be carried out to assess the adequacy of the selected mesh size. It should be noted that the result convergence will not be attained at geometric discontinuities of the structure where singularities exist. At those locations, stresses and strains will always increase with further mesh refinements.

Mesh sensitivity studies require additional modeling and computation time and may not always be justified. Section 3, Table 7 contains guidance regarding the recommended mesh size for certain common types of NLFEA of marine and offshore structures.

For hull girder ultimate strength and residual analyses, small geometric details, such as cutouts for welds and stiffeners and stiffener brackets, may be neglected. However, larger cutouts, such as manholes and pipe and ventilation duct openings, should be modeled.

TABLE 7
Mesh Size Recommendations

Type of Analysis	*Mesh Size*
Simulation of tensile tests Small scale ductile fracture analysis Plate forming simulations	$t \times t$ for shell and $t \times t \times t$ for solid elements
Low-cycle fatigue of a critical detail	$t \times t$ for shell and $t \times t \times t$ for solid elements (second-order solid elements should be used, and weld should be modeled)

Type of Analysis	*Mesh Size*
Stiffened panel structural collapse and indentation	8 elements between stiffeners with aspect ratio close to 1 3 to 6 elements across the stiffener web height with aspect ratio close to 1 and size not larger than the size of the plate elements 2 elements across the full flange breadth of T type stiffeners with size not larger than the size of the plate elements 1 element across the flange breadth for L type stiffeners with size not larger than the size of the plate elements(1)
Hull girder ultimate strength and residual strength analyses	**Fine Mesh:** Extent: Hull girder compression flange extending five stiffener spaces from the deck or inner bottom in the vertical sense and five web-frame spaces in the longitudinal sense. • 6 to 8 elements between stiffeners with aspect ratio close to 1 • 3 to 6 elements across the stiffener web height with aspect ratio close to 1 with size not larger than the size of the plate elements • 2 elements across the full flange breadth of T type stiffeners with size not larger than the size of the plate elements • 1 element across the flange breadth for L type stiffeners with size not larger than the size of the plate elements(1)
	Coarse Mesh: 1 stiffener spacing with aspect ratio close to 1
Impact with ice	**Fine Mesh:** Extent: Ice belt. • 6 to 8 elements between stiffeners with aspect ratio close to 1 • 3 to 6 elements across the stiffener web height with aspect ratio close to 1 with size not larger than the size of the plate elements • 2 elements across the full flange breadth with size not larger than the size of the plate elements • 3 elements in the area where the bracket meets the longitudinal flange.
	Coarse Mesh: ½ stiffener spacing with aspect ratio close to 1
Plate forming	$r/5$; r = indenter radius
Local crushing analysis of thin plates (e.g., web frames)	8 elements per half-length of one structural fold H $H = 0.983b^{2/3}t^{1/3}$; b = plate breadth, t = plate thickness
Ship-to-ship collision	**Fine Mesh:** Extent: Area to be impacted by the striking ship. $10t \times 10t$, but not greater than 200 mm (7.874 in.) with aspect ratio close to 1
	Coarse Mesh: 1 stiffener spacing with aspect ratio close to 1

Note:

1. In case of stiffeners with bulb profile that are modeled with solid elements, finer mesh size may be required to adequately capture the shape of the bulb.

14 Element Choice

The element choice will depend on the type of the structure to be analyzed and the type of the analysis. Commercial NLFEA programs usually offer a large selection of elements to be used in the nonlinear analysis. A number of constitutive formulations usually exist for one element type (e.g., shell) each with its own set of advantages/disadvantages and application areas. In that regard, three main features of each element are:

- Element geometric shape (truss/beam, shell, or solid)
- Element order (first-order linear or second-order quadratic)
- Element integration level (full integration or reduced integration)

The structural analyst should be aware of any unwanted element behavior, such as *shear locking*, *volumetric locking,* and *hourglassing*, as these may impact the nonlinear analysis more than they do linear analysis.

14.1 Element Geometric Shape and Order

For the NLFEA of typical thin-walled marine and offshore structures, general-purpose first-order quadrilateral shell elements are usually sufficient for modeling all structural members. The elements should have at least five points through the thickness at each integration location to adequately model the nonlinear material behavior. The usage of triangular shell elements should be minimized in the locations of interest. Second-order elements will provide higher solution accuracy but should only be used when the expected solution is smooth. In other cases, first-order elements are preferred.

In cases where the through-thickness distribution of stresses and strains is important (e.g., low-cycle fatigue analysis), 3-D solid elements may be used. If second-order solid elements are used, one element across the plate thickness is usually sufficient, but if linear solid elements are used, then at least four elements across the plate thickness are recommended. Solid triangular prisms (wedge elements) may be used to model welds. Tetrahedral elements should be avoided in the areas of interest.

The use of beam and truss elements should be avoided in the areas of interest, except that first-order beam elements may be used to model stiffeners on primary structural members and flanges of longitudinals outside the fine mesh region. The use of beam elements may significantly increase the computation time when explicit dynamic analysis is performed, as stated in 3/5.2.2, and selective subcycling is recommended.

It is not recommended to mix first- and second-order elements in the model.

14.2 Element Integration Level

A finite element stiffness matrix is obtained by numerical integration of constitutive equations that model structural behavior of springs/trusses, beams, shells, and homogeneous solids. Most commercial NLFEA programs offer fully integrated and reduced integration elements. Reduced integration significantly reduces the computation time, and in some cases, may provide more accurate results because it eliminates element shear and volumetric locking. Shear locking may occur in first-order fully integrated elements where the spurious (parasitic) shear strains give rise to excessive stiffness in bending. Volumetric locking may occur in fully integrated elements where spurious pressure stresses render the element too stiff to deformations that cause no change in the volume of the element.

However, first-order elements with reduced integration are prone to hourglassing. This is a numerical issue that arises because the bending modes (which combined mode resembles the shape of an hourglass) of first-order elements with reduced integration have no strain energy associated with them. These spurious zero-energy modes need to be stabilized. Most commercial NLFEA programs have automatic hourglass control, which is recommended for all first-order reduced integration elements. Hourglassing can also be reduced by mesh refinements and by distributing the concentrated load over a larger area. The energy associated with hourglass control should be less than 5% of the total internal strain energy of the system.

For shell elements with three translational and three rotational DOF per node, only two in-plane rotational DOF are associated with the element stiffness. The element will have no rotational stiffness (or *drilling stiffness*) about the direction normal to the plane of the element. Most commercial NLFEA programs automatically add a small rotational stiffness to avoid this singularity while minimally affecting the solution accuracy. As with numerical stabilization, contact stabilization, and hourglass control, the energy associated with drilling stiffness should be less than 5% of the total internal strain energy of the system.

SECTION 4

Quality Control

1 Choice of NLFEA Program

The use of a well-tested and validated program is strongly recommended. The NLFEA program should be able to adequately model all types of nonlinearity and all relevant failure modes that are expected in the analyzed system. The selected NLFEA program should be well documented, and its basic theoretical background should be available to the structural analyst.

The structural analyst should possess a sound theoretical knowledge of the nonlinear finite element method and should be familiar with the selected NLFEA program, and its strengths and limitations. The analyst should be familiar with the behavior of the system to be analyzed and all its relevant failure modes in order to exercise sound professional judgment when assessing the adequacy of the nonlinear finite element analysis techniques and results.

2 General Recommendations for Improving Results Reliability

The following general recommendations are given in order to assist the structural analyst in achieving more reliable and accurate results when using NLFEA. More information can be found in Section 3.

i) Apply the load in multiple steps, each of which will contain multiple load increments. The static loads (gravity, hydrostatic pressure, etc.) are applied first, followed by the dynamic loads.

ii) If the NLFEA program fails to converge at the beginning of the analysis when the structure is expected to behave linearly, investigate the adequacy of the FE model, the boundary conditions, and the applied loads. The initial load increment may be too large, preventing the iteration algorithm from converging to a valid solution. The convergence issue may appear at the beginning of the analysis even if the initial increment is too small, especially if the loads or displacements are applied using the smooth step function.

iii) If needed, use numerical damping to stabilize sudden material or geometric instabilities. It should be verified that the stabilization energy does not exceed 5% of the total internal energy of the system.

iv) Apply initial geometric imperfections to convert bifurcation buckling into a continuous buckling problem, this avoiding sudden instability at the critical buckling load.

v) If needed, use surface smoothing and contact stabilization. The energy used to stabilize the contact should be monitored and should not exceed 5% of the total internal energy of the system.

vi) Discontinuity of the first derivative of the material flow curve may cause convergence issues. The flow curve should be specified at sufficiently large number of points to adequately describe the yielding of the material. Sudden changes in the tangent stiffness, as when the material starts to yield, may require smoothing out.

vii) If reversed loading or cyclic loading is applied, then the combined nonlinear kinematic/isotropic hardening material model is recommended.

viii) When running quasi-static analysis, kinetic energy should be monitored and should not exceed 5% of the total internal energy of the system, except at the beginning of the analysis. The linear behavior of the structure should be verified by comparing it to the solution of the linear FE analysis. To minimize the inertial effects at the beginning of the analysis, the loads or displacements should be applied using the smooth step function.

ix) When running dynamic analysis, input time series should be specified with sufficient resolution. Smoothing should be used when prescribed displacement time series are specified to provide continuity of the calculated accelerations. Smoothing of velocity time series is also recommended.

x) Sampling of the results during the dynamic analysis should be done with twice the highest vibration frequency of interest in the response of the structure.

xi) Caution should be exercised when using beam elements in explicit analysis as the beam cross-sectional properties, and not just the element length, density, and modulus of elasticity, can have a significant effect on the critical time increment.

xii) The use of triangular or tetrahedral elements should be minimized, and the aspect ratio of element sides should not exceed 3.

xiii) If first-order reduced integration elements are used, hourglass control should be applied. The energy needed to control the hourglassing should stay below 5% of the total internal energy of the system. A ratio greater than 5% indicates that mesh refinement or a different element type is needed.

xiv) The energy associated with adding the drilling stiffness to shell elements should stay below 5% of the total internal energy of the system.

3 Validating the Analysis Methodology and Results

The analysis methodology and the results should be validated against existing numerical and test results, when available. The reports from the International Ship and Offshore Structures Congress (ISSC) contain benchmark studies performed using various NLFEA programs (e.g., [16]).

Material parameters should be carefully calibrated against the experimental data. If such data is not available, data given in these Guidance Notes may be used.

Sensitivity studies with respect to the mesh size, material parameters, element type, and imperfection size and shape may be necessary, especially for novel designs.

4 Documenting the Analysis

Upon conclusion of the NLFEA, modeling techniques, input parameters, final results, and conclusions should be documented. The analysis report and model database should be submitted to ABS for review as deemed necessary. The level of detail in the report should enable an independent analysis. The report should cover the following items:

i) The objective of the analysis

ii) Relevant failure modes of the structure and its sources of nonlinearity

iii) Main assumptions

iv) Model geometry with reference to the technical drawings needed to create it

v) Model geometry simplifications

vi) Relevant load cases and loading approach including the load sequence

vii) Boundary conditions

viii) Finite element model extent, mesh size, and element type (hourglassing, locking, drilling stiffness)

ix) Geometric imperfections

x) Analysis type (e.g., static, quasi-static, dynamic)

xi) The plot of kinetic to internal energy ratio for quasi-static analysis

xii) Iteration algorithms (e.g., N-R, modified N-R, Arc Length)

xiii) Load (displacement) incrementation procedure

xiv) Time domain integration scheme (e.g., implicit, explicit)

xv) Result sampling frequency

xvi) Numerical stabilization and the plot of the ratio of stabilization energy to total internal energy

xvii) Materials and their respective models including the flow curve, hardening rule, and strain rate effects, if considered

xviii) Ductile fracture modeling details

xix) Contact modeling details

xx) The choice of applied partial safety factors and failure criteria with justifications

xxi) Detailed presentation of relevant results and the discussion of the same

xxii) Analysis conclusions and recommendations

APPENDIX **1**

Application Examples

1 General *(2021)*

The following examples highlight the practical application of the NLFEA. The main model and analysis input parameters are given, as well as the summary of the results. The examples are prepared with the commercial NLFEA program Abaqus [17], for illustrative purposes only, and not as an endorsement of the program. ABS will accept results from any reliable commercial FE program.

2 Ultimate Strength and Post-Collapse Analysis of a Stiffened Panel

A stiffened panel similar to the one shown in Section 3, Figure 13 is analyzed under uniaxial compression and biaxial-compression combined with the normal pressure acting on the unstiffened side of the panel. The force-displacement curves are given for various analysis types. Also, the effect of initial imperfections is shown.

2.1 Geometry, Material, and Initial Imperfections

The stiffened panel consists of the plate and four "T" stiffeners with dimensions as given in Appendix 1, Table 1 (also refer to Section 3, Figure 13). Three transverse web frames are not modeled. Instead, they are represented in the model with adequate boundary conditions (see A1/2.2). Initial imperfections are generated using trigonometric functions as explained in 3/10.3.

The material is taken as higher-strength steel HS32 with parameters described in Section 3, Table 4. Since the load application is without load reversals, isotropic hardening model is used.

TABLE 1
Model Geometry Parameters

Dimension	*Value mm (in.)*	*Description*
A	9000 (354.331)	Overall panel length ($1/2a + a + a + 1/2a$)
B	4200 (165.354)	Overall panel breadth
a	3000 (118.110)	Web frame spacing
b	840 (33.071)	Stiffener spacing
h_w	350 (13.780)	Height of web
b_f	150 (5.906)	Breadth of flange
t_p	20 (0.787)	Thickness of plate

Dimension	*Value mm (in.)*	*Description*
t_w	12 (0.472)	Thickness of web
t_f	18 (0.709)	Thickness of flange

2.2 Boundary Conditions and Loads

Appendix 1, Figure 1 shows the boundary conditions of the stiffened panel with four corners 1, 2, 3, and 4. To enable the application of biaxial loads and pressure, the panel is allowed to be compressed in both the *x* and *y* axes and is allowed to shear while all the edges 1-2 and 3-4 remain straight, as shown in Appendix 1, Figure 1. Also, the edge 1-2 remains parallel to the edge 3-4. Multi point constraints (MPC) of Slider type are used in Abaqus to enforce the edges 1-2 and 3-4 to remain straight. The edge 1-4 is restrained in the *x* direction, while all the nodes on the edge 2-3 are enforced to have an equal translation in the *x* direction.

FIGURE 1
Stiffened Panel Boundary Conditions

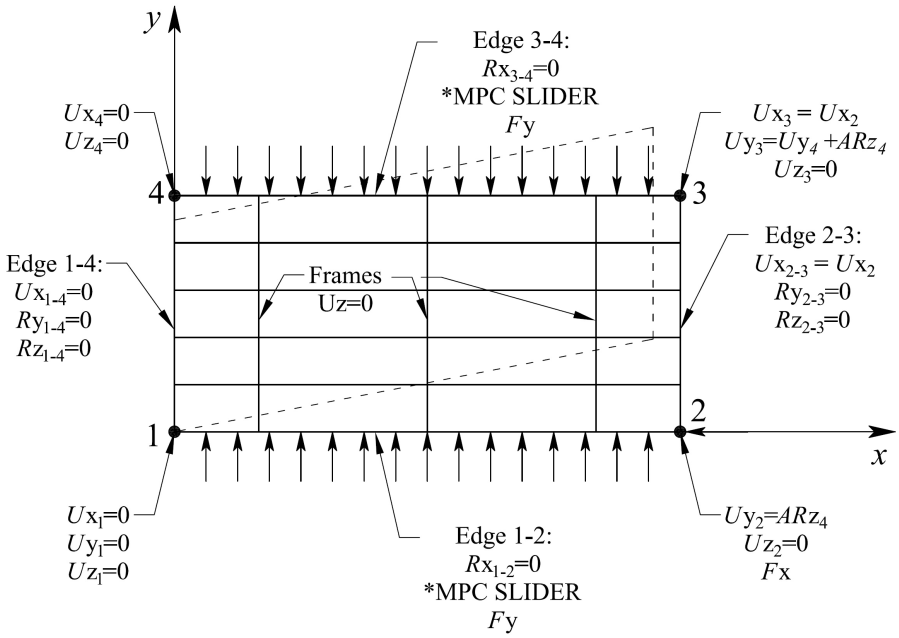

Making sure that the edges 1-2 and 3-4 remain parallel and that the edge 2-3 translates parallel to the *y* axis (all nodes of the edge 2-3 have the same translation in the *x* direction) is achieved by Equation type Constraints in Abaqus. For example:

$$
\begin{aligned}
Uy_3 &= Uy_4 + ARz_4 \\
Ux_3 &= Ux_2 \\
Ux_{2-3} &= Ux_2 \qquad (A1.1) \\
Uy_2 &= ARz_4
\end{aligned}
$$

where

Uy_3	=	translation in the *y* direction of corner 3
Uy_4	=	translation in the *y* direction of corner 4
Ux_3	=	translation in the *x* direction of corner 3

Ux_2 = translation in the x direction of corner 2

Ux_{2-3} = translation in the x direction of edge 2-3

Uy_2 = translation in the y direction of corner 2

Rz_4 = rotation around the z axis of corner 4

A = overall stiffened panel length as specified in Appendix 1, Table 1.

In order to properly model the stiffener web to web frame welded connection, Kinematic Coupling is used to connect the master node at the intersection of plate, stiffener web, and plane of the transverse web frame to all the slave nodes of the stiffener web in the plane of the transverse web frame (see Appendix 1, Figure 2). Only the translation in the y direction is coupled. Also, displacement in the z direction, Uz, is prevented at the intersections of the transverse web frames and the stiffened panel plate.

A compressive load along the edges 1-2 and 3-4 in the y direction, Fy, is applied as a concentrated force distributed uniformly at all the edge nodes (corner nodes should be loaded with ½ of the force at other nodes). A compressive load along the edge 2-3 in the x direction, Fx, is applied as a concentrated force at node 2. The boundary conditions and constraints at nodes 2, 3, and edge 2-3 provide a uniform distribution of Fx along the edge 2-3. In some analyses, the uniform pressure of 0.2 N/mm^2 (0.020 kgf/mm^2, 29.01 psi) is also applied on the unstiffened side of the panel before the uniaxial or biaxial compression are applied.

FIGURE 2
Kinematic Coupling Between Stiffener Web and Web Frame

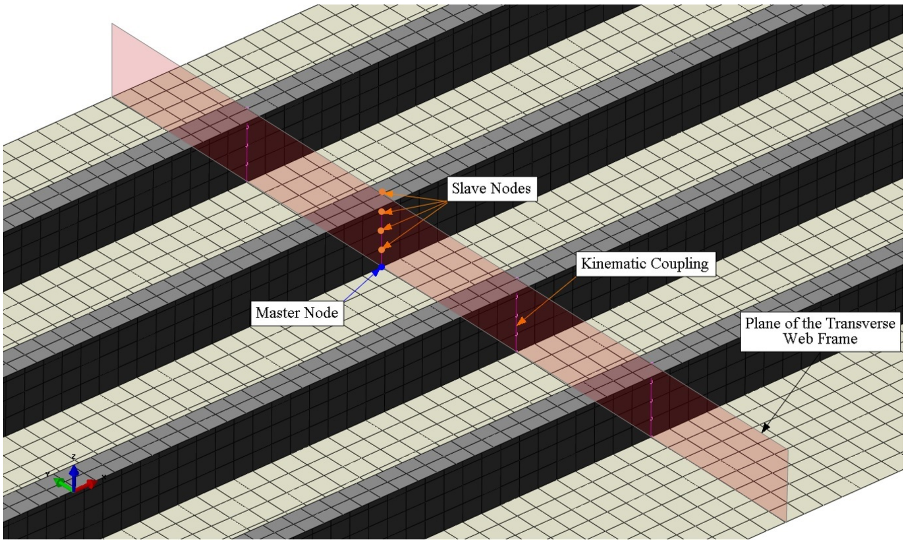

Instead of applying compressive concentrated force at corner 2 (load control), in some analyses, the displacements in the x direction are applied at corner 2 (displacement control). The difference in the results between the load control and the displacement control are shown in A1/2.4.

The following three load cases are considered:

i) Uniaxial compression

ii) Constant pressure and uniaxial compression

iii) Constant pressure and biaxial compression applied proportionally so that $Fy = 0.5Fx$

2.3 Mesh Size and Element Type

Mesh size is selected in accordance with the recommendations in Section 3, Table 7. Eight elements are generated across the stiffener spacing, four elements across the stiffener web, and two elements across the stiffener flange. Element side aspect ratio of all the elements is close to one.

All generated elements are first-order shell quadrilaterals with full integration – S4 elements in Abaqus. These are general purpose shell elements applicable to small and finite strains and thick and thin plates.

2.4 Analysis Type

Two different analysis types are used: static and quasi-static. Also, two different loading approaches are used: displacement control and load control.

Static analysis is performed using both the Arc-Length and the Newton-Raphson algorithms. The N-R static analysis is stabilized using adaptive stabilization with the maximum ratio of stabilization to internal strain energy not exceeding 1%.

Quasi-static analysis is performed using an implicit time integration scheme. The implicit analysis is run using the "Quasi-Static" settings in Abaqus. The effect of the inertia forces is further minimized by reducing the material density (reversed mass scaling; see 3/5.2.3 and 3/5.3) by an order of magnitude and by extending the load application time to ten seconds (from the original one second for the static analysis).

In the implicit quasi-static analyses, the loads or displacements are applied using a Smooth Step amplitude option in Abaqus (see 3/5.3). This helps with the convergence, and it also minimizes the inertial effect at the beginning of the analysis by gradually increasing the load application rate.

Nonlinear geometry is considered in all analysis types using NLGEOM = on in Abaqus.

2.5 Results

2.5.1 Uniaxial Compression *(2021)*

Appendix 1, Figure 3 compares the load-displacement curves obtained using different analysis types for the case of pure uniaxial compression.

FIGURE 3
Load-Displacement Curves for Uniaxial Compression *(2021)*

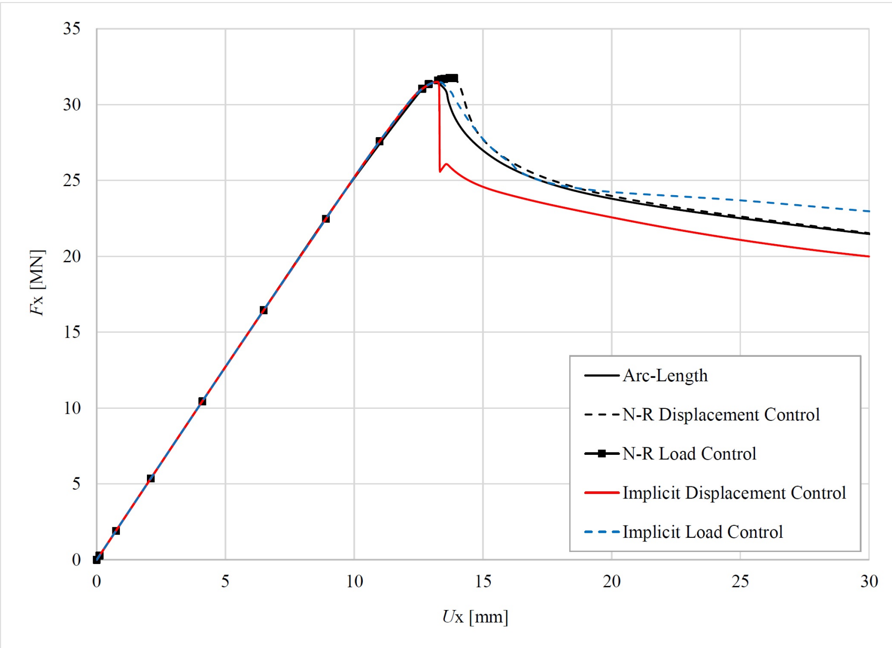

Since the Arc-Length algorithm treats the load increments as part of the solution, they can either be positive or negative (applied load increases or decreases during the analysis). Therefore, the Arc-Length algorithm can trace the load-displacement curve beyond the limit point (ultimate strength). The static N-R algorithm can only do that when displacement control is used. Otherwise, if the load control is used, the static N-R algorithm stops at the limit point. Up to the limit point, load and displacement controls yield the same results with the static N-R algorithm.

The implicit quasi-static analysis can trace the load-displacement curve beyond the limit point with either the load control or the displacement control. However, when the load control is used, the implicit quasi-static analysis starts to experience the accelerated collapse once the limit point is reached. After the limit state is reached, the internal forces in the panel are no longer purely static, but also contain the inertia component, which grows as the applied load is increased. Therefore, the implicit quasi-static load-displacement curve for the load control is above all the other curves for axial displacements greater than 20 mm (0.866 in.).

Appendix 1, Figure 4 shows the ratio of kinetic (*ALLKE*) and internal strain energies (*ALLIE*) for the implicit quasi-static analysis with displacement and load control. The energy ratio is plotted against the displacement. At the ultimate strength point, the energy ratio starts to increase. During the displacement control, the inertial effects are quickly dampened, always staying well below the 5% threshold as mentioned in 3/5.2.2 and 3/5.3. During the load control, the inertial effects cannot be dampened as the applied load keeps increasing beyond the limit point, and the kinetic energy quickly crosses the threshold. This part of the load-controlled analysis can no longer be considered quasi-static.

FIGURE 4
Kinetic to Internal Energy Ratio for Implicit Quasi-Static Analyses *(2021)*

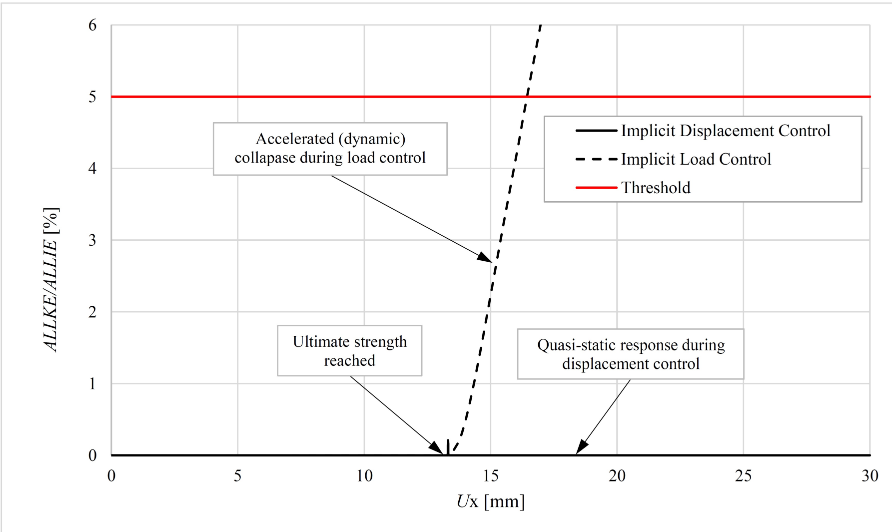

All the analysis types provide very similar estimates of the ultimate strength of the panel, although there are some differences in the post-ultimate strength region. Appendix 1, Figure 5 shows the von Mises stresses in the top surface of the plate and the deformed shape of the stiffened panel at the ultimate strength and at the end of the Arc-Length static analysis. The panel collapses between the second and third transverse web frame where the size and shape of the initial imperfections is critical for the initiation and progression of the collapse.

2.5.2 Pressure and Biaxial Compression

Appendix 1, Figure 6 shows the load displacement curves for the three load cases mentioned in A1/2.2. The Arc-Length algorithm is used in all three analyses. The load-displacement curves in the *x* direction are plotted for all three load cases as the load in the x direction is common for all of them. The uniaxial load-displacement curve is the same as in Appendix 1, Figure 3.

It is seen how the constant pressure of 0.2 N/mm^2 (0.020 kgf/mm^2, 29.01 psi) decreases the ultimate strength of the panel. If compression in the *y* direction is added, the ultimate strength of the panel decreases even further. It is also seen that the addition of the compression in the *y* direction slightly increases the initial linear stiffness of the panel in the *x* direction.

2.5.3 The Effect of Initial Imperfections

The load displacement curves for the case with and without the initial imperfections are given in Appendix 1, Figure 7. In order to facilitate the convergence, the case with "No Imperfections" contains 5% of the standard initial imperfections as calculated using the expressions in 3/10.3. It is seen that the imperfections cause approximately 9.4% decrease in the ultimate strength of the panel. The "No Imperfections" curve clearly shows when the material starts to yield (yield plateau), and when the stiffened panel suddenly buckles. When the imperfections are present, it is difficult to clearly separate yielding from buckling as there will be some response in the buckling mode right from the start of the analysis.

FIGURE 5
von Mises Stresses in the Stiffened Panel

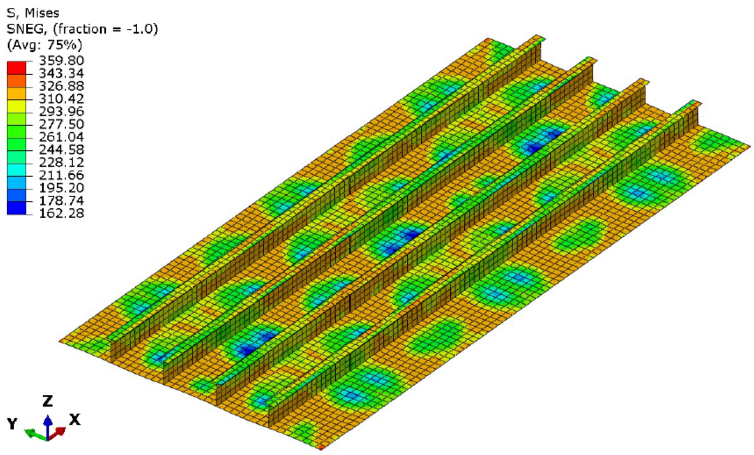

a) At the ultimate strength point – axial displacement in the x direction = 13.14 mm (0.517 in.)

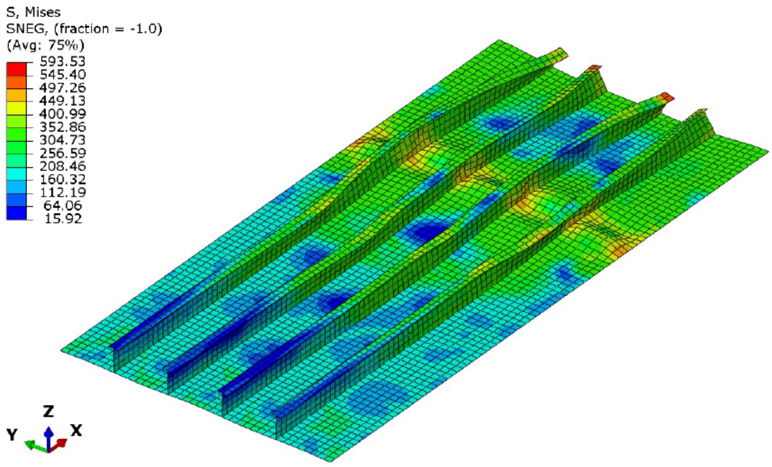

b) At the end of the analysis – axial displacement in the x direction = 60.60 mm (2.386 in.)

FIGURE 6
Load-Displacement Curves for All Three Load Cases

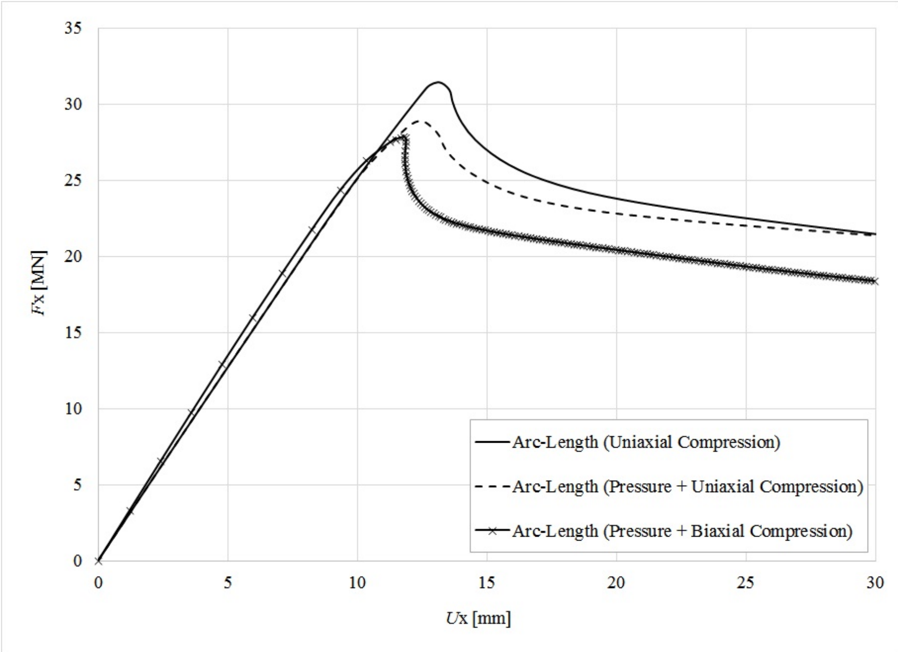

FIGURE 7
The Effect of Imperfections on the Load Displacement Curve

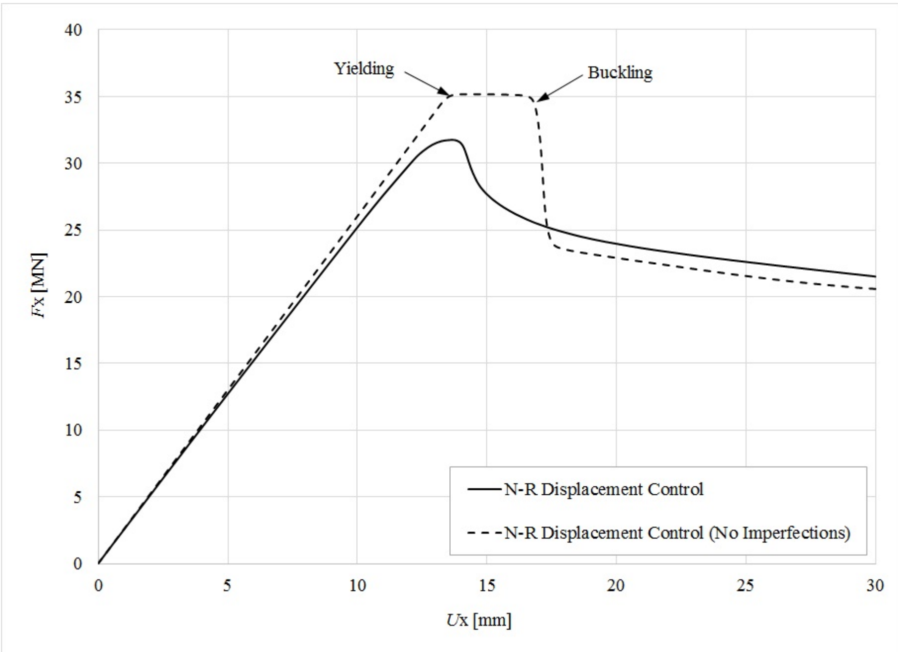

3 Ultimate Strength and Post-Collapse Analysis of a Hull Girder

An ultimate strength and post-collapse behavior of a bulk carrier is analyzed in the intact and damaged (residual strength) conditions. Only the vertical bending moment is considered in the analysis. Hogging and sagging conditions are considered for the intact hull girder. Hogging is considered for the grounding damage and sagging is considered for the collision damage. More information about this example can be found in [18].

3.1 Geometry, Material, and Initial Imperfections

The computer aided design (CAD) model of a bulk carrier is shown in Appendix 1, Figure 8. A ½ + 1 + ½ hold model is considered in accordance with Section 3, Table 3.

FIGURE 8
CAD Model of the Bulk Carrier

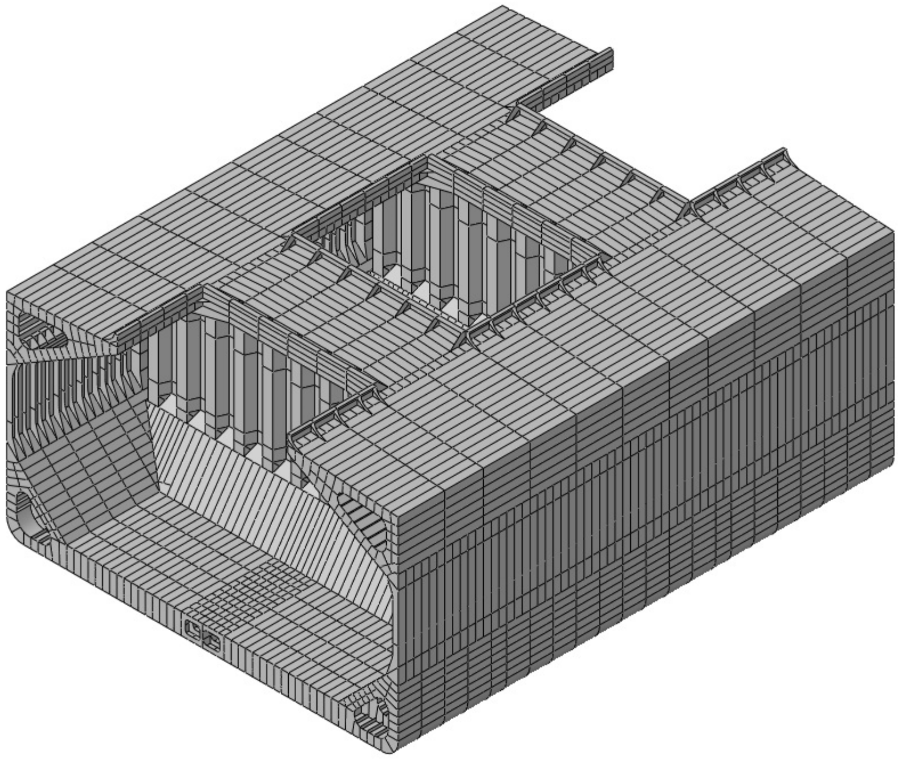

The hull is made of mild steel (MS), and higher-strength steels HS32 and HS36. Since the load application is without load reversals, the isotropic hardening model is used.

The method of superposition of buckling modes is used because of its convenience when large structures are considered and the fact that such imperfections will conservatively trigger the main plate and stiffener buckling modes during the analysis. The scaling of the buckling modes is calculated so that the largest plate out-of-plane deformation is equal to $b/200$, where b is the width of the plate between the stiffeners.

3.2 Boundary Conditions and Loads

Curvature control is used to apply a pure vertical bending moment on the hull girder. Equal in magnitude, but opposite in sign, rotations of the cross sections around the horizontal transverse axis are simultaneously incremented at the reference points at both ends of the model (see Appendix 1, Figure 9). All DOF of the reference point are kinematically coupled with the corresponding DOF of all the nodes on the two end cross sections. The two reference points are placed at the neutral axis level. At the aft end of the model, the vertical and transverse translations of the reference point are restricted ($Uy = Uz = 0$), while at the forward end, all translations are restricted ($Ux = Uy = Uz = 0$), as well as the rotation around the longitudinal axes ($Rx = 0$). Rotation around the transverse axis is prescribed symmetrically at the reference points on both ends of the model ($Ry = c$ and $Ry = -c$) where c is the rotation magnitude. Such constraints prevent rigid body motion of the model, and the kinematic coupling forces the cross sections to remain in plane. In order to achieve a pure vertical bending loading away from the model boundaries, it is important that one end of the model is not restrained in the longitudinal direction. This eliminates the axial forces throughout the model and allows the neutral axis to freely shift and rotate for asymmetrically damaged and/or loaded hulls. In this example, both collision and grounding damage are asymmetric about the vessel's centerline.

FIGURE 9
Hull Girder Boundary Conditions

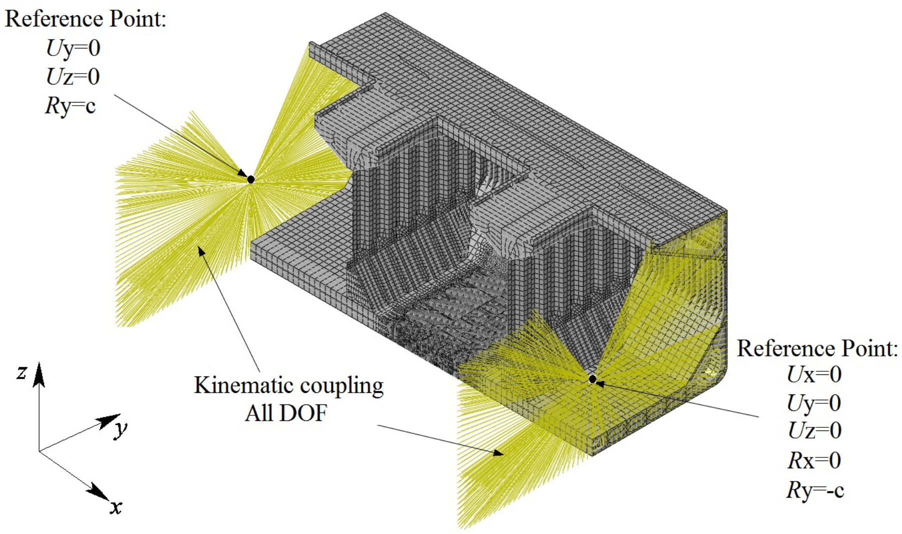

3.3 Mesh Size and Element Type

The regions of the model that are expected to have high compressive stresses should have a mesh that is fine enough to be able to capture main buckling failure modes of structural members. Away from the hull compression flanges (e.g., deck in sagging and double bottom in hogging), the fine mesh is gradually transitioned into a coarser mesh in order to minimize the computation time.

The following mesh characteristics are applied in accordance with Section 3, Table 7:

i) Only the compression hull girder flange is modeled using finer mesh with an element size of about 100 mm (3.937 in.) (eight elements between the longitudinals and at least three elements across the web of the longitudinal)

ii) Other parts of the model are meshed using an element size approximately equal to the spacing of longitudinals

iii) At least two shell elements across the full flange of the longitudinals are used in the region of finer mesh

iv) The finer mesh is gradually transitioned into the coarser mesh

v) The longitudinal extent of the finer mesh is limited to the middle portion of the two-hold model (approximately five web frame spacings)

vi) All longitudinals in the fine mesh region are meshed using shell elements as well as the webs of longitudinals in the coarser mesh region

vii) Beam elements are used only for the stiffeners on transverse structural members and for flanges of longitudinals outside the fine mesh region

viii) All large openings in structural members are modeled in the fine mesh region

All quadrilateral shell elements are first-order full integration general purpose elements (S4) applicable to small and finite strains and thick and thin plates. The usage of triangular shell elements is minimized, especially in the fine mesh region. Timoshenko beam elements (B31) are used for the stiffeners on transverse structural members and for flanges of longitudinals outside the fine mesh region.

3.4 Damage Extent

Collision and grounding damage are considered as two separate cases. Damage is assumed to have a rectangular shape with transverse dimensions similar to the ones specified for collision and grounding in [19]. Appendix 1, Figure 10 shows schematically the transverse damage extent for the bulk carrier. The collision and grounding damage extents are shown on the same figure for simplicity only. The grounding damage is positioned so that it includes the bilge, thus creating the greatest amount of geometric asymmetry. The grounding damage reaches three quarters of the double bottom height, leaving only the inner bottom plating with its longitudinals.

In the longitudinal direction, the collision and grounding damage spans three web frame spacings, including the transverse structure at the ends of the damage extent. The ends of the damage include sharp stress concentration raisers that are left on purpose in the FE models to simulate stress concentrations in the real-world damage case.

FIGURE 10
Damage Extent

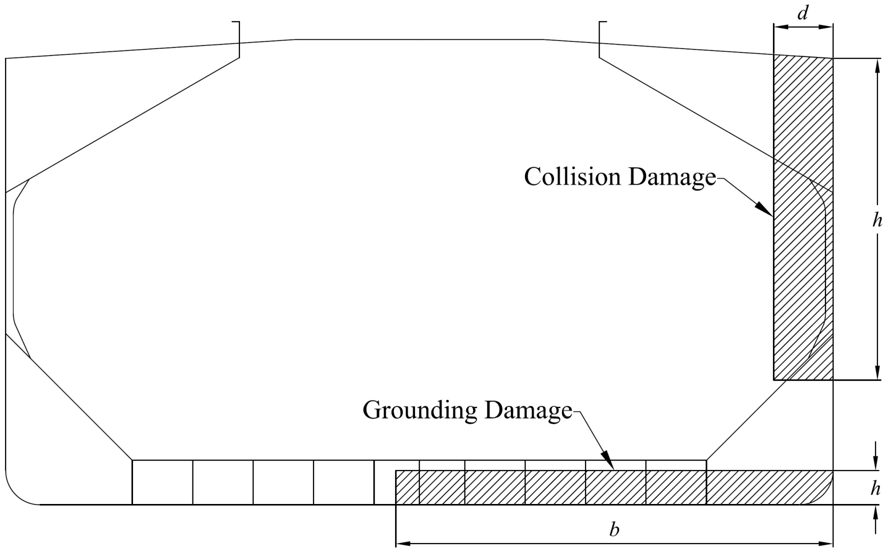

3.5 Analysis Type

Results are obtained using explicit quasi-static analysis with reversed mass scaling where the density of the material is reduced by an order of magnitude to minimize the inertial effects. Explicit analysis is selected because it is very effective on large systems.

The curvature is applied using a Smooth Step amplitude option in Abaqus (see 3/5.3). This minimizes the inertial effect at the beginning of the analysis by gradually increasing the curvature application rate. Curvature application time is one second.

The relatively small number of beam elements in the model governs the critical time increment of the explicit analysis. Therefore, selective subcycling is used to decrease the computation time, as stated in 3/5.2.2.

Nonlinear geometry is considered in all analyses using NLGEOM = on in Abaqus. Also, double precision is used for the analysis and the packager (preprocessor).

A small amount of viscous damping should be introduced when running explicit analysis to control high frequency oscillations. In Abaqus, this is achieved by specifying linear and quadratic bulk viscosity parameters. The default values are 0.06 and 1.2, respectively, and are considered suitable for most types of analysis.

3.6 Results

Appendix 1, Figure 11 shows the moment curvature (load-displacement) plots for the sagging and hogging conditions of the intact and damaged structure. It is seen how the collision and grounding damage decrease the ultimate strength of the hull girder.

Appendix 1, Figure 12 shows the interframe collapse mode of the intact bulk carrier in the hogging condition. Interframe collapse mode is very common for intact ship structures.

Appendix 1, Figure 13 shows the non-interframe collapse mode of the bulk carrier with the grounding damage in hogging. It is seen that the entire inner bottom on the damaged side has buckled due to the lack of the primary support members such as floors and longitudinal girders. The intact side of the double bottom experiences the interframe collapse.

Appendix 1, Figure 14 shows the collapse mode of the bulk carrier with collision damage in sagging. It is seen how the interframe collapse mechanism originates at the sharp corner of the damage in the deck subjected to compressive loads.

In order to verify that the quasi-static stable response is obtained using explicit analysis, the ratio of kinetic (*ALLKE*) and internal strain energies (*ALLIE*) is plotted for all analyses in Appendix 1, Figure 15. Except at the beginning of each analysis, the ratio of energies stays below the 5% threshold, as stated in 3/5.2.2 and 3/5.3. It is also a good practice to check the behavior of the structure at the beginning of the analysis by comparing the response of the NLFEA with the response of a purely linear analysis. This is shown in Appendix 1, Figure 16 for the case of the intact bulk carrier in hogging. It is seen that a stable quasi-static response is achieved at the beginning of the analysis as well.

FIGURE 11
Moment-Curvature Curves for Intact and Damaged Conditions

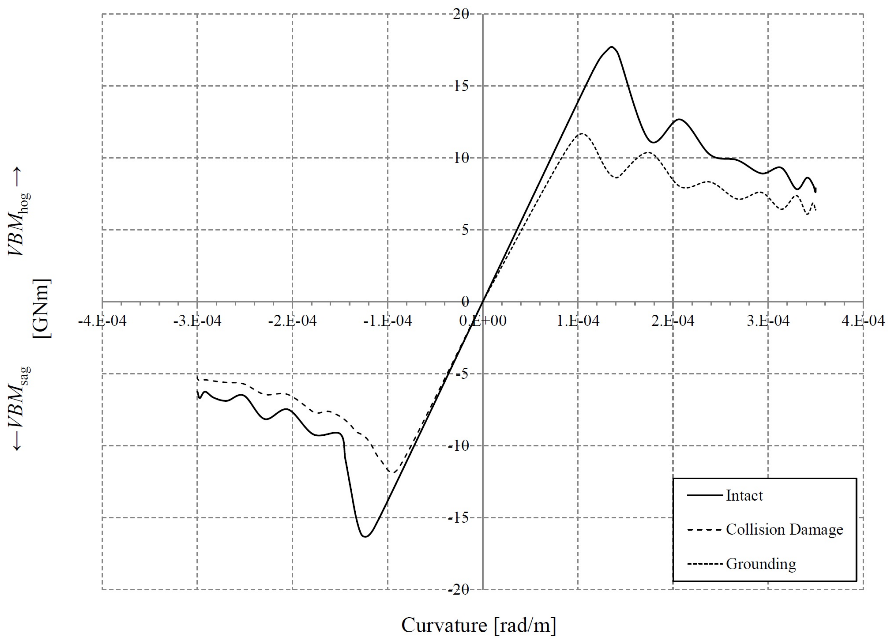

FIGURE 12
Interframe Collapse mode of the Intact Bulk Carrier in Hogging

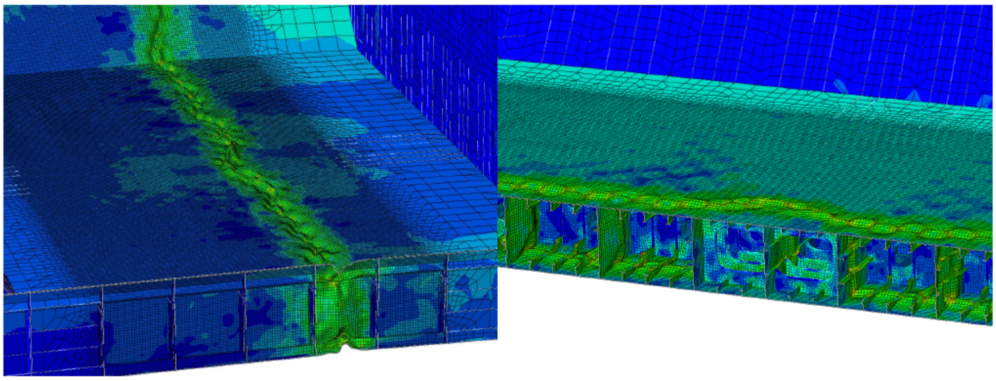

FIGURE 13
Collapsed Bulk Carrier with Grounding Damage in Hogging

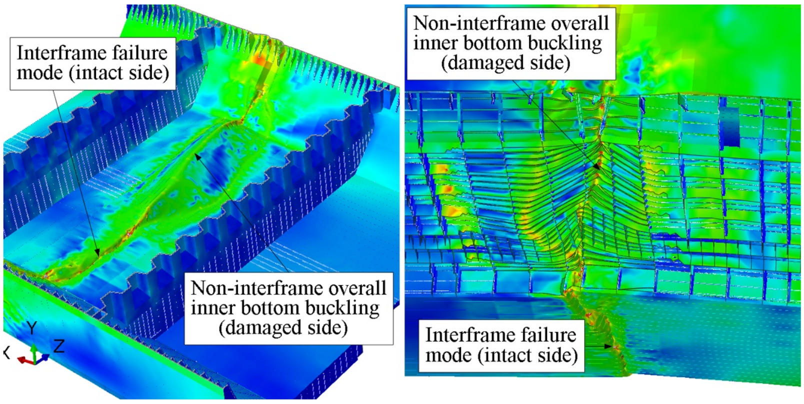

FIGURE 14
Collapsed Bulk Carrier with Collision Damage in Sagging

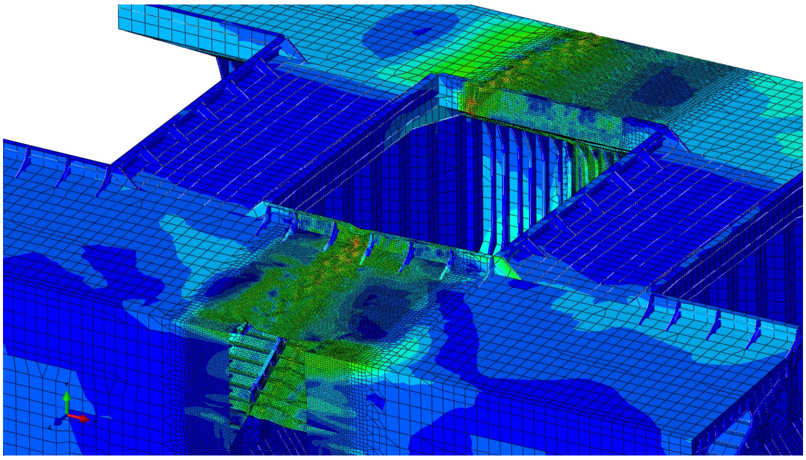

FIGURE 15
Kinetic to Internal Energy Ratios

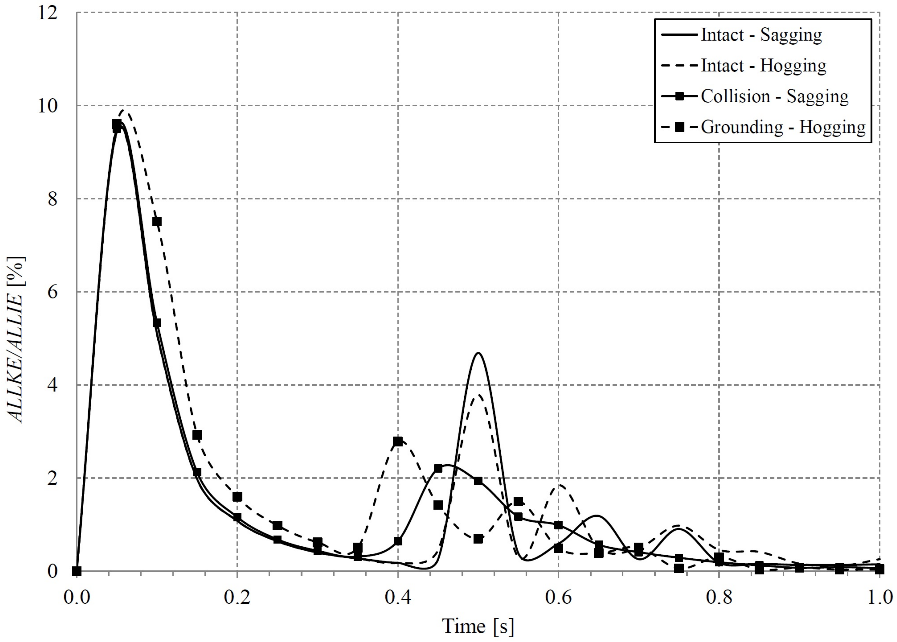

FIGURE 16
Comparison Between Linear and Nonlinear FEA

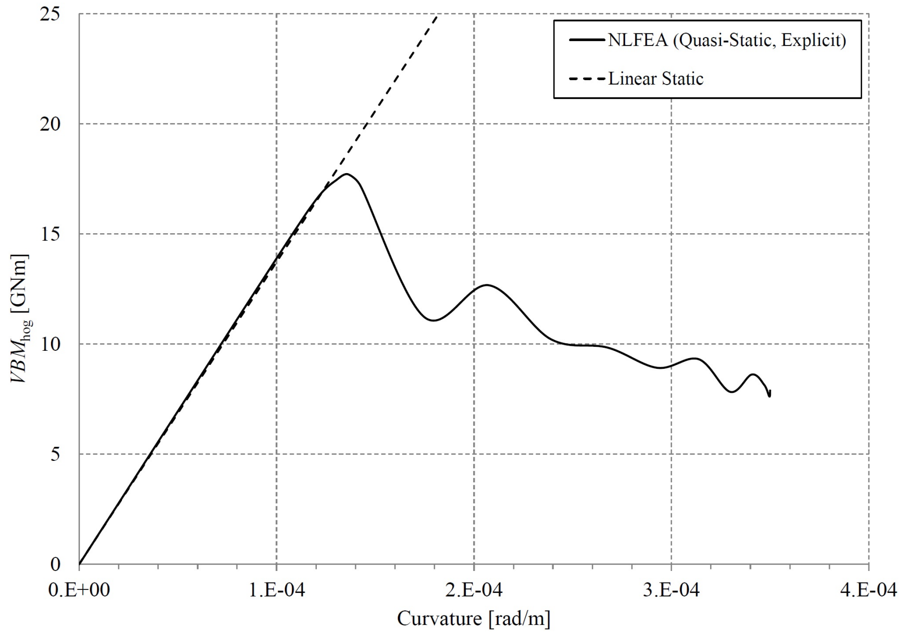

4 Time-Domain Analysis of Container Lashing System

A single nine-tier container stack with double external lashing and a rigid 2-tier lashing bridge is analyzed under significant harmonic roll. Maximum twistlock tension, corner post compression, and lashing rod tension are calculated.

Tall container stacks exhibit strong nonlinear behavior caused primarily by:

i) Container corner separations (containers can separate without any resistance until the twistlock clearance value is exhausted and the twistlock engages)

ii) Inability of the lashing rod to carry compressive loads

iii) Coupling between the overturning moment about the base of the stack and the relative transverse deformation of the stack caused mainly by the container corner separations on the tension side of the stack and the resulting container rigid body rotations

Material nonlinearity does not significantly affect the stack forces up to their allowable limits and does not need to be considered in nonlinear static or time-domain analyses.

4.1 Container Stack Modeling

All nine containers are standard International Organization for Standardization (ISO) 40 feet high cube containers.

4.1.1 Twistlocks

The containers are mutually connected with twistlocks. Fully automatic twistlocks (FATs) are used above the highest lashing point, and semi-automatic twistlocks (SATs) are used below the highest lashing point. Twistlocks are modeled in Abaqus using Cartesian Connectors with prescribed clearance (gap) values in all three directions (see Appendix 1, Table 2). Appendix 1, Figure 17 shows the nonlinear force-separation behavior of the twistlocks. Friction in the twistlocks is also modeled using Coulomb's Law.

TABLE 2
Twistlock Clearances

	Clearance mm (in.)		
	Vertical	*Transverse*	*Longitudinal*
FAT	0-30 (0-1.181)	± 0.75 (± 0.030)	± 4 (± 0.157)
SAT	0-12 (0-0.472)	± 0.75 (± 0.030)	± 4 (± 0.157)

FIGURE 17
Nonlinear Behavior of Twistlocks

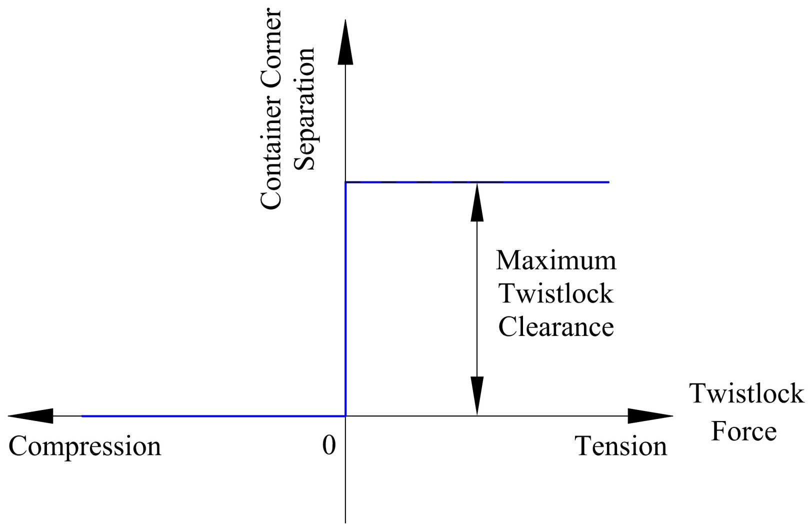

4.1.2 Lashing Rods

The container stack is secured to the 1-tier lashing bridge with the double external lashing pattern that connects the bottom container corners of the third tier and top container corners of the second tier with the top platform of the lashing bridge, as can be seen in Appendix 1, Figure 19. Lashing rods are modeled as nonlinear springs having almost zero stiffness in compression and linear stiffness in tension. The lashing rod stiffness in tension is determined based on the lashing rod diameter, length, and the effective modulus of elasticity, as specified in the ABS *Guide for Certification of Container Securing Systems*. Appendix 1, Figure 18 shows the nonlinear behavior of the lashing rod when transitioning from tension to compression.

FIGURE 18
Nonlinear Behavior of Lashing Rods

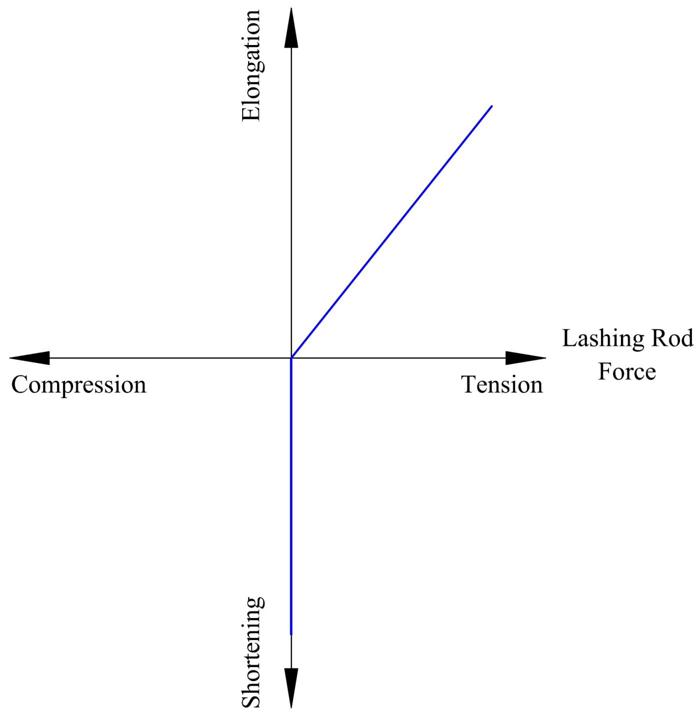

4.1.3 Container Masses and Mass Proportional Damping

Container cargo is modeled as a point mass located in the middle of the container in the longitudinal and transverse directions and at 45% of the container height. The cargo mass moments of inertia are specified under the assumption of a homogeneous mass distribution inside the container up to 90% of the container height. The cargo mass is then connected using Distributed Continuum coupling to all four corners of the container so that it can follow the motion of the container in an average sense. The cargo mass and the container structural mass give the total mass of the loaded container which can be seen in Appendix 1, Figure 19 for each tier.

Mass proportional damping from the Rayleigh damping model is specified for container cargo and structural masses. The damping coefficient α is calibrated based on measurement data for a similar nine tier stack with double external lashing.

4.2 Boundary Conditions and Loads

Harmonic rolling is prescribed at the instantaneous center of roll (COR) of the vessel. All other DOF are fixed at the COR, which is then kinematically coupled with the twistlocks at the bottom of the stack and with the bottom ends of each lashing rod, as shown in Appendix 1, Figure 19.

Gravity is first applied in a separate step of the analysis over a time period of two seconds using Smooth Step function to avoid numerical issues and noise in the results.

In the next step, harmonic roll with an amplitude of 14° and a period of 26 seconds is applied as a time series of prescribed roll motion at the COR of the vessel. Five full roll cycles are analyzed. The roll amplitude is gradually increased from 0° to 14° over the first 26 seconds of the analysis in order to avoid numerical issues at the start of the analysis and results that have too much noise. Appendix 1, Figure 20 shows the time history of applied roll motion at the COR.

FIGURE 19
Container Stack Modeling

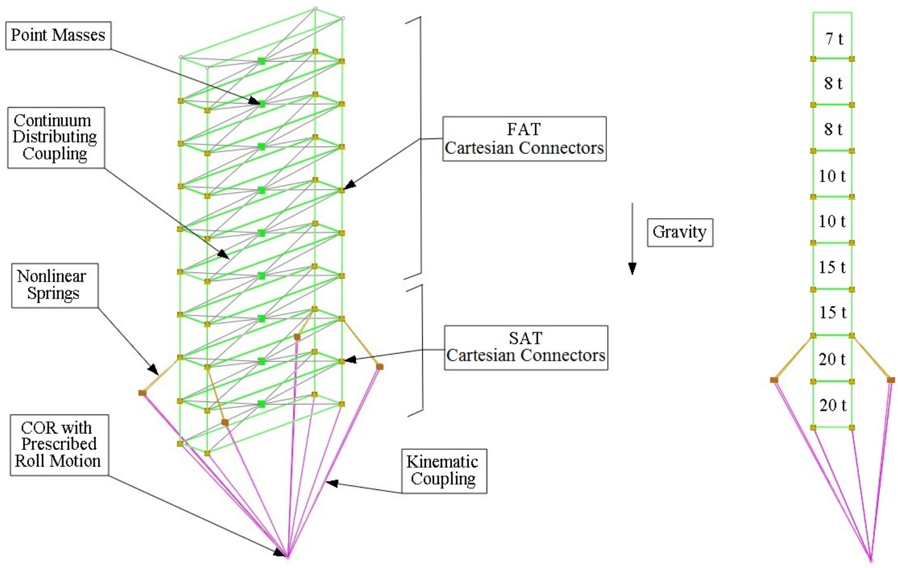

FIGURE 20
Time History of Applied Roll Motion at COR

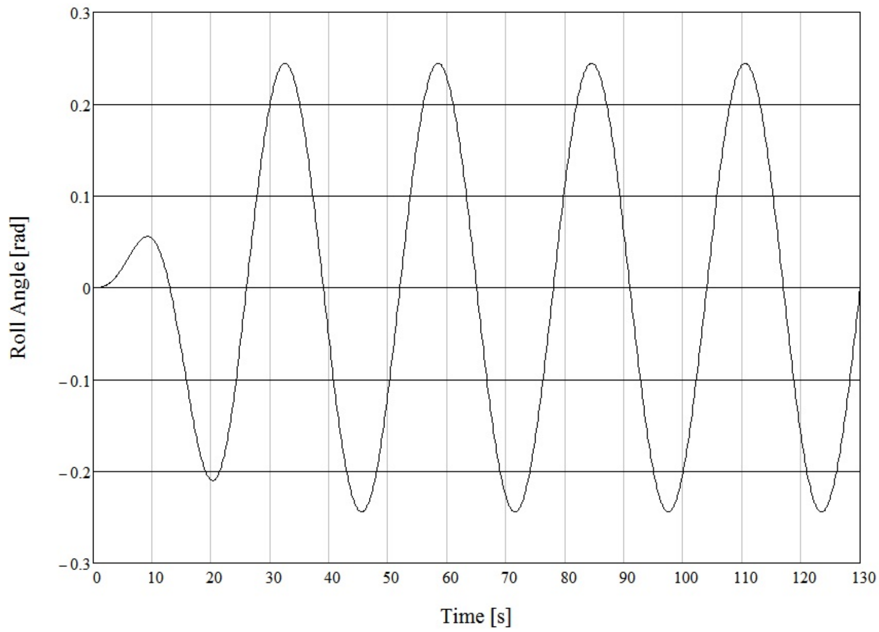

The prescribed roll motion time series is entered tabularly into Abaqus. Care should be taken that the input time series is smooth enough, since the tabular data will be linearly interpolated and will not have continuous first derivatives. If a time derivative of the input time series is required (e.g., in order to get velocity and acceleration from a prescribed displacement), and if the resolution of the input time series is coarse, this can create a substantial amount of noise in the results. In this case, smoothing of the input time series should be used. Abaqus applies quadratic smoothing across a fraction of the time intervals before and after each point of the input time series. A fraction value equal to 0.05 is recommended when input time series are coarse. In this example, the input roll time series interval is very small (1 ms), and the smoothing does not have a big impact.

When performing dynamic analysis, attention should be paid to the sampling frequency of the response (frequency at which the results are saved). If this frequency is less than twice the highest frequency expected in the response of the structure, then *aliasing* will occur, meaning that the time series of the results will not be completely defined, and loss of information and distortion of the time series will occur. In this example, a sampling frequency of 23 Hz is used, which is sufficient since the highest expected relevant frequency is about 5 Hz. Anything above 5 Hz can be considered as numerical noise and can be filtered out. In this example, time series of the results are filtered using the Butterworth filter with a cutoff frequency of 5 Hz. The amount of noise present in the results is found to be very small, however.

4.3 Mesh Size and Element Type

Each container is constructed using only Timoshenko beam elements (B31) with one element per container edge. Beam General Section is used in Abaqus to directly define the cross-sectional properties of each element (cross-sectional area, moments of inertia, torsion constant, modulus of elasticity, Poisson ratio, density, damping, and transverse shear). All these properties are calibrated so that the container has matching racking stiffness constants on all sides as required by the ABS *Guide for Certification of Container Securing Systems*. This modeling technique enables an adequate simulation of the container global structural response without the need for modeling the container corrugated plating.

4.4 Analysis Type

Explicit time-domain nonlinear analysis is used to determine the response of the container stack to harmonic roll motion. This type of analysis has proven very effective in simulating the dynamic behavior of container stacks, especially when multiple stacks, even whole bays, are modeled and the contact between containers is simulated. Also, twistlock and lashing rod failure can be simulated, which may lead to stack collapse and loss of containers.

Nonlinear geometry is considered using NLGEOM = on in Abaqus. Also, double precision is used for the analysis and the packager (preprocessor).

A small amount of viscous damping should be introduced when running explicit analysis to control high frequency oscillations. In Abaqus, this is achieved by specifying linear and quadratic bulk viscosity parameters. The default values are 0.06 and 1.2, respectively, and are considered suitable for most types of analysis.

4.5 Results

Time series of maximum twistlock tension, corner post compression, and lashing rod tension occurring in the stack are given in Appendix 1, Figure 21, Figure 22, and Figure 23, respectively. It is seen that all force time series exhibit a periodic, albeit not harmonic, response, which is a characteristic of a nonlinear system. Since the roll amplitude is slowly ramped up during the first roll cycle, the results reach a steady state during the second cycle. Another feature common to all the results is the local vibratory response of the stack as it rolls over to one side. This is evident in the oscillations of the time series around the peak values.

Appendix 1, Figure 21 shows the time series with the maximum twistlock tension of 247.8 kN (25.27 tf, 24.87 Ltf) (positive twistlock force) which occurs in the first FAT above the highest lashing point. This is very common since this is the first twistlock unprotected by the lashing rods with all the above containers pulling on it. The twistlock separation time series is also plotted on the same graph. It is seen that the tension force in the twistlock only exists when the maximum twistlock clearance of 20 mm (0.787 in.) is exhausted and the twistlock engages.

Appendix 1, Figure 22 shows the maximum corner post compression of 715.7 kN (72.98 tf, 71.83 Ltf). It occurs in tier-2 container, which is also common for this type of lashing pattern and lashing bridge height.

Corner post compression is calculated by combining the top corner twistlock force with the vertical component of the lashing rod tension attached to the same container corner, if present. Care should be taken regarding signs of the forces when combining the two time series.

FIGURE 21
Maximum Twistlock Tension (TT)

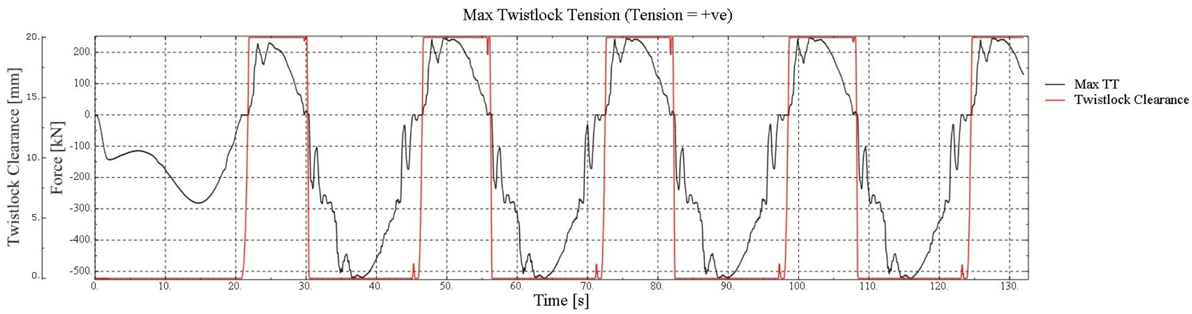

FIGURE 22
Maximum Corner Post Compression (CPC)

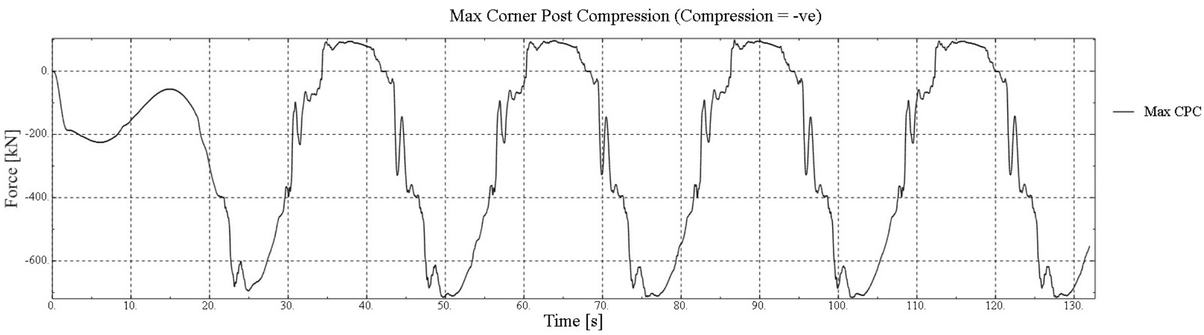

Appendix 1, Figure 23 shows two lashing rod tension time series: the maximum lashing rod tension among all upper lashing rods (rods connecting the bottom container corners of the third tier with the lashing bridge) and the maximum lashing rod tension among all lower lashing rods (rods connecting the top container corners of the second tier with the lashing bridge). Due to the separation of the corners between the upper and lower lashing rods, caused by the twistlock clearance, the upper lashing rod will have larger elongation, and thus, larger tensile forces. Maximum tension in the upper lashing rods is 233.9 kN (23.85 tf, 23.47 Ltf) and the maximum tension in the lower lashing rods is 89.0 kN (9.08 tf, 8.93 Ltf). Linear analysis cannot account for the twistlock clearance and thus predicts equal forces in both lashing rods. It is also seen in Appendix 1, Figure 23 that there is no compression force in the lashing rods due to the specified nonlinear behavior of the lashing rods. The maximum upper and lower lashing rod tension forces occur on the opposite sides of the container (port side and starboard side). This is why the two time series are out of phase.

FIGURE 23
Maximum Lashing Rod Tension (LRT)

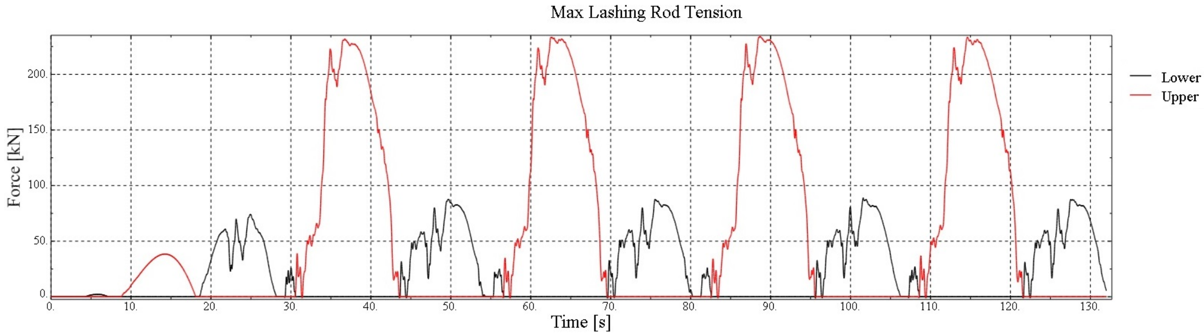

In the absence of twistlock clearances, the container stack will deform, relative to its base, only due to container racking, and these transverse deformations are generally small. However, twistlock clearances enable additional rigid body rotation of each container, and this causes the container stack to significantly deform relative to its base. Such significant deformation causes coupling between the overturning moment about the base of the stack and the relative transverse deformation of the stack. As the stack deforms, the moment around the base of the stack increases. This effect cannot be captured by linear stack analysis. Appendix 1, Figure 24 shows the maximum relative stack deformation of the stack at the instant of largest roll angle. The stack is shown such that its base is in the horizontal position, and its roll angle is indicated in Appendix 1, Figure 24 by the orientation of the coordinate system.

FIGURE 24
Relative Transverse Deformation of the Stack

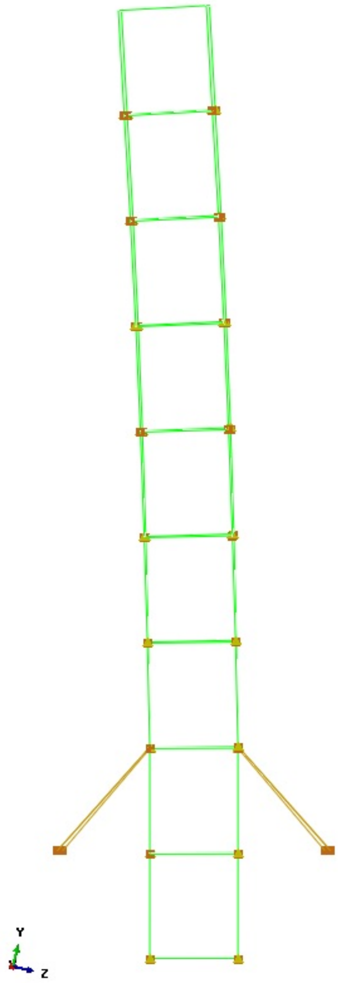

5 Indentation of a Stiffened Panel *(2021)*

This example demonstrates the use of NLFEA to analyze the impact between a stiffened panel and a rounded rigid indenter causing plastic deformation and ductile fracture of the stiffened panel. The problem is treated dynamically. Strain-rate hardening is simulated using the Cowper-Symonds mode, in accordance with 3/9.5. The fracture is also modeled using the linear damage accumulation law with the Liu ductile fracture criteria described in 3/11.

5.1 Geometry and Material *(2021)*

The stiffened panel geometry is shown in Appendix 1, Figure 25 and the panel particulars are given in Appendix 1, Table 3. The stiffened panel is impacted by a small semi-spherical indenter with a radius r = 300 mm (11.811 in.) and a mass of 12 t (26455.5 lb) from the unstiffened side. The indenter is placed in the middle of the model between the stiffeners. At the beginning of the analysis, the top of the indenter is one millimeter away from the plate, including the thickness of the plate. This is done to avoid initial contact overclosures.

FIGURE 25
Model Geometry and Boundary Conditions *(2021)*

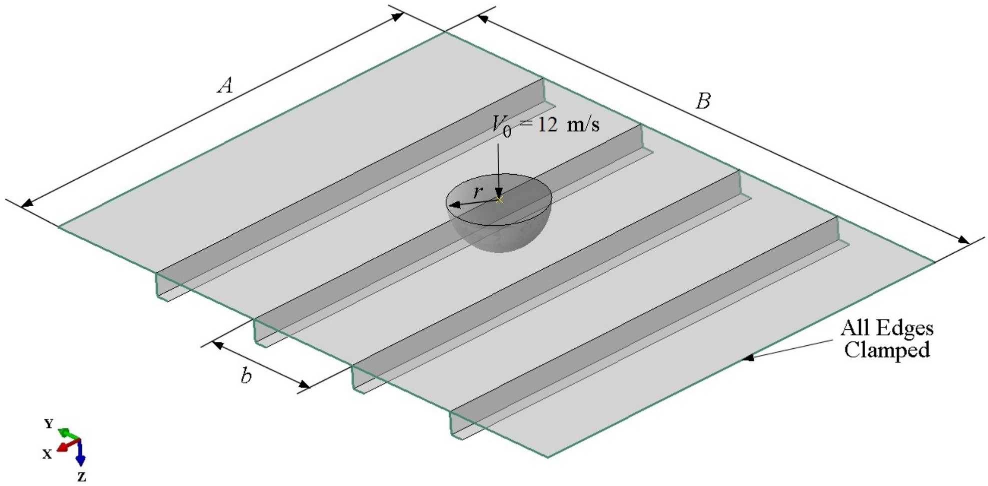

TABLE 3
Model Geometry Parameters

Dimension	*Value mm (in.)*	*Description*
A	3000 (118.110)	Overall panel length
B	4050 (159.449)	Overall panel breadth
b	810 (31.890)	Stiffener spacing
h_w	150 (5.906)	Height of web
b_f	90 (3.543)	Breadth of flange
t_p	6 (0.236)	Thickness of plate
t_w	9 (0.354)	Thickness of web
t_f	9 (0.354)	Thickness of flange
r	300 (11.811)	Radius of the indenter

Material of the panel is HS32 steel with parameters described in Section 3, Table 4. Since there are no load reversals or cyclic loads, isotropic hardening model is used. Strain rate hardening is simulated using the Cowper-Symonds model, which for high tensile steels has C = 3200 s^{-1} and q = 5, in accordance with recommended values from Section 3, Table 5. In Abaqus, this is selected as the Power Law Rate Depended hardening suboption of the Plastic material behavior with Multiplier = 3200 and Exponent = 5.

In this example, Liu ductile fracture criteria [20] is used. This criterion is of the form given by Eq. 3.31 with a constant critical fracture strain for a certain element size and plate thickness. The Liu criterion is given in Eq. A1.2, which also shows how the criterion is modeled in Abaqus using the Johnson-Cook linear damage accumulation law (only available for explicit analysis):

$$\varepsilon_{cf} = 0.5 - 0.01\frac{L}{t}$$

$$d_1 = 0.5 - 0.01\frac{L}{t} = 0.5 - 0.01\frac{30}{6} = 0.45 \quad \ldots\ldots\ldots\ldots \quad (A1.2)$$

$$d_2 = d_3 = d_4 = d_5 = 0$$

as explained in 3/11, where L = 30 mm (1.181 in.) is the size of the stiffened panel plate elements and t = 6 mm (0.236 in.) is the plate thickness. As described in [12], the Liu criterion is particularly suitable for simulating penetrations with a rounded indenter, such as the one used in this example. The criterion is valid for L/t in the range from 5 to 20 for mild and high tensile steels. The Liu criterion assumes there is no ductile fracture evolution. In Abaqus, this is modeled using Displacement at failure = 0 in the Damage Evolution suboption of the Johnson-Cook Damage material behavior.

No initial imperfections are modeled, as they have a negligible impact on this kind of analysis.

5.2 Boundary Conditions and Loads *(2021)*

All edges of the panel are clamped, as can be seen in Appendix 1, Figure 25. This is a conservative assumption. In a real case scenario (e.g., object dropped onto a deck of a vessel), the edges of the panel will be allowed to deform, and the energy of the impact will be absorbed by a larger part of the deck structure.

The indenter has an initial velocity of 12 m/s (39.37 ft/s) in the z direction perpendicular to the stiffened panel plate (see Appendix 1, Figure 25). There are no other externally applied loads. Therefore, once the simulation starts, the energy of the system remains constant, and the initial kinetic energy of the indenter is mainly transformed into the internal strain energy of the stiffened panel. A part of the initial kinetic energy is dissipated through friction, contact, ductile fracturing, and bulk viscous dissipation. As the kinetic energy of the indenter is transformed into the internal energy of the stiffened panel or dissipated, the indenter slows down. The analysis is run for one second, during which the indenter penetrates through the stiffened panel and continues moving in the same direction at a significantly reduced speed.

5.3 Mesh Size and Element Type

The entire stiffened panel is meshed using first-order shell quadrilaterals with full integration (S4). These are general purpose shell elements applicable to small and finite strains and thick and thin plates.

A uniform mesh size of 30 mm (1.181 in.) is used with an element side ratio equal to one for all elements. The mesh size was selected to be $5t$, where t = 6 mm (0.236 in.) is the plate thickness. This is the finest mesh admissible by the Liu ductile fracture criteria, as noted in 3/11.

A rigid semi-spherical indenter is meshed using R3D4 bilinear rigid quadrilaterals and a small number of R3D3 linear rigid triangles. Mesh size for the indenter is also 30 mm (1.181 in.). This enables a smooth contact.

5.4 Contact Modeling

The General contact algorithm is used to model contact between the indenter and the stiffened panel, where Abaqus assigns the contact pairs automatically, including the self-contact.

The Hard Contact pressure-overclosure relationship is used in the normal direction with the Penalty constraint enforcement method.

Frictional behavior is specified in the tangential direction using the Penalty frictional formulation with a coefficient of friction equal to 0.3.

5.5 Analysis Type

Explicit dynamic analysis is performed. Nonlinear geometry is considered using NLGEOM = on. A small amount of viscous damping should be introduced when running explicit analysis to control high frequency oscillations. In Abaqus, this is achieved by specifying linear and quadratic bulk viscosity parameters. The default values are 0.06 and 1.2, respectively, and are considered suitable for most types of analysis.

5.6 Results *(2021)*

Appendix 1, Figure 26 shows the distribution of the equivalent plastic strain, $\bar{\varepsilon}_p$ (PEEQ in Abaqus), on a punctured stiffened panel at the end of the analysis. As soon as the equivalent plastic strain reaches the fracture limit (PEEQ = 0.45) at all through thickness sections of a shell element on at least one integration point, the element is deleted, and the fracture occurs. This is clearly indicated in Appendix 1, Figure 26, where the maximum contour of PEEQ is 0.45 and occurs close to the rim of the fracture.

FIGURE 26
Equivalent Plastic Strain Distribution on a Punctured Stiffened Panel *(2021)*

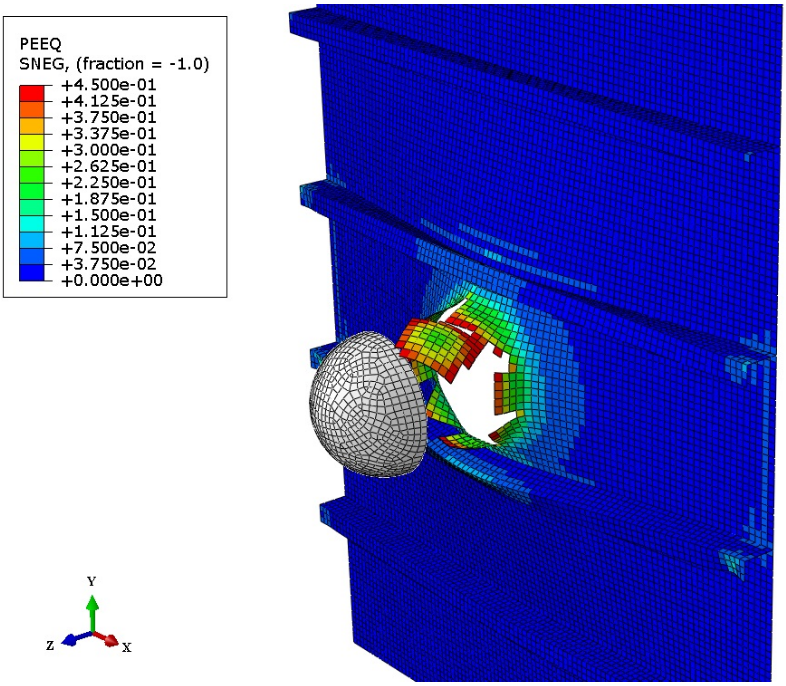

Appendix 1, Figure 26 also shows the areas with permanent plastic deformation (*PEEQ* > 0). At the end of the analysis, the elastic strains are recovered, and the small vibrations of the panel caused by a sudden impact are faded.

The average displacement of the plate in the *z* direction around the fracture (not including the jagged edges of the puncture) is approximately equal to 300 mm (11.811 in.). Using Eq. 3.17, the strain rate can be estimated at 20 s^{-1}. At this strain rate, the hardening effect on the material flow curve will be significant. The relationship between the dynamic and static true flow curves can be obtained by using Eq. 3.16:

$$\sigma(\varepsilon)_{dyn} = 1.36\sigma(\varepsilon) \quad \text{(A1.3)}$$

where $\sigma(\varepsilon)_{dyn}$ is the dynamic true flow curve and $\sigma(\varepsilon)$ is the static true flow curve. Therefore, the dynamic yield stress is 36% greater than the static yield stress.

Appendix 1, Figure 27 shows plots of the energy absorbed by the stiffened panel (internal astrain energy *ALLIE*) over time. Cases with and without the strain rate effect are shown. The initial kinetic energy of the indenter is 0.864 MJ. It is seen that about 92.4% of that kinetic energy is absorbed by the stiffened panel when strain rate hardening effect is considered. When it is not considered, only 57.6% of the initial kinetic energy of the indenter is absorbed by the stiffened panel.

6 Impact with Ice

For an example of the application of NLFEA to analyze the impact of vessel's side structure with ice, see the ABS *Guidance Notes on Ice Class*.

FIGURE 27
Absorbed Energy Over Time *(2021)*

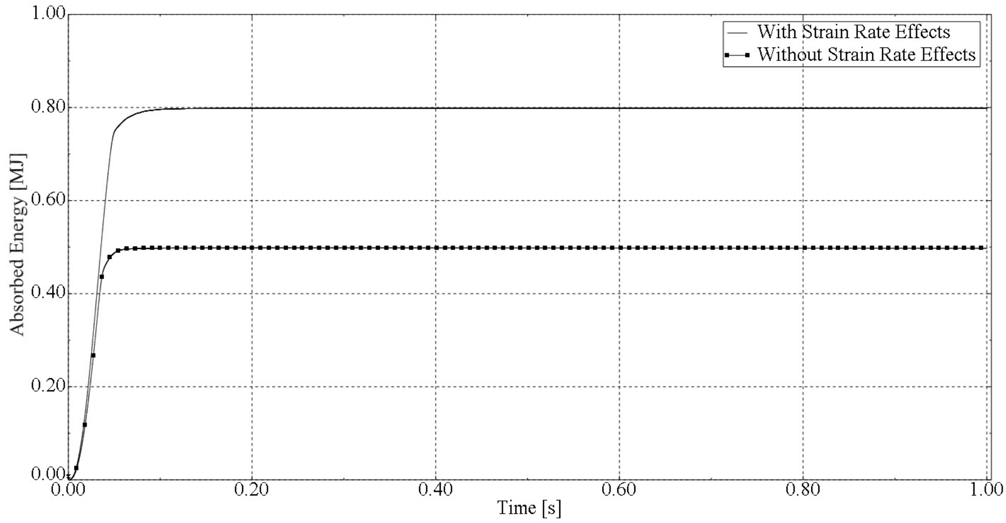

APPENDIX 2

Tabulated True Flow Curves

TABLE 1
Steel Grades MS, HS32, HS36

MS			*HS32*			*HS36*		
True Strain ε *[%]*	*True Plastic Strain* $\varepsilon_p=\varepsilon-\sigma/E$ *[%]*	*True Stress* σ *[N/mm²]*	*True Strain* ε *[%]*	*True Plastic Strain* $\varepsilon_p=\varepsilon-\sigma/E$ *[%]*	*True Stress* σ *[N/mm²]*	*True Strain* ε *[%]*	*True Plastic Strain* $\varepsilon_p=\varepsilon-\sigma/E$ *[%]*	*True Stress* σ *[N/mm²]*
0.000	0.000	0.000	0.000	0.000	0.000	0.000	0.000	0.000
0.112	0.000	235.263	0.150	0.000	315.473	0.169	0.000	355.600
0.456	0.344	236.074	0.485	0.334	316.530	0.499	0.329	356.775
0.800	0.688	236.888	0.819	0.668	317.592	0.829	0.659	357.955
1.145	1.032	237.705	1.154	1.003	318.657	1.159	0.988	359.138
1.489	1.375	238.525	1.489	1.337	319.725	1.489	1.318	360.325
1.861	1.744	245.974	1.861	1.705	328.349	1.861	1.685	369.970
2.233	2.113	253.499	2.233	2.073	337.061	2.233	2.053	379.713
2.606	2.481	261.102	2.606	2.441	345.858	2.606	2.420	389.551
2.978	2.850	268.781	2.978	2.809	354.733	2.978	2.788	399.473
3.878	3.742	287.661	3.878	3.700	376.322	3.878	3.677	423.558
4.779	4.633	306.820	4.779	4.591	397.021	4.779	4.567	446.402
5.680	5.525	325.823	5.680	5.483	414.730	5.680	5.459	465.522
6.581	6.417	343.841	6.581	6.377	428.375	6.581	6.353	480.019
7.481	7.310	359.896	7.481	7.273	438.962	7.481	7.248	491.330
8.382	8.205	373.450	8.382	8.169	447.952	8.382	8.144	501.090
9.283	9.100	384.704	9.283	9.066	456.254	9.283	9.041	510.216
10.184	9.996	394.290	10.184	9.963	464.304	10.184	9.937	519.131
11.084	10.893	402.841	11.084	10.860	472.301	11.084	10.834	528.024
11.985	11.790	410.813	11.985	11.757	480.338	11.985	11.730	536.980

MS			HS32			HS36		
True Strain ε [%]	*True Plastic Strain ε_p=ε-σ/E [%]*	*True Stress σ [N/mm²]*	*True Strain ε [%]*	*True Plastic Strain ε_p=ε-σ/E [%]*	*True Stress σ [N/mm²]*	*True Strain ε [%]*	*True Plastic Strain ε_p=ε-σ/E [%]*	*True Stress σ [N/mm²]*
12.886	12.687	418.491	12.886	12.654	488.463	12.886	12.627	546.044
13.787	13.584	426.044	13.787	13.551	496.700	13.787	13.523	555.239
14.687	14.481	433.572	14.687	14.447	505.063	14.687	14.419	564.578
15.588	15.378	441.135	15.588	15.344	513.561	15.588	15.316	572.641
16.489	16.276	448.767	16.489	16.242	518.785	16.489	16.215	577.584
17.390	17.173	456.493	17.390	17.141	523.147	17.390	17.113	582.303
18.290	18.070	464.328	18.290	18.040	527.321	18.290	18.012	586.819
19.191	18.967	472.283	19.191	18.939	531.326	19.191	18.910	591.150
20.092	19.863	480.364	20.092	19.838	535.176	20.092	19.809	595.313
20.993	20.760	488.578	20.993	20.737	538.883	20.993	20.708	599.321
21.893	21.657	496.931	21.893	21.636	542.458	21.893	21.607	603.185
22.794	22.555	502.353	22.794	22.535	545.911	22.794	22.506	606.917
23.695	23.454	506.677	23.695	23.434	549.251	23.695	23.405	610.526
24.596	24.353	510.874	24.596	24.333	552.486	24.596	24.304	614.021
25.496	25.251	514.954	25.496	25.232	555.623	25.496	25.203	617.409
26.397	26.150	518.923	26.397	26.132	558.667	26.397	26.102	620.697
27.298	27.049	522.788	27.298	27.031	561.625	27.298	27.001	623.891
28.199	27.948	526.555	28.199	27.930	564.502	28.199	27.901	626.997
29.099	28.847	530.229	29.099	28.830	567.303	29.099	28.800	630.021
30.000	29.746	533.815	30.000	29.729	570.031	30.000	29.699	632.966

TABLE 2
Steel Grades HS40, HS43, HS47

HS40			HS43			HS47		
True Strain ε [%]	*True Plastic Strain ε_p=ε-σ/E [%]*	*True Stress σ [N/mm²]*	*True Strain ε [%]*	*True Plastic Strain ε_p=ε-σ/E [%]*	*True Stress σ [N/mm²]*	*True Strain ε [%]*	*True Plastic Strain ε_p=ε-σ/E [%]*	*True Stress σ [N/mm²]*
0.000	0.000	0.000	0.000	0.000	0.000	0.000	0.000	0.000
0.186	0.000	390.724	0.200	0.000	420.840	0.219	0.000	461.008
0.511	0.325	391.999	0.522	0.322	422.198	0.536	0.317	462.474
0.837	0.650	393.279	0.844	0.643	423.561	0.854	0.634	463.944
1.163	0.976	394.562	1.167	0.965	424.928	1.171	0.950	465.420

HS40			*HS43*			*HS47*		
True Strain ε [%]	*True Plastic Strain ε_p=ε-σ/E [%]*	*True Stress σ [N/mm^2]*	*True Strain ε [%]*	*True Plastic Strain ε_p=ε-σ/E [%]*	*True Stress σ [N/mm^2]*	*True Strain ε [%]*	*True Plastic Strain ε_p=ε-σ/E [%]*	*True Stress σ [N/mm^2]*
1.489	1.301	395.850	1.489	1.286	426.300	1.489	1.267	466.900
1.861	1.668	406.116	1.861	1.654	437.172	1.861	1.634	478.728
2.233	2.036	416.486	2.233	2.021	448.152	2.233	2.000	490.673
2.606	2.403	426.951	2.606	2.387	459.224	2.606	2.367	502.707
2.978	2.770	437.482	2.978	2.754	470.323	2.978	2.733	514.723
3.878	3.659	462.576	3.878	3.643	495.987	3.878	3.621	541.755
4.779	4.549	484.478	4.779	4.534	516.166	4.779	4.513	561.513
5.680	5.442	500.666	5.680	5.428	530.013	5.680	5.407	574.908
6.581	6.337	512.583	6.581	6.324	540.768	6.581	6.303	585.860
7.481	7.233	522.601	7.481	7.220	550.517	7.481	7.198	596.150
8.382	8.130	531.956	8.382	8.116	560.017	8.382	8.094	606.332
9.283	9.026	541.134	9.283	9.013	569.520	9.283	8.990	616.583
10.184	9.922	550.324	10.184	9.909	579.121	10.184	9.886	626.967
11.084	10.819	559.605	11.084	10.805	588.858	11.084	10.782	636.811
11.985	11.715	569.014	11.985	11.701	597.469	11.985	11.680	642.286
12.886	12.611	578.568	12.886	12.600	602.572	12.886	12.579	647.405
13.787	13.509	585.317	13.787	13.498	607.369	13.787	13.477	652.216
14.687	14.407	590.229	14.687	14.397	611.898	14.687	14.376	656.754
15.588	15.306	594.887	15.588	15.296	616.187	15.588	15.274	661.051
16.489	16.204	599.316	16.489	16.194	620.263	16.489	16.173	665.132
17.390	17.103	603.541	17.390	17.093	624.147	17.390	17.072	669.019
18.290	18.002	607.579	18.290	17.992	627.857	18.290	17.971	672.731
19.191	18.901	611.449	19.191	18.891	631.410	19.191	18.870	676.284
20.092	19.800	615.164	20.092	19.790	634.818	20.092	19.769	679.691
20.993	20.699	618.737	20.993	20.690	638.094	20.993	20.668	682.964
21.893	21.598	622.179	21.893	21.589	641.248	21.893	21.568	686.115
22.794	22.497	625.501	22.794	22.488	644.289	22.794	22.467	689.153
23.695	23.396	628.710	23.695	23.388	647.226	23.695	23.366	692.085
24.596	24.296	631.816	24.596	24.287	650.067	24.596	24.266	694.920
25.496	25.195	634.824	25.496	25.186	652.817	25.496	25.165	697.664
26.397	26.094	637.741	26.397	26.086	655.482	26.397	26.065	700.323
27.298	26.994	640.573	27.298	26.985	658.068	27.298	26.964	702.902

HS40			*HS43*			*HS47*		
True Strain ε *[%]*	*True Plastic Strain* $\varepsilon_p=\varepsilon-\sigma/E$ *[%]*	*True Stress* σ *[N/mm²]*	*True Strain* ε *[%]*	*True Plastic Strain* $\varepsilon_p=\varepsilon-\sigma/E$ *[%]*	*True Stress* σ *[N/mm²]*	*True Strain* ε *[%]*	*True Plastic Strain* $\varepsilon_p=\varepsilon-\sigma/E$ *[%]*	*True Stress* σ *[N/mm²]*
28.199	27.893	643.326	28.199	27.885	660.580	28.199	27.864	705.407
29.099	28.792	646.002	29.099	28.784	663.023	29.099	28.763	707.841
30.000	29.692	648.608	30.000	29.684	665.399	30.000	29.663	710.209

TABLE 3
Steel Grades HS51, HS56, HS63

HS51			*HS56*			*HS63*		
True Strain ε *[%]*	*True Plastic Strain* $\varepsilon_p=\varepsilon-\sigma/E$ *[%]*	*True Stress* σ *[N/mm²]*	*True Strain* ε *[%]*	*True Plastic Strain* $\varepsilon_p=\varepsilon-\sigma/E$ *[%]*	*True Stress* σ *[N/mm²]*	*True Strain* ε *[%]*	*True Plastic Strain* $\varepsilon_p=\varepsilon-\sigma/E$ *[%]*	*True Stress* σ *[N/mm²]*
0.000	0.000	0.000	0.000	0.000	0.000	0.000	0.000	0.000
0.238	0.000	501.190	0.262	0.000	551.440	0.295	0.000	621.830
0.551	0.312	502.760	0.568	0.306	553.135	0.593	0.298	623.690
0.863	0.624	504.335	0.875	0.612	554.835	0.892	0.595	625.554
1.176	0.936	505.915	1.182	0.918	556.540	1.190	0.893	627.424
1.489	1.248	507.500	1.489	1.224	558.250	1.489	1.191	629.300
1.861	1.614	520.302	1.861	1.590	572.327	1.861	1.555	645.172
2.233	1.980	533.227	2.233	1.955	586.540	2.233	1.920	661.175
2.606	2.346	546.234	2.606	2.321	600.840	2.606	2.285	677.057
2.978	2.712	559.151	2.978	2.686	615.033	2.978	2.650	691.970
3.878	3.600	587.219	3.878	3.572	645.748	3.878	3.538	717.836
4.779	4.491	606.351	4.779	4.463	666.542	4.779	4.432	733.335
5.680	5.386	619.522	5.680	5.357	680.899	5.680	5.326	746.507
6.581	6.281	630.847	6.581	6.252	693.305	6.581	6.221	759.394
7.481	7.177	641.762	7.481	7.147	705.288	7.481	7.115	772.379
8.382	8.072	652.669	8.382	8.042	717.270	8.382	8.011	782.886
9.283	8.968	663.692	9.283	8.937	729.384	9.283	8.909	789.308
10.184	9.863	674.876	10.184	9.832	741.677	10.184	9.807	795.180
11.084	10.761	681.297	11.084	10.729	748.271	11.084	10.705	800.593
11.985	11.659	686.788	11.985	11.627	754.262	11.985	11.603	805.616
12.886	12.558	691.920	12.886	12.525	759.862	12.886	12.502	810.302
13.787	13.456	696.739	13.787	13.424	765.120	13.787	13.400	814.696

HS51			HS56			HS63		
True Strain ε [%]	True Plastic Strain $\varepsilon_p=\varepsilon-\sigma/E$ [%]	True Stress σ [N/mm^2]	True Strain ε [%]	True Plastic Strain $\varepsilon_p=\varepsilon-\sigma/E$ [%]	True Stress σ [N/mm^2]	True Strain ε [%]	True Plastic Strain $\varepsilon_p=\varepsilon-\sigma/E$ [%]	True Stress σ [N/mm^2]
14.687	14.355	701.284	14.687	14.322	770.079	14.687	14.299	818.834
15.588	15.253	705.586	15.588	15.221	774.772	15.588	15.198	822.744
16.489	16.152	709.669	16.489	16.119	779.227	16.489	16.097	826.452
17.390	17.051	713.558	17.390	17.018	783.469	17.390	16.996	829.978
18.290	17.950	717.269	18.290	17.917	787.518	18.290	17.895	833.339
19.191	18.849	720.821	19.191	18.816	791.392	19.191	18.794	836.552
20.092	19.748	724.225	20.092	19.715	795.105	20.092	19.694	839.629
20.993	20.647	727.496	20.993	20.614	798.673	20.993	20.593	842.582
21.893	21.547	730.642	21.893	21.513	802.105	21.893	21.493	845.420
22.794	22.446	733.675	22.794	22.412	805.413	22.794	22.392	848.153
23.695	23.345	736.602	23.695	23.311	808.605	23.695	23.291	850.788
24.596	24.245	739.431	24.596	24.211	811.690	24.596	24.191	853.332
25.496	25.144	742.168	25.496	25.110	814.676	25.496	25.091	855.793
26.397	26.044	744.820	26.397	26.009	817.568	26.397	25.990	858.174
27.298	26.943	747.392	27.298	26.909	820.373	27.298	26.890	860.482
28.199	27.843	749.889	28.199	27.808	823.096	28.199	27.790	862.721
29.099	28.742	752.315	29.099	28.708	825.742	29.099	28.689	864.895
30.000	29.642	754.675	30.000	29.607	828.315	30.000	29.589	867.008

TABLE 4
Steel Grades HS70, HS91, HS98

HS70			HS91			HS98		
True Strain ε [%]	True Plastic Strain $\varepsilon_p=\varepsilon-\sigma/E$ [%]	True Stress σ [N/mm^2]	True Strain ε [%]	True Plastic Strain $\varepsilon_p=\varepsilon-\sigma/E$ [%]	True Stress σ [N/mm^2]	True Strain ε [%]	True Plastic Strain $\varepsilon_p=\varepsilon-\sigma/E$ [%]	True Stress σ [N/mm^2]
0.000	0.000	0.000	0.000	0.000	0.000	0.000	0.000	0.000
0.328	0.000	692.267	0.423	0.000	893.772	0.456	0.000	964.389
0.618	0.289	694.279	0.689	0.265	896.157	0.714	0.257	966.882
0.908	0.579	696.297	0.956	0.531	898.548	0.972	0.514	969.381
1.199	0.868	698.320	1.222	0.796	900.946	1.231	0.771	971.887
1.489	1.157	700.350	1.489	1.061	903.350	1.489	1.028	974.400
1.861	1.521	718.578	1.861	1.427	916.985	1.861	1.397	982.140

HS70			HS91			HS98		
True Strain ε [%]	True Plastic Strain $\varepsilon_p=\varepsilon-\sigma/E$ [%]	True Stress σ [N/mm^2]	True Strain ε [%]	True Plastic Strain $\varepsilon_p=\varepsilon-\sigma/E$ [%]	True Stress σ [N/mm^2]	True Strain ε [%]	True Plastic Strain $\varepsilon_p=\varepsilon-\sigma/E$ [%]	True Stress σ [N/mm^2]
2.233	1.884	736.782	2.233	1.793	930.573	2.233	1.765	989.870
2.606	2.248	753.444	2.606	2.159	942.899	2.606	2.134	997.104
2.978	2.615	765.963	2.978	2.527	952.241	2.978	2.503	1003.152
3.878	3.507	783.941	3.878	3.421	967.498	3.878	3.398	1014.885
4.779	4.401	798.169	4.779	4.315	980.857	4.779	4.294	1025.910
5.680	5.295	812.223	5.680	5.210	994.207	5.680	5.190	1036.983
6.581	6.191	822.193	6.581	6.106	1003.488	6.581	6.086	1046.190
7.481	7.089	828.596	7.481	7.003	1011.018	7.481	6.983	1054.040
8.382	7.987	834.312	8.382	7.901	1017.737	8.382	7.880	1061.045
9.283	8.885	839.477	9.283	8.798	1023.808	9.283	8.778	1067.374
10.184	9.784	844.192	10.184	9.697	1029.348	10.184	9.676	1073.150
11.084	10.682	848.530	11.084	10.595	1034.444	11.084	10.574	1078.462
11.985	11.581	852.548	11.985	11.493	1039.164	11.985	11.473	1083.383
12.886	12.480	856.292	12.886	12.392	1043.561	12.886	12.371	1087.968
13.787	13.379	859.798	13.787	13.291	1047.677	13.787	13.270	1092.259
14.687	14.278	863.095	14.687	14.190	1051.548	14.687	14.169	1096.295
15.588	15.178	866.207	15.588	15.089	1055.201	15.588	15.068	1100.104
16.489	16.077	869.155	16.489	15.988	1058.661	16.489	15.967	1103.710
17.390	16.976	871.955	17.390	16.887	1061.947	17.390	16.866	1107.136
18.290	17.876	874.622	18.290	17.786	1065.077	18.290	17.765	1110.399
19.191	18.775	877.168	19.191	18.686	1068.064	19.191	18.664	1113.514
20.092	19.675	879.604	20.092	19.585	1070.923	20.092	19.564	1116.494
20.993	20.575	881.940	20.993	20.485	1073.663	20.993	20.463	1119.350
21.893	21.474	884.184	21.893	21.384	1076.294	21.893	21.363	1122.094
22.794	22.374	886.342	22.794	22.284	1078.826	22.794	22.262	1124.733
23.695	23.274	888.422	23.695	23.183	1081.265	23.695	23.162	1127.276
24.596	24.174	890.428	24.596	24.083	1083.618	24.596	24.061	1129.729
25.496	25.073	892.367	25.496	24.982	1085.891	25.496	24.961	1132.100
26.397	25.973	894.243	26.397	25.882	1088.090	26.397	25.861	1134.392
27.298	26.873	896.059	27.298	26.782	1090.220	27.298	26.760	1136.612
28.199	27.773	897.820	28.199	27.682	1092.284	28.199	27.660	1138.764

HS70			*HS91*			*HS98*		
True Strain ε ***[%]***	***True Plastic Strain*** $\varepsilon_p=\varepsilon-\sigma/E$ ***[%]***	***True Stress*** σ ***[N/mm²]***	***True Strain*** ε ***[%]***	***True Plastic Strain*** $\varepsilon_p=\varepsilon-\sigma/E$ ***[%]***	***True Stress*** σ ***[N/mm²]***	***True Strain*** ε ***[%]***	***True Plastic Strain*** $\varepsilon_p=\varepsilon-\sigma/E$ ***[%]***	***True Stress*** σ ***[N/mm²]***
29.099	28.673	899.529	29.099	28.581	1094.287	29.099	28.560	1140.853
30.000	29.573	901.188	30.000	29.481	1096.233	30.000	29.459	1142.881

APPENDIX 3
References

[1] J. K. Paik and A. K. Thayamballi, Ship–Shaped Offshore Installations: Design, Building, and Operation, Cambridge: Cambridge University Press, 2007.

[2] O. Hughes and J. K. Paik, Ship Structural Analysis and Design, Jersey City, NJ: The Society of Naval Architects and Marine Engineers, 2010, pp. 8.1-8.22.

[3] N. E. Dowling, Mechanical Behavior of Materials, Third ed., Upper Saddle River, NJ: Pearson Prentice Hall, 2007.

[4] P. Wriggers, Nonlinear Finite Element Methods, Heidelberg: Springer-Verlag, 2008.

[5] M. A. Crisfield, "A fast incremental/iterative solution procedure that handles "snap-through"," *Computers & Structures,* vol. 13, no. 1-3, pp. 55-62, 1981.

[6] E. Riks, "An incremental approach to the solution of snapping and buckling problems," *International Journal of Solids and Structures,* vol. 15, no. 7, pp. 529-551, 1979.

[7] H. M. Hilber, T. J. R. Hughes and R. L. Taylor, "Improved numerical dissipation for time integration algorithms in structural dynamics," *Earthquake Engineering and Structural Dynamics,* vol. 5, no. 3, pp. 283-292, 1977.

[8] E. Lehmann, "Discussion on Report of Committee III. 1: Ultimate Strength," in *Proceedings of 16th ISSC, pp. 121–131*, 2006.

[9] J. Lubliner, Plasticity Theory, Berkeley, CA: Jacob Lubliner, 2006.

[10] X. Yun and L. Gardner, "Stress-strain curves for hot-rolled steels," *Journal of Constructional Steel Research,* vol. 133, pp. 36-46, 2017.

[11] N. Jones and C. Jones, "Inelastic failure of fully clamped beams and circular plates under impact loading," *Proceedings of the Institution of Mechanical Engineers, Part C: Journal of Mechanical Engineering Science,* vol. 216, no. 2, pp. 133-149, 2002.

[12] S. Zhang, P. T. Pedersen and R. Villavicencio, Probability and Mechanics of Ship Collision and Grounding, Oxford: Butterworth-Heinemann, 2019.

[13] R. Törnqvist, Design of Crashworthy Ship Structures (Phd Thesis), Kongens Lyngby: Technical University of Denmark, 2003.

[14] M. Storheim, J. Amdahl and I. Martens, "On the accuracy of fracture estimation in collision analysis of ship and offshore structures," *Marine Structures,* vol. 44, pp. 254-287, 2015.

[15] G. R. Johnson and W. H. Cook, "Fracture characteristics of three metals subjected to various strains, strain rates, temperatures and pressures," *Engineering Fracture Mechanics,* vol. 21, no. 1, pp. 31-48, 1985.

[16] J. e. a. Czujko, "Committee III.1 - Ultimate Strength," in *Proceedings of the 20th International Ship and Offshore Structures Congress*, 2018.

[17] Simulia Corp, SIMULIA User Assistance 2018, Providence, RI: Dassault Systèmes Simulia Corp., 2017.

[18] M. Petričić, "Survivability of Hull Girder in Damaged Condition," Ship Structure Committee, Washington, 2015.

[19] IACS, Common Structural Rules for Bulk Carriers and Oil Tankers – External Release 1, London: International Association of Classification Societies, 2014.

[20] B. Liu, R. Villavicencio, S. Zhang and C. Guedes Soares, "A simple criterion to evaluate the rupture of materials in ship collision simulations," *Marine Structures,* vol. 54, pp. 92-111, 2017.